INFORMATION TO USERS

This dissertation was produced from a microfilm copy of the original document. While the most advanced technological means to photograph and reproduce this document have been used, the quality is heavily dependent upon the quality of the original submitted.

The following explanation of techniques is provided to help you understand markings or patterns which may appear on this reproduction.

1. The sign or "target" for pages apparently lacking from the document photographed is "Missing Page(s)". If it was possible to obtain the missing page(s) or section, they are spliced into the film along with adjacent pages. This may have necessitated cutting thru an image and duplicating adjacent pages to insure you complete continuity.

2. When an image on the film is obliterated with a large round black mark, it is an indication that the photographer suspected that the copy may have moved during exposure and thus cause a blurred image. You will find a good image of the page in the adjacent frame.

3. When a map, drawing or chart, etc., was part of the material being photographed the photographer followed a definite method in "sectioning" the material. It is customary to begin photoing at the upper left hand corner of a large sheet and to continue photoing from left to right in equal sections with a small overlap. If necessary, sectioning is continued again — beginning below the first row and continuing on until complete.

4. The majority of users indicate that the textual content is of greatest value, however, a somewhat higher quality reproduction could be made from "photographs" if essential to the understanding of the dissertation. Silver prints of "photographs" may be ordered at additional charge by writing the Order Department, giving the catalog number, title, author and specific pages you wish reproduced.

University Microfilms

300 North Zeeb Road
Ann Arbor, Michigan 48106

A Xerox Education Company

72-24,144

PARETSKY, Leon Carl, 1943-
FILTRATION OF AEROSOLS BY GRANULAR BEDS.

The City University of New York, Ph.D., 1972
Engineering, chemical

University Microfilms, A XEROX Company, Ann Arbor, Michigan

FILTRATION OF AEROSOLS BY GRANULAR BEDS

by

Leon Carl Paretsky

A dissertation submitted to the Graduate Faculty in Chemical Engineering in partial fulfillment for the degree of Doctor of Philosophy, The City University of New York

1972

This manuscript has been read and accepted for the Graduate Faculty in Engineering in satisfaction of the dissertation requirement for the degree of Doctor of Philosophy.

5/12/72
Date

Chairman of Examining Committee

5/12/72
Date

Jacques E. Benveniste
Executive Officer

Prof. Robert Pfeffer (Chairman & Mentor)

Prof. Sylvan M. Edmonds

Prof. Robert A. Graff

Prof. Arthur M. Squires (Co-mentor)

Supervisory Committee

The City University of New York

ABSTRACT

An investigation into the mechanics governing the filtration of both monodispersed dilute aerosols and power station fly ash by granular beds was undertaken.

Initially, experimental studies of the filtration of dilute aerosols of Dow microspheres by beds of sand were conducted with flows passing vertically upward, vertically downward, and horizontally. Face velocities of 0.3 to 70 cm/sec, using 10-14 mesh and 20-30 mesh sand were investigated. The single particle collection efficiency was found to be independent of bed height. Filtration was primarily by diffusion and gravity settling at low velocities, and by inertial impaction at high velocities. Direct interception was negligible in this investigation. Upshot flow gave lower single particle collection efficiencies than downshot flow, indicating the importance of gravity settling as a filtration mechanism.

With the use of Happel's "free surface" model for granular beds, the experimental results were correlated reasonably well by semi-empirical, semi-theoretical considerations taking into account filtration by the

above-mentioned mechanisms. An overall theoretical-empirical filtration model was obtained by adding the single particle collection efficiencies of each of the filtration mechanisms.

Fly ash filtration was studied at velocities low enough to promote formation of a filter cake. Filter cakes were deposited on both horizontal sand surfaces and on the free surfaces of a panel bed filter fitted for cleaning by puffback. Studies on the horizontal sand bed indicated that the structure of the fly ash filter cake varied with the face velocity and the method of deposition. Shifts in the face velocity on a deposited filter cake were found to alter the structure of the filter cake. A filter cake thickness of 0.14 grams/cm^2 was found to have a collection efficiency of over 99.99% against the 1.1 micron Dow microspheres.

Cyclic operation of the panel bed filter was found to produce fly ash collection efficiencies in excess of 99.9% at a face velocity of about 11 ft/min, and with a fly ash filter cake pressure drop of about one-half inch water. Steady-state operation was easily attained and maintained. The nature of the filter

cake was investigated by passing a dilute aerosol of 1.1 micron Dow microspheres through the filter cake. It was found best to perform this test at the same velocity at which the filter cake was deposited.

ACKNOWLEDGEMENTS

I thank Professor Robert Pfeffer and Professor Arthur M. Squires for their guidance and interest in this research.

Thanks are also due to the Chemical Engineering Shop, especially John Bodnaruk and George DiIorio, for their assistance in constructing and setting up the experimental apparatus.

I acknowledge the financial support received from the City University of New York, the NSF traineeship program, and the NDEA fellowship program.

I also wish to thank Dean and Professor Emeritus A.X. Schmidt, former Chairman of the Department of Chemical Engineering, for enabling me to obtain teaching experience while pursuing my doctorate.

Grant Number AP-00693 from the Air Pollution Control Office of the Environmental Protection Agency supported a major part of this work.

DEDICATION

This research is dedicated to my wife, Celia, for her encouragement and patience in understanding the sometimes strange existence that this research effort required.

PRESENTATIONS AND PUBLICATIONS

Portions of this research appear in the following:

L. Paretsky, L. Theodore, R. Pfeffer, and A.M. Squires, "Panel Bed Filters for Simultaneous Removal of Fly Ash and Sulfur Dioxide: II. Filtration of Dilute Aerosols by Sand Beds", Presented at the 63rd Annual Meeting of the Air Pollution Control Association, June 1970. Published in the Journal of the Air Pollution Control Association, 21, 204 (1971).

TABLE OF CONTENTS

LIST OF TABLES

LIST OF FIGURES

NOMENCLATURE

A = area of filter in direction of fluid flow

$\bar{A}(t)$ = fluctuating force per unit mass which is characteristic of the Brownian motion of an aerosol particle

A_e = $(2 + 3\gamma^5)/2W$

a_c = projected area of single collector particle

B = mobility of aerosol particle = $C/(6\pi\mu r_p)$

B_e = $1/2W$

b = thickness of fibrous filter or height or depth of sand bed

C = Cunningham correction factor

C_L = arbitrary constant in velocity profile around stationary cylinder

C_e = $- (3 + 2\gamma^5)/2W$

D_e = $- \gamma^5/2W$

E = single particle collection efficiency of a collector taking into account the presence of neighboring collectors

E^* = single particle collection efficiency of an isolated collector

E_D, E_D^* = single particle collection efficiency due to Browian diffusion

E_{DI}, E_{DI}^* = single particle collection efficiency due to direct interception

E_G, E_G^* = single particle collection efficiency due to gravity settling

E_I, E_I^* = single particle collection efficiency due to inertial impaction

E_T, E_T^* = total single particle collection efficiency

E_δ, E_δ^* = loss in collection efficiency due to effect of gravity settling (equation 48)

ΔE_T = difference between downshot and upshot single particle collection efficiencies

$\overline{F}_D$ = drag force on an isolated fibrous collector

F_i = fraction of incoming aerosols remaining after passing through section i

F_{ijk} = fraction of incoming aerosols remaining after passing through sections i, j, and k

$f(\sigma)$ = a function accounting for the aerosol removal caused by ash collected in the interior of the bed

$f_1(Z_{ao})$ = a function accounting for the aerosol removal caused by Z_{ao}

$\overline{g}$ = gravitational vector

g_o = acceleration of gravity

$\overline{g}'$ = dimensionless gravitational vector = $\overline{g}/g_o$

K_f = permeability constant of the fly ash filter cake

K_o = permeability constant of the clean sand bed

k_c = mass transfer coefficient

l = length of an individual fiber

m_p = mass of aerosol particle

N_G = gravity settling parameter = $\frac{2}{9} \frac{\rho_p r_p^2 g_o C}{\mu U_o}$

N_I = inertial parameter = $\frac{2}{9} \frac{\rho_p r_p^2 U_o C}{\mu r_c}$

n = aerosol concentration

n_o = free stream aerosol concentration

n' = dimensionless aerosol concentration = n/n_o

Pe = Peclet number = $(2\ r_c\ U_o/\Delta\ )$

ΔP = pressure loss or drop through filter

ΔP_d = pressure loss across bed after puffback

ΔP_f = pressure loss attributed to presence of fly ash in sand bed (i.e., $\Delta P_t - \Delta P_o$)

ΔP_o = clean bed pressure drop

ΔP_t = dirty bed pressure drop

ΔP_σ = pressure loss caused by ash collected in the interior of the bed

Q = volumetric flow rate upstream of filter

r = spherical coordinate

$\bar{r}$ = position coordinate vector of aerosol particle

r_b = radius of cell boundary

r_c = radius of collector or sand particle

r_f = effective fiber radius

r_o = initial position of aerosol particle

r_p = radius of aerosol particle

$r_{p_{max}}$ = aerosol size at which the penetration through a filter is the maximum (at constant velocity)

R = direct interception parameter = r_p/r_c

Re_c = collector Reynolds number = $(2\ r_c\ U_o\ \rho_f/\mu)$

Re_p = particle Reynolds number = $(2\ r_p\ U_o\ \rho_f/\mu)$

R_s = specific resistance of dust on fabric filter (equation 79)

$\bar{r}'$ = dimensionless position coordinate vector of aerosol particle = $\bar{r}/r_c$

Sh = Sherwood number = $(2\ r_c\ k_c/\Delta)$

S_R = residual drag of fabric filter media (equation 79)

s_c = projected area of collector per unit total volume of filter

t = time

t' = dimensionless time = $t/(r_c/U_o)$

$\bar{U}_M$ = fluid velocity vector

U_{M_r} = radial fluid velocity component

U_{M_y} = fluid velocity in y direction

U_{M_z} = fluid velocity in z direction

U_{M_θ} = angular fluid velocity component

U_o = free stream velocity

$\bar{U}_M'$ = dimensionless fluid velocity vector = $\bar{U}_M/U_o$

U_{M_y}' = dimensionless fluid velocity in y direction = U_{M_y}/U_o

U_{M_z}' = dimensionless fluid velocity in z direction = U_{M_z}/U_o

V = particle velocity equal to fluid velocity

V_A = test aerosol face velocity

V_A^B = test aerosol face velocity equal to velocity at which filter cake was developed

V_{Bed} = face velocity at which filter cake was developed

$\bar{V}_B$ = fluctuating velocity vector, characteristic of the Brownian motion of an aerosol particle

V_f = filter velocity

$\bar{V}_I$ = instantaneous particle velocity vector

V_o = superficial velocity

$\bar{V}_P$ = average particle velocity vector

V_{P_y} = particle velocity in y direction

V_{P_z} = particle velocity in z direction

v_c = volume of single collector particle

$\bar{V}_B'$ = dimensionless Brownian velocity vector = $\bar{V}_B/U_o$

$\bar{V}_P'$ = dimensionless particle velocity vector = $\bar{V}_P/U_o$

V_{P_y}' = dimensionless particle velocity in y direction = V_{P_y}/U_o

V_{P_z}' = dimensionless particle velocity in z direction = V_{P_z}/U_o

W = $2 - 3\gamma + 3\gamma^5 - 2\gamma^6$

x_o = distance from surface of collector at angle 90^o with respect to direction of flow within which all particles are collected by diffusion (Table 3)

y = coordinate axis

y_{crit} = starting point of the critical trajectory of the aerosol particle

y_o = initial position of aerosol particle

y' = dimensionless coordinate axis = y/r_c

y_o' = dimensionless initial position of aerosol particle = y_o/r_c

Z = weight of fly ash deposited on the sand surface per unit area of sand bed

Z_{ao} = critical value of Z for development of stable filter cake; obtained from test aerosol analysis

Z_{po} = critical value of Z for development of stable filter cake; obtained from pressure loss analysis

z = coordinate axis

z_o = initial position of aerosol

z' = dimensionless coordinate axiz = z/z_o

z_o' = dimensionless initial position of aerosol particle = z_o/r_c

γ = $r_c/r_b = (1 - \epsilon)^{1/3}$

Δ = diffusion coefficient

ϵ = porosity or voidage of fibrous filter or sand bed

ϵ_f = porosity of fly ash filter cake deposited on surface

ξ = fractional penetration of aerosols through a filter media

ξ^* = fractional penetration of aerosols through a filter media composed of ideal collectors

ξ_c = fractional penetration of aerosols through a clean sand bed

ξ_d = fractional penetration of aerosols through a dirty sand bed

ξ_f = fractional penetration of aerosols through the fly ash retained in a sand bed

ρ_f = density of fluid

ρ_p = density of aerosol particle

σ = fraction of fly ash deposited on a sand surface that goes to forming a filter cake

η = attenuation factor for a clean sand bed defined in equation (29)

η_f = attenuation factor for a fly ash filter cake

θ = spherical coordinate

μ = viscosity of fluid stream

φ = spherical coordinate

$\varphi(z_{po})$ = function to account for pressure loss due to z_{po}

ψ = stream function

Ω = Effectiveness factor, defined in equation (89)

∇' = dimensionless operator = $r_c \nabla$

∇'^2 = dimensionless operator = $r_c^2 \nabla^2$

$\rho(\epsilon)$ = function of ϵ = $\dfrac{W}{1 - \gamma^5}$

$= \dfrac{2 - 3\gamma + 3\gamma^5 - 2\gamma^6}{1 - \gamma^5}$

1. INTRODUCTION

The problem of removing dust from a gas stream has received considerable attention. The dust can be fly ash from the stack gas of a coal fired power-station, or the fines from a metallurgical process such as a steel furnace. Brandt (6) reviews many of the present dust removal techniques. Most of these involve the use of electrostatic precipitators, cyclones, wet scrubbers and fabric filters. Brandt enumerates the deficiencies in these methods, and urges the desirability of finding better methods of dust removal.

The Lurgi filter (17) was a recent attempt in devising a gravel bed filter for dust collection. Collection efficiencies of over 99 percent were reported. The objections of Brandt to the Lurgi filter are not applicable to a panel bed filter having free renewable surfaces, such as the filter of Squires (53,54). The advantages of a filter of this type are that in addition to effectively treating dusts, if a suitable reactive filter solid is utilized, it can also be used for removal of certain gases that may be present in the dust stream. This may be, for example, half-calcined dolomite for

removal of SO_2.

In its simplest form, the panel consists of a tall narrow bed of a granular solid retained between two parallel, vertical, perforated walls. Construction permits the fly ash in the entering gas to be deposited upon a free surface of the granular solid, which is retained there at its angle of repose. The filter would be operated at a velocity low enough to permit formation of a filter cake of fly ash at the gas-entry surfaces and to limit the degree to which the deposited fly ash penetrates into the sand bed. The fly ash filter cake is removed periodically, along with a small amount of the granular solid, allowing a new free surface to form.

The dusts (or heavy aerosols) treated by the above mentioned devices generally have a dirty-side loading of the order of several grams per cubic meter. The filtration behavior of these dusts is clearly time dependent; that is, the filtration efficiency and pressure loss across the filter increases with time (20).

Insight into the behavior of these heavy aerosols could be obtained by developing an understanding of the filtration of monodispersed dilute aerosols by granular beds. These aerosols have a loading of approximately 10^{-6} grams per cubic meter, and do not have

a time-dependent filtration behavior.

Experimental study of granular bed filtration is quite limited. It is confined essentially to the work of Thomas and Yoder (62,63), who investigated the penetration of highly dilute aerosols through particulate beds, and to the work of Taub (59), who studied the time-dependent filtration efficiency of a sand bed capturing fly ash under conditions such that the fly ash deposits appear throughout the bed and are not concentrated in a filter cake at the gas-entry surface.

Analytical work on aerosol filtration by granular beds could not be found in the literature. Rather, it is necessary to draw on the studies of aerosol filtration by fibrous filters where fairly extensive analytical and experimental work has been reported. A typical analytical approach has been Dorman's method (15) of treating Ramskill and Anderson's data (47) for the filtration of dilute aerosols by fibrous filters. Dorman developed a semi-empirical curve fitting model that correlated filtration efficiency vs. velocity for constant aerosol particle size.

Dorman's approach is to consider independently each of the filtration mechanisms - diffusion, inertial

impaction, and direct interception. He assumes that a certain fraction of the particles are removed by each mechanism, and the total removal is affected by the product of these mechanisms.

For diffusion and direct interception, Dorman used analytical models which had been previously developed by other investigators (13,37), while for inertial impaction the dependence of aerosol penetration on velocity was determined by fitting an empirical equation to the experimental data.

Thomas and Yoder (62,63) demonstrated that for sand beds, as for fabric filters, there exists a particular aerosol size that at constant velocity exhibits a maximum penetration. In other words, there is a particular size that is the most difficult to filter for a given velocity and sand bed. Their study indicated that the penetration varies with respect to bed orientation. An aerosol passed upshot gave consistantly higher penetration than one passed downshot in the range of sand size, particle size and aerosol velocity which they investigated. This illustrated the importance of gravity settling in the filtration of aerosols by sand beds. There were insufficient data from the work of Thomas and Yoder for a rigorous test of the applicability of Dorman's

technique to sand bed filtration.

It is apparent there is a need for a study of the filtration of dilute aerosols by sand beds, and the literature on aerosol filtration by fabric filters can be used as a guide for the investigation.

No work has been done on the filtration of heavy aerosols under conditions conducive to the formation of a filter cake at the gas-entry surface of the sand bed.

Research was undertaken in each of the two foregoing areas. Results will be presented in two sections, first the dilute aerosol studies, then the fly ash work.

2. OBJECT OF THE RESEARCH

The object of this research is two-fold. (1) Extend the breadth of knowledge of the filtration of dilute aerosols by granular beds, and (2) initiate a study into the mechanics of the formation and retention of a fly ash filter cake deposited upon free renewable surfaces of a granular solid, as in a panel bed filter.

For the former, experimental studies are made of the filtration of dilute aerosols of Dow microspheres by sand beds, with flows vertically upwards, vertically downwards, and horizontally. This information is utilized in the construction of a model that would predict filtration efficiencies of a granular bed for a dilute aerosol stream.

For the latter, work is performed in developing an operation representative section of a panel bed filter, along with ancillary equipment such as a feeder which can deliver the fly ash. The steady-state behavior (consisting of deposition of a filter cake, subsequent cleaning by puffback and then repetition of this cycle) is examined for various bed velocities and thicknesses of filter cake. At various stages in the cycles a dilute aerosol stream is passed through the fly ash filter cake

and sand bed. Upon correction for the removal of aerosols by the sand bed, the penetration of the aerosols through the fly ash filter cake is obtained. These measurements provide additional information as to the structure of the filter cake.

A fly ash filter cake is also deposited on a vertical cylindrical packed bed. Aerosol measurements on this unit aid in interpreting the measurements on the panel.

3. SIGNIFICANCE OF THE RESEARCH

This research should advance the understanding and technology of dust removal from a gaseous stream through the use of a granular filter media.

Granular beds, used with a filter aid or a pre-coat, could be used as an "absolute" filter for dilute aerosols under conditions where conventional membrane HEPA filters are suitable, as well as for conditions (e.g., at high temperature) where such filters cannot be used.

The use of a panel bed filter in a power station promises higher efficiencies than possible with current dust capturing techniques. In addition, the granular solid present in the panel can be reactive to noxious gaseous such as sulfur dioxide so as to cause their removal.

A panel could also be used to suppress both alkali fumes and hydrogen sulfide present in the offgas from a fluidized bed gasifying coal so that the hot gases can be used in a gas turbine (27). Filter aids (such as fly ash) could be used to improved the filtration efficiency of the granular solid.

The use of the test aerosol to probe the nature of the fly ash filter cake provides a technique whereby

the structure of the cake can be examined at different time intervals without disturbing the cake.

PART ONE: DILUTE AEROSOL STUDIES

4. BACKGROUND

Mechanisms of Filtration of Dilute Aerosols

The primary mechanisms involved in the filtration of aerosols are diffusion, direct interception, inertial impaction, and gravity settling. Electrical and thermal effects may also appear, but generally these effects are induced external to the filtration process and will not be considered here.

Figure 1 illustrates the collection of an aerosol particle by a spherical collector. Deposition by diffusion is caused by the Brownian motion of the aerosol particle which results in a deviation from its normal flow and subsequent deposition and adherence to the filter media. This effect is prevalent at low velocities and for small particles. In analyzing collection by this mechanism it is customary to consider the particles as points with no mass or size. The aerosol particle velocity, upon which the Brownian velocity is superimposed, is assumed equal to the fluid velocity.

Deposition by direct interception occurs when the particles moving along streamlines of a fluid approach

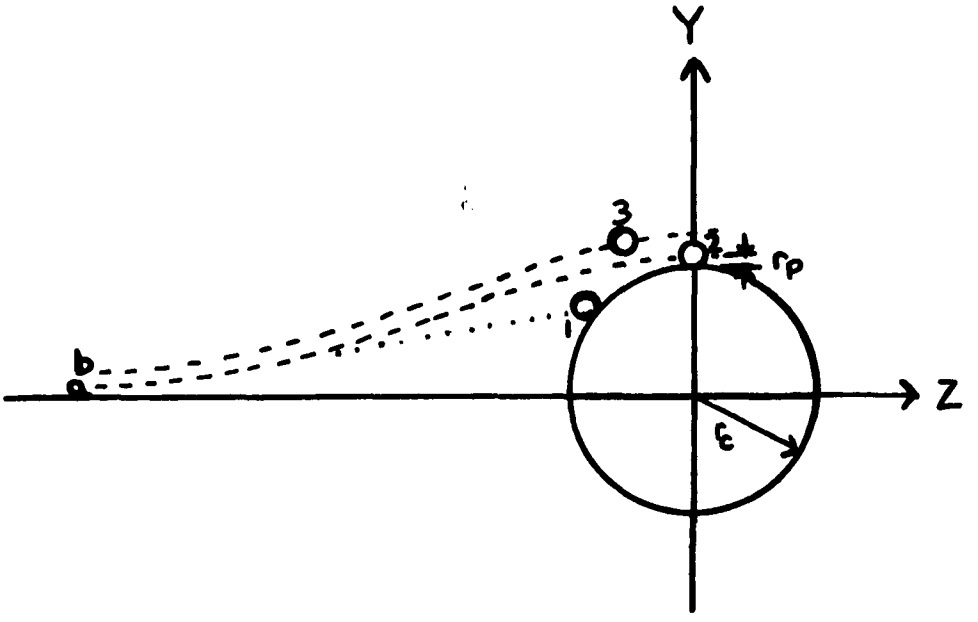

Figure 1. Aerosol Particles Approaching a Collector.

r_c = collector radius

r_p = aerosol particle radius

a, b = typical fluid streamlines

1, 2, 3 = typical aerosol particles

the collector within a distance equal to the radius of the impinging particle. From Figure 1 it is seen that particle 2 which is carried by streamline a will be filtered by this mechanism. Particle 3 which is carried along streamline b will not be filtered. This mechanism is independent of the fluid velocity, but increases with the size of the aerosol particle, and decreases as the size of the collector increases. In analyzing filtration by this mechanism the particles are considered to have a length dimension but no mass.

The mechanism of removal by inertial impaction occurs when the size or velocity of the particle is so large that the particle does not follow the streamline of the fluid but resists the directional change imposed by the collector and strikes it. Particle 1 on streamline a illustrates typical deposition by this mechanism. An increase in velocity and mass of the impinging particle increases the effect of this mechanism. In analyzing deposition by inertial impaction the particles are considered to be point masses in the calculation of the collection efficiency. However, their size is accounted for in evaluation of the fluid's resistance to the particles' motion.

Deposition by gravity settling can be considered as a removal mechanism superimposed on any of the above. It is most prevalent at lower velocities and for larger particles.

The above description applies for each of the mechanisms acting independently of one another. Table 1 lists the various mechanisms and the parameters associated with each mechanism (48).

Unfortunately, for the purpose of mathematical analysis of the filtration process, these mechanisms usually are superimposed upon one another.

Consider initially the case of diffusion of particles of finite size (but no mass). This is equivalent to diffusion coupled with direct interception. The particles are collected by the combined mechanisms when they diffuse not to the surface of the collector (as for pure diffusion), but within a distance equal to the radius of the aerosol particle from the surface of the collector. This change reflects itself in an altering of the boundary conditions on the diffusion equation.

For direct interception combined with inertial impaction, the particles are considered to be captured when their trajectories are less than a distance equal to the radius of the particle from the collector surface.

Table 1. Filtration Parameters (48)

MECHANISM	CHARACTERISTIC PARAMETER	SIGNIFICANCE
Brownian Diffusion	$\frac{1}{Pe} = \frac{\Delta}{2r_c U_o}$	$\frac{\text{Diffusional Forces}}{\text{Inertial Forces}} = \frac{\Delta U_o/(2r_c)^2}{U_o^2/2r_c}$
Direct Interception	$R = \frac{r_p}{r_c}$	$\frac{\text{Characteristic Dimension of Particle}}{\text{Characteristic Dimension of Collector}} = \frac{r_p}{r_c}$
Inertial Impaction	$N_I = \frac{2}{9}\frac{\rho_p r_p^2 U_o C}{\mu r_c}$	$\frac{\text{Force Necessary to Stop Particle in Distance Equal to Radius of Collector}}{\text{Fluid Resistive Force to Particle}} = \frac{\frac{4}{3}\pi r_p^3 \rho_p U_o^2/2r_c}{6\pi r_p \mu U_o/C}$
		$\frac{\text{Stopping Distance of Particle}}{\text{Radius of Collector}} = \frac{2U_o r_p^2 \rho_p C/9\mu}{r_c}$
Gravity Settling	$N_G = \frac{2}{9}\frac{\rho_p r_p^2 g_o C}{\mu U_o}$	$\frac{\text{Force of Gravity}}{\text{Fluid Resistive Force}} = \frac{\frac{4}{3}\pi r_p^3 \rho_p g_o}{6\pi r_p \mu U_o/C}$
	$= \frac{g_o r_c}{U_o^2} N_I$	$\frac{\text{Settling Velocity of Particle}}{\text{Free Stream Velocity}} = \frac{2g_o \rho_p r_p^2 C/9\mu}{U_o}$

As with the diffusion - direct interception coupling, this involves altering the boundary condition at the surface of the collector.

If diffusion is included with direct interception and inertial impaction, one has the random Brownian motion superimposed on the inertial motion of the particle. As will be shown latter, however, the latter two mechanisms virtually never occur simultaneously.

Historical Survey

Aerosol filtration theory as applied to single particle targets is fairly well established. The limiting factor is a thorough knowledge of the fluid dynamics around the target. Obviously, as the targets become more numerous, and the voidage becomes smaller, the hydrodynamic problem becomes more complicated. The problem is usually approached by modifying a single particle filtration model to one which will fit multiple target filtration data, as in a fibrous filter or a sand bed.

The two basic filtration phenomena that have been investigated are the effect of velocity on penetration and the effect of aerosol size on penetration. The currently accepted trends are illustrated in Figures 2 and 3.

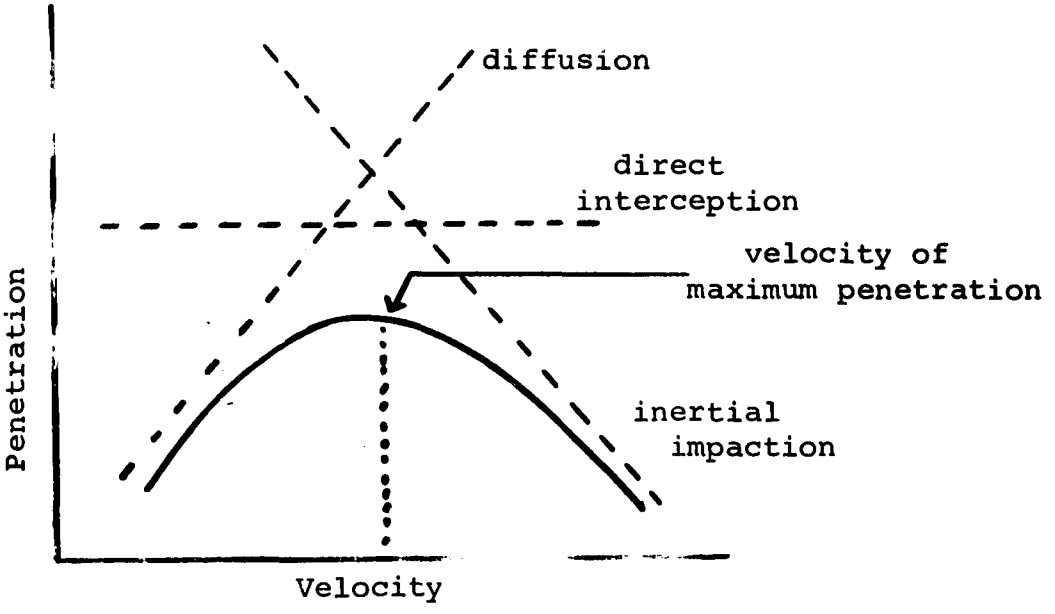

Figure 2. Effect of Velocity on Penetration (constant particle size).

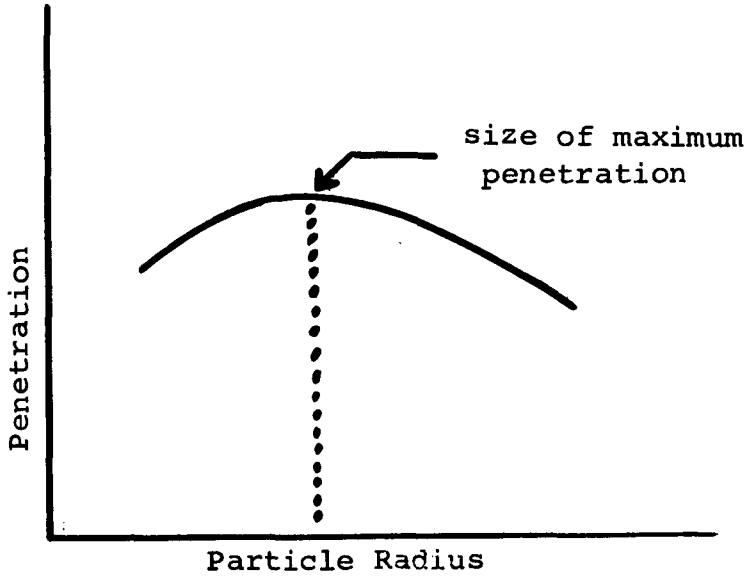

Figure 3. Effect of Particle Radius on Penetration (constant velocity).

The work of Langmuir (37) is the historical starting point in any treatment of filtration of aerosols. He considered only direct interception and Brownian diffusion to be the important mechanisms of capture, which is true in the small particle size and low velocity regime which he studied. Langmuir also calculated a critical value of N_I for single particle targets (about 0.05 - 0.10 for potential flow) below which no deposition by inertia occurs. This value was arrived at by obtaining the velocity field and particle flow lines around the collector. With this knowledge it is possible to find the particles which, starting at infinity in the direction of fluid flow and at a certain limiting distance from the axis of the cylinder, will just touch the surface of the collector. This limiting distance is a function of N_I.

Langmuir's approach to obtain the efficiency of the filter medium was to calculate what the pressure loss would be for a single fiber. An arbitrary proportionality constant was then included in the velocity distribution equations for a single fiber, and the total pressure loss was obtained by summing the pressure loss over all the fibers in the filter.

Langmuir then measured the actual pressure drop through the filter and calculated the value of the arbitrary constant which he called an interference function. This was used to correct the velocity distribution for neighboring fibers, and to calculate the actual collection efficiency. The existence of a size of aerosol particle which has a maximum penetration at constant velocity was mentioned, but no criteria for predicting its value were disclosed.

The question of whether an aerosol size of maximum penetration at constant velocity actually exists was seriously questioned for some time. La Mer et al (35) did not find a size of maximum penetration, and claimed that such a size does not exist. Ramskill and Anderson (47) also did not find this size, but believed it to exist. These workers felt that their experiments were run at too high a velocity to indicate a size of maximum penetration at constant velocity.

The work of Chen (9), who also surveyed previous work in his paper on filtration of aerosols through fibrous mats, showed that a size of maximum penetration at constant velocity does exist, and furthermore, such a size exists only when the face velocity is below a certain value. Chen's limitation was 5 cm/sec for the type of filters and

aerosols used. This might explain failures in previous attempts to find a minimum collection efficiency at constant velocity.

The existence of a minimum value of the inertial parameter N_I below which there is no deposition by inertia for isolated collectors has been noted by Chen and others.

The work of Thomas and Yoder (62,63), the only available experimental work on aerosol filtration through sand, showed the same general trends as those shown by fibrous filters. Their experiments illustrated that the size of maximum penetration increased with a decrease in velocity. The importance of gravity settling as a filtration mechanism (in the range of variables tested) was clearly demonstrated since the efficiency of penetration varied with orientation with respect to gravity in addition to varying with face velocity, size of aerosol particles, and size of sand granules.

The approach of Dorman (15) in correlating the data of Ramskill and Anderson (47) is noteworthy, and will be described in detail later. Dorman combined the diffusional and interception model of Langmuir (37) with the inertial model of Davies (13) (with some modification) to present a semi-empirical curve fitting model that fits the above data (47) quite well.

The effect of aerosol particle size on penetration was illustrated by Ramskill and Anderson (47), and Stern, Zeller and Schekman (57). At high velocities the larger aerosol particles give lower penetrations, while at low velocities the condition is reversed. Figure 4 illustrates this along with the existence of an "iso-efficiency point", a velocity where the collection efficiencies are the same for all sizes of particles (9,57).

The effect of filter fiber diameter on the penetration curves is illustrated in Figure 5, where the larger fiber sizes give higher penetrations. It should be noted that this is data for relatively high velocities, from 20 to over 250 cm/sec (47).

The different behavior of liquid and solid aerosols upon capture is mentioned by Fuchs (25). Liquid aerosols could deform upon collisions with the fibers and upon collisions among themselves. However, Stern et al (57) did not find any noticeable difference in the filtration efficiencies of liquid DOP and solid polystyrene aerosols of about 0.30 microns diameter, in penetration studies through fibrous filter mats.

A more complete discription of aerosol filtration theory is available in Chen (9), Fuchs (25), or Green

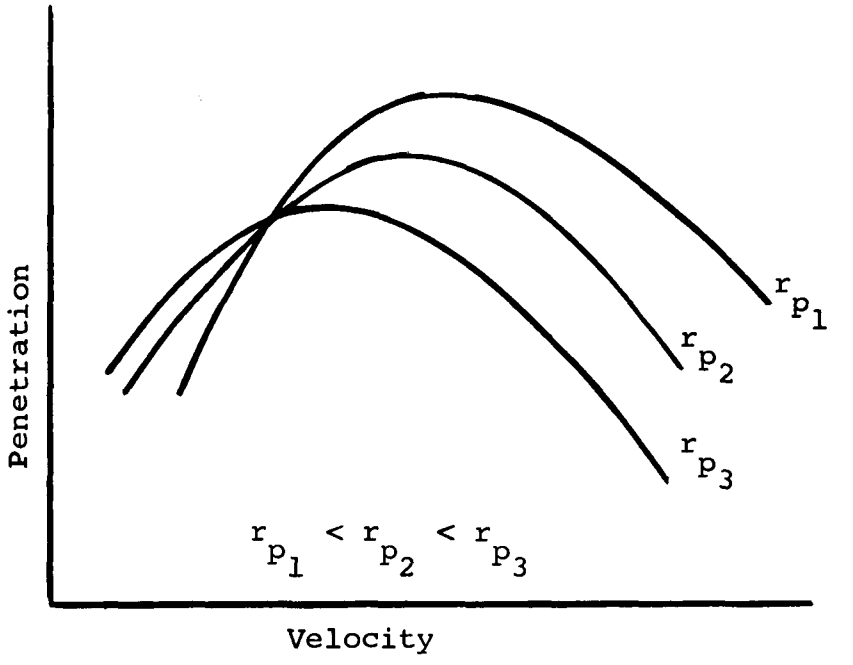

Figure 4. Effect of Particle Size on Velocity vs Penetration

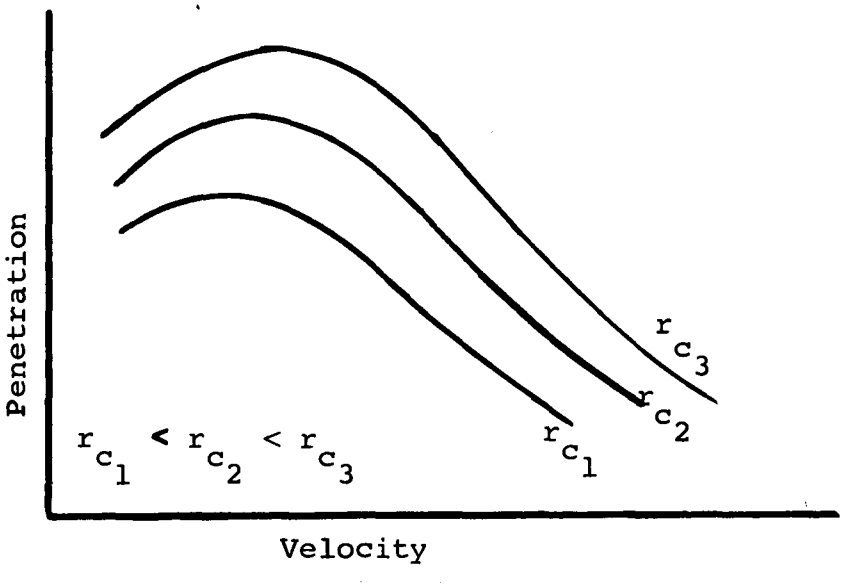

Figure 5. Effect of Fibrous Collector Size on Velocity vs Penetration

and Lane (29).

Dorman's Model

Several models have been proposed for the capture of aerosols by fibrous filters, assuming only one mechanism predominates. Dorman combined these individual mechanisms into a model that would predict the filtration efficiency of a fibrous filter when several mechanisms are simultaneously involved. He then applied this model to aerosol penetration data, and showed that empirical adjustments in the model would give excellent agreement between the resultant semi-empirical model and the experimental data.

Dorman took the filtration equation for fibers

$$\frac{n}{n_o} = \exp - \frac{2}{\pi} \frac{1 - \epsilon}{\epsilon} E_T \frac{b}{r_c} \qquad (1)$$

and assumed the single particle collection efficiency, E_T, to be composed of the sum of the single particle collection efficiencies of the individual mechanisms. That is, with the following notation of subscripts being adopted:

DI - indicates direct interception

I - indicates inertial impaction

D - indicates capture by Brownian diffusion

$$E_T = E_{DI} + E_I + E_D \qquad (2)$$

Therefore, for direct interception, inertial impaction and Brownian diffusion Dorman proceeded to write the filtration equation in terms of the total fraction penetration, ξ_T, as

$$\xi_T = \exp - \frac{2}{\pi} (E_{DI} + E_I + E_D) \frac{1 - \epsilon}{\epsilon} \frac{b}{r_c} \qquad (3)$$

Dorman used Langmuir's (37) calculations for capture by direct interception. The efficiency of capture of aerosols by a pad composed of ideal fibers was calculated, assuming that the velocity profile around a fiber could be approximated by Lamb's solution (36) for flow around a stationary cylinder. It is assumed that all particles that pass within a distance r_p of the collector are captured. Langmuir replaced the coefficienct of the radial and angular velocity components, $\frac{1}{2(2 - \ln Re_c)}$ in Lamb's solution by an arbitrary constant C_L instead. Experimental pressure drop measurements over the actual fiber enables one to calculate an effective fiber radius which is used to replace the actual fiber radius.

The measured drop is then equated to the pressure drop which would be obtained if the fibers behaved individually with no interference effects due to the proximity of other fibers. This enables one to solve for the constant, C_L. By this procedure the filtration equation for direct interception alone is obtained, and since the pressure drop, ΔP, is proportional to the velocity, V, E_{DI} is found to be independent of velocity (Table 2).

Langmuir's calculations were also used to obtain the filtration efficiency due to diffusion. The procedure involved finding the distance from which particles, carried by the fluid, will diffuse to the surface of a cylinder. It is then assumed that all particles that pass within this distance x_o, at angular location $\theta = 90^o$, of the collector are captured.

Langmuir assued the effective time a particle can diffuse to the surface of the collector is the time it takes a particle to pass from $\theta = 30^o$ to $\theta = 150^o$ through the point x_o. The root mean square distance from the surface of the above movement is the effective distance of the layer from which particles can diffuse.

As before, this single collector model is corrected for the presence of other fibers, and E_D is obtained. Since the pressure loss is proportional to

Table 2. Collection by Direct Interception

$$E_{DI} = \frac{\text{particles removed by collector}}{\text{particles removed if flow was straight}}$$

$$= \frac{2n_o \int_{r_c}^{r_c+r_p} U_\theta \big|_{\theta=90^o} \cdot 1 \, dr}{n_o \, U_o \, 1 \, 2r_c} \qquad (a)$$

where 1 is length of fiber.

Use Lamb's equation for the tangential velocity, replacing $[\, 2 \, (\, 2 - \ln Re_c \,) \,]^{-1}$ by C_L

$$U_\theta = U_o \, C_L \left[1 - \left(\frac{r_c}{r}\right)^2 + 2 \ln\left(\frac{r}{r_c}\right) \right] \sin \theta \qquad (b)$$

Integrate and non-dimensionalize

$$E_{DI} = C_L \left[\, 2(1 + R) \ln(1 + R) - R\left(1 + \frac{R}{1 + R}\right) \right] \qquad (c)$$

Drag force on an isolated fibrous collector based on Lamb's equation

$$F_D = 8 \pi \mu U_o \, 1 \, C_L \qquad (d)$$

Pressure drop across actual filter obtained by summing over all fibers in filter

$$\Delta P = 8 \pi \mu U_o \, 1 \, C_L \frac{1 - \epsilon}{\pi r_c^2 \, 1} b \qquad (e)$$

Experimental correlation utilized to relate ΔP to an effective fiber radius, r_f. r_f obtained from pressure drop measurements. Use r_f and experimental ΔP in (e), thus obtain C_L. Use C_L and r_f in (c), obtain E_{DI}.

the velocity, E_D is found to be proportional to $V^{-2/3}$ (Table 3).

The model of Davies (13) was used to predict capture due to inertial impaction. It is assumed that all the particles carried in the fluid upstream of a particular fiber will strike and adhere to the fiber if the particles are within a certain region y_{crit} about the axis of flow perpendicular to the cylinder. Again, it is assumed the fibers act independently. Measurements of pressure drop through the filter pad are used to replace the radius of the fiber with an effective fiber radius. Davies related the region y_{crit} to the inertial parameter N_I, and the pad voidage ϵ by fitting a quadratic equation of numerical values of y_{crit}/r_f vs ϵ and N_I obtained from a numerical solution of the flow field. This results in a solution for the efficiency of capture including inertia and direct interception. However, by setting R (the direct interception parameter) equal to zero, the filtration efficiency due only to direct interception is obtained (Table 4).

Dorman was interested in the dependence of the single particle collection efficiency on velocity

Table 3. Collection by Diffusion

$$E_D = \frac{\text{particles removed by collector}}{\text{particles removed if flow was straight}}$$

$$= \frac{2n_o \int_{r_c}^{r_c+x_o} U_\theta \Big|_{\theta=90^o} \; 1 \; dr}{n_o \; U_o \; 1 \; (2r_c)} \qquad (a)$$

As with Table 2 for Direct Interception, use Lamb's expression for the tangential velocity, letting $x_o' = x_o/r_c$

$$E_D = C_L \left[2(1 + x_o')\ln(1 + x_o') - x_o'\left(1 + \frac{1}{1 + x_o'}\right) \right] \qquad (b)$$

Expanding the above, with $x_o' << 1$

$$E_D = 2 \; C_L \; x_o'^{\,2} \qquad (c)$$

The average displacement of an aerosol particles in a time t is

$$x = \left(\frac{4}{\pi} \Delta t \right)^{1/2} \qquad (d)$$

Langmuir found the effective distance from which particles diffuse to the collector to be

$$x = 1.120 \; x_o \qquad (e)$$

and the effective time of this diffusion is

$$t = \left(0.556 \; r_c^{\,2}/C_L \; U_o \; x_o \right) \qquad (f)$$

Using (e) and (f) in (d) and non-dimensionalizing

$$x_o' = \left(\frac{1.13}{C_L}\right)^{1/3} \; Pe^{\,-1/3} \qquad (g)$$

Substituting in (c)

$$E_D = 2.17 \; C_L^{\,1/3} \; Pe^{\,-2/3} \qquad (h)$$

Obtain C_L and use r_f in place of r_c as with Direct Interception (Table 2)

Table 4. Collection by Inertial Impaction

$$E_I = \frac{\text{particles removed by collector}}{\text{particles removed if flow was straight}}$$

$$= \frac{n_o U_o (2 y_{crit} 1)}{n_o U_o (2 r_c 1)}$$

$$= \frac{y_{crit}}{r_c} \qquad \text{(a)}$$

Replace r_c with r_f, as with Direct Interception.

y_{crit}/r_c obtained from Davies' relationship which includes both inertial and direct interception effects

$$\frac{y_{crit}}{r_c} = [R + (\frac{1}{4} + 0.4R) N_I - 0.0263 R N_I^2]$$

$$[0.16 + 10.9 (1 - \epsilon) - 17 (1 - \epsilon)^2] \qquad \text{(b)}$$

Want only effect of inertial impaction, hence $R = 0$

$$E_I = \frac{1}{4} N_I [0.16 + 10.9 (1 - \epsilon) - 17 (1 - \epsilon)^2] \qquad \text{(c)}$$

for the purpose of testing his model. The velocity is related to the single particle collection efficiency as follows:

$$E_{DI} \propto V^{0}$$

$$E_{D} \propto V^{-2/3}$$

$$E_{I} \propto V^{1}$$

The complete filtration equation can be written using the above proportionality relationships in equation (3). Thus

$$\xi = \exp - (A'V + D'V^{-2/3} + I')b \qquad (4)$$

where A', D', and I' are the inertial, diffusion and interception coefficients respectively. If $\bar{\xi}$, the percent penetration is introduced where

$$\bar{\xi} = 100\xi \qquad (5)$$

equation (4) becomes

$$2 - \log_{10}\bar{\xi} = (AV + DV^{-2/3} + I)b \qquad (6)$$

At V_{max}, the velocity of maximum penetration, $\frac{d\bar{\xi}}{dV} = 0$. This condition permits one to reduce the above relation to

$$2 - \log_{10}\bar{\xi} = [\, A(V + \frac{3}{2} V_{max}^{5/3} V^{-2/3}) + I \,]b \qquad (7)$$

A plot of $2 - \log_{10}\bar{\xi}$ vs $V + \frac{3}{2} V_{max}^{5/3} V^{-2/3}$ for velocity-penetration data should yield a straight line if the model is correct, with the slope giving A and the intercept I.

Application of Dorman's Model

Dorman applied his model to Ramskill's and Anderson's data of filtration through fabric filters. A typical set of data from the latter's work on the effect of aerosol velocity on penetration is illustrated in Figure 6. Typical values give $N_I = 1$ and $r_p/r_c = 0.1$. For these values inertial impaction should depend on the velocity to the first power (Table 4). The filtration model is then just equation (7) written above. Figure 7 illustrates a test of this model for the data of Ramskill and Anderson presented in Figure 6. If the original functions were chosen correctly, a plot of $2 - \log_{10}\bar{\xi}$ vs $V + \frac{3}{2} V_{max}^{5/3} V^{-2/3}$ should generate a straight line. Since this is not found to be the case, Dorman concluded that the proposed mechanism does not appear to be correct.

Dorman then assumed that the inertial

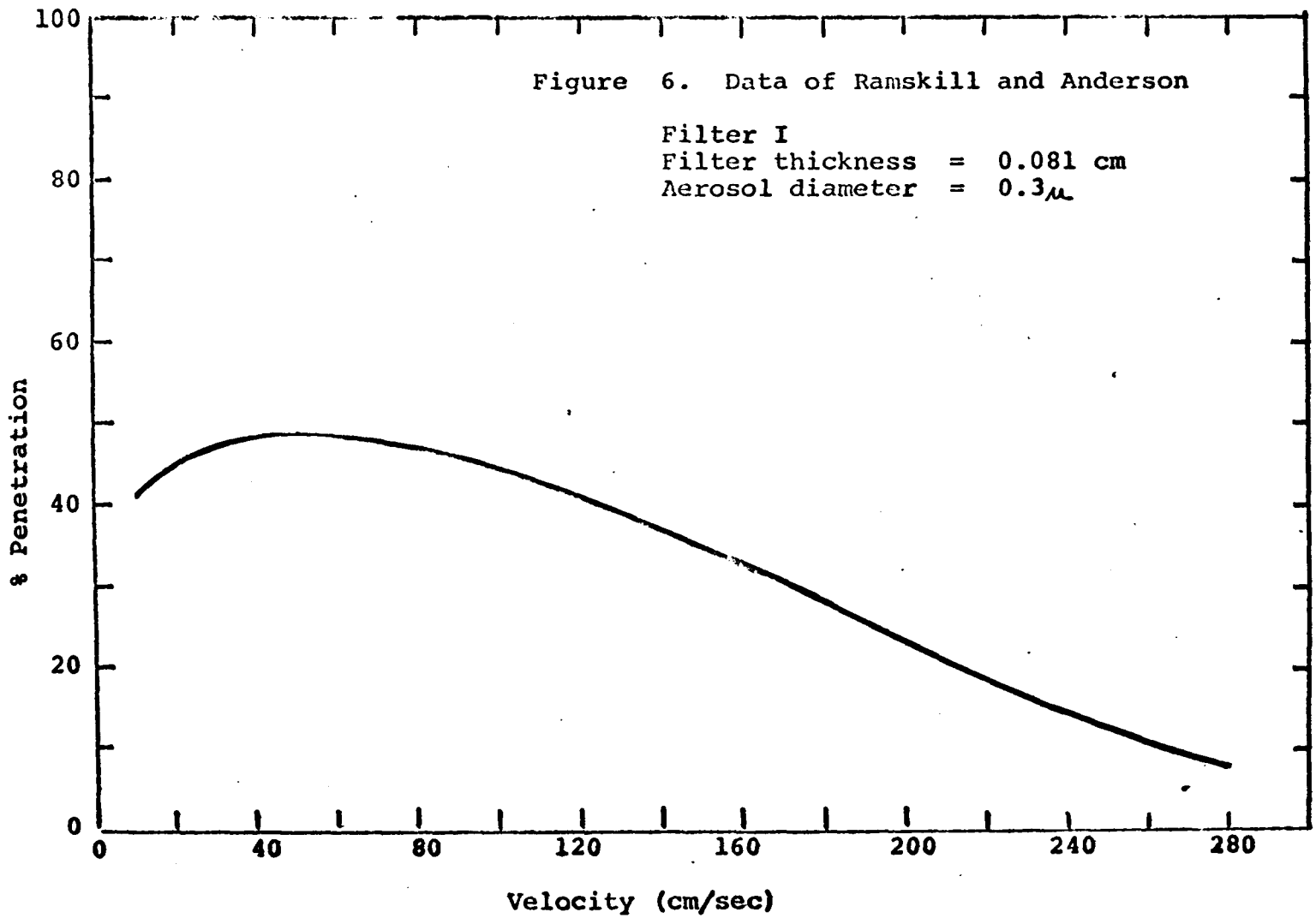

Figure 6. Data of Ramskill and Anderson

Filter I
Filter thickness = 0.081 cm
Aerosol diameter = 0.3μ

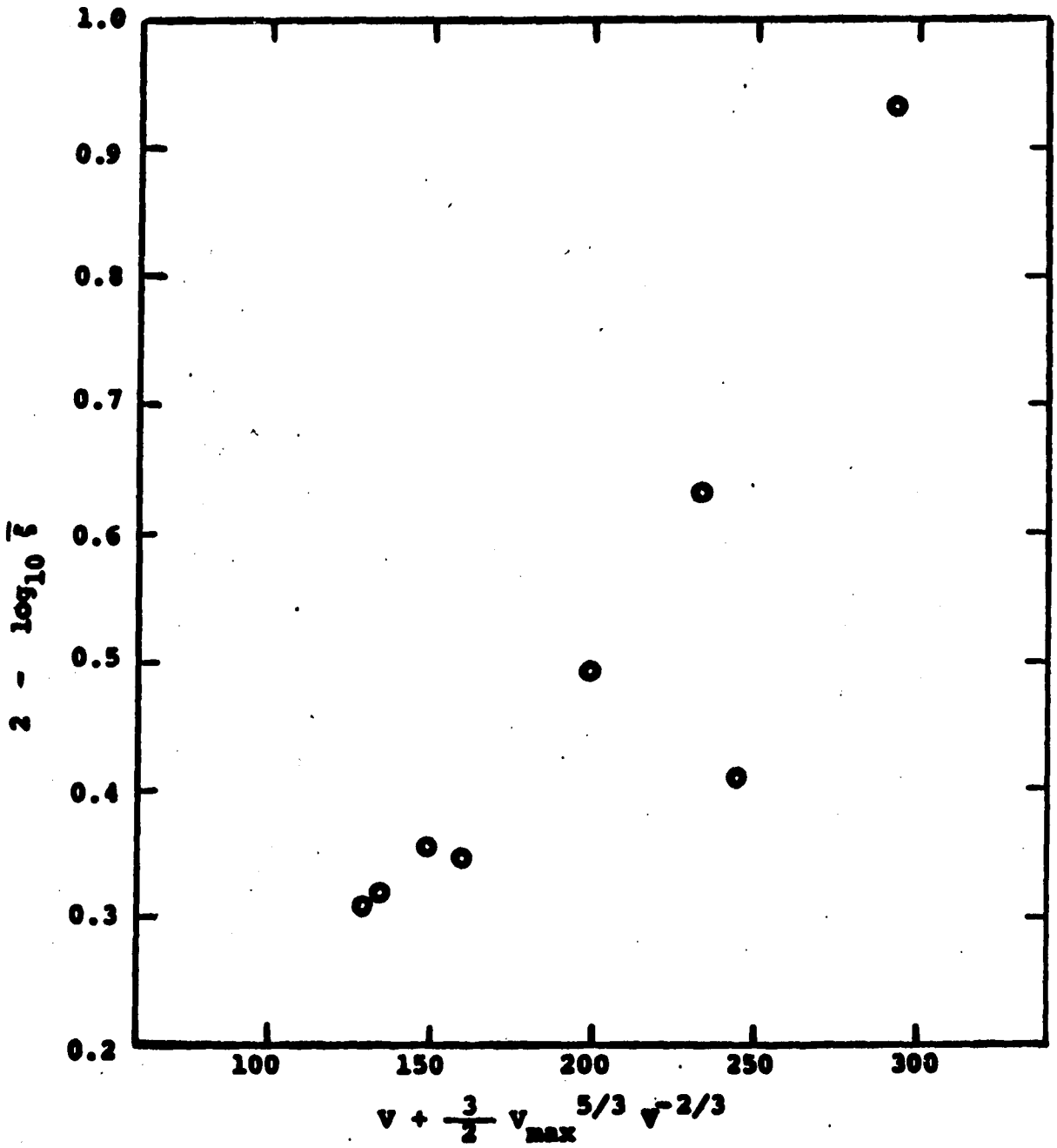

Figure 7. Test of Dorman's model on data of Ramskill and Anderson (Figure 6).

dependence on velocity is to the second power. This model would give:

$$\bar{\xi} = \exp - (I' + D'V^{-2/3} + A_2'V^2)b \qquad (8)$$

and

$$2 - \log_{10}\bar{\xi} = (A_2V^2 + DV^{-2/3} + I)b \qquad (9)$$

A plot of $2 - \log_{10}\bar{\xi}$ vs $V^2 + 3V_{max}^{8/3} V^{-2/3}$ resulted in a straight line (Figure 8), indicating that the proposed mechanism appears to be correct.

Further arbitrary manipulation by Dorman indicated that an inertial dependence on V^2 and a diffusional dependence on $V^{-1/2}$ gave the best possible fit (Figure 9). The percent difference between the numerical coefficients of the corresponding inertial, diffusional, and direct interception terms for the two successful models (Figures 8 and 9) is about 8% for the inertial term, about 17% for the diffusional term (for a velocity of 20 cm/sec), and about 6% for the direct inception term.

Apparently the models developed for diffusion

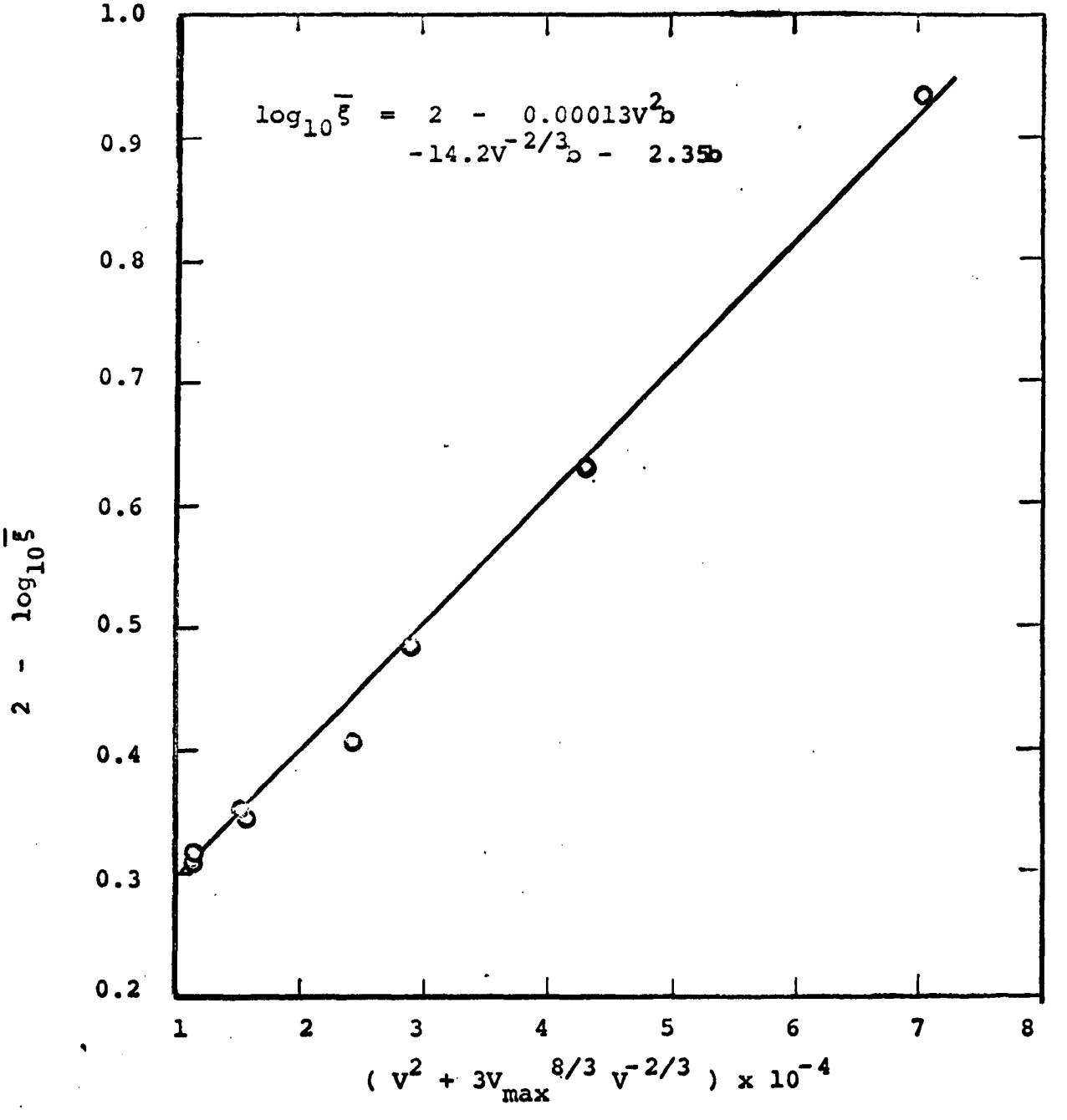

Figure 8. Successful test of Dorman's model to data of Ramskill and Anderson (Figure 6).

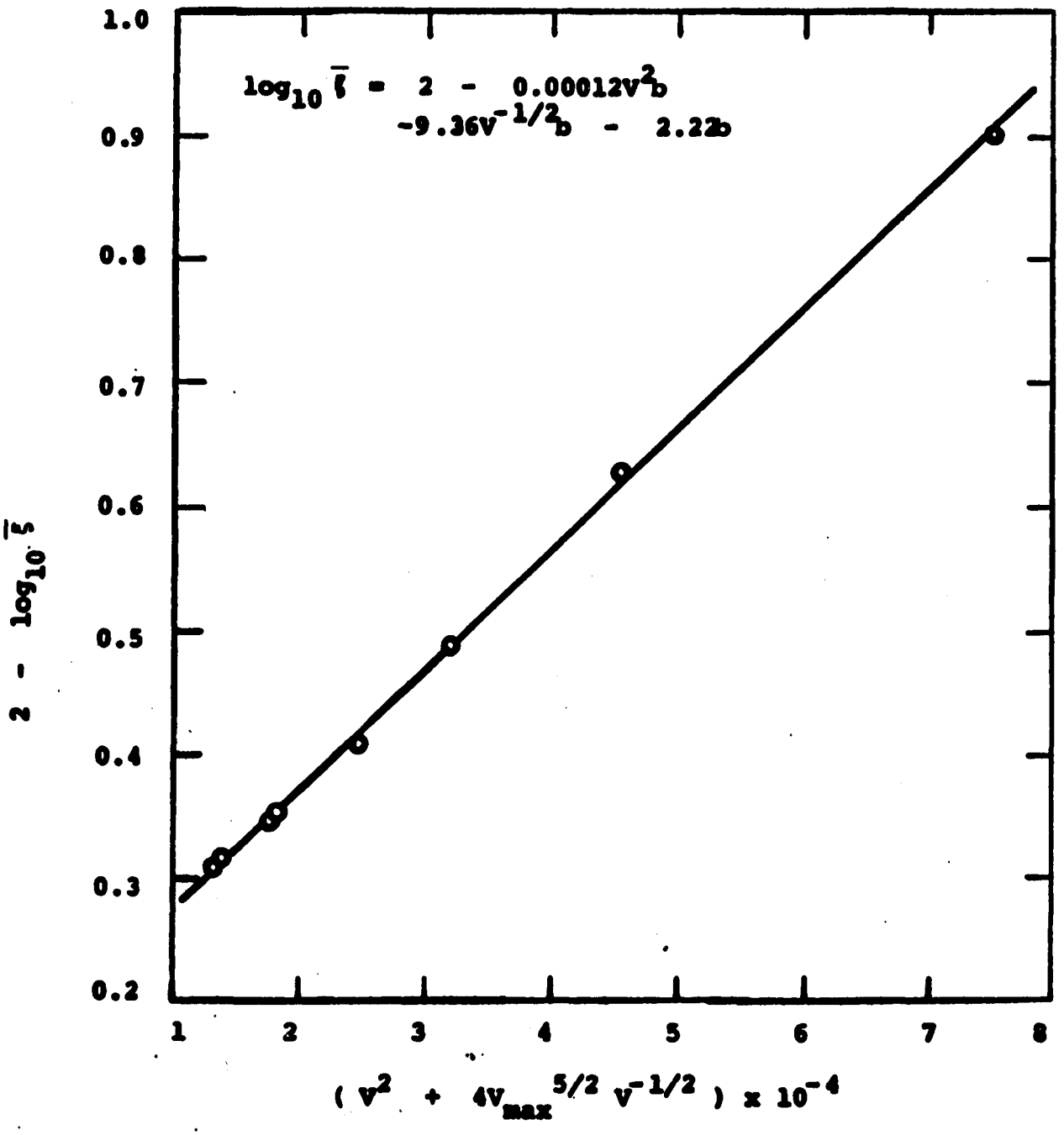

Figure 9. Successful test of Dorman's model on data of Ramskill and Anderson (Figure 6).

and direct interception are correct, whereas further analytical work must be done on the mechanism of inertial capture. It appears, however, that the best way to obtain a working model for aerosol filtration lies through a combination of theory and empiricism.

Studies of Aerosol Filtration in Granular Beds

Studies of granular bed filtration of aerosols are few. Thomas and Yoder (62,63) studied the penetration of beds of sand and lead shot by monodispersed liquid aerosols produced in a Sinclair-La Mer generator and monodispersed solid aerosols obtained from the atomization of a dilute suspension of polystyrene latexes. This work established the existence of a size of maximum penetration (at constant face velocity), of about 0.30 microns radius, which increased with decreasing face velocity. As the velocity increased, the penetration increased, presenting a family of curves as shown in Figure 10.

Flow was either upshot or downshot - the importance of gravity settling was illustrated by the penetration varying with direction. Upshot gave consistently higher penetration. Face velocities were in the range 0.1 to 1.5 cm/sec. Sand size was between 8 - 50 mesh.

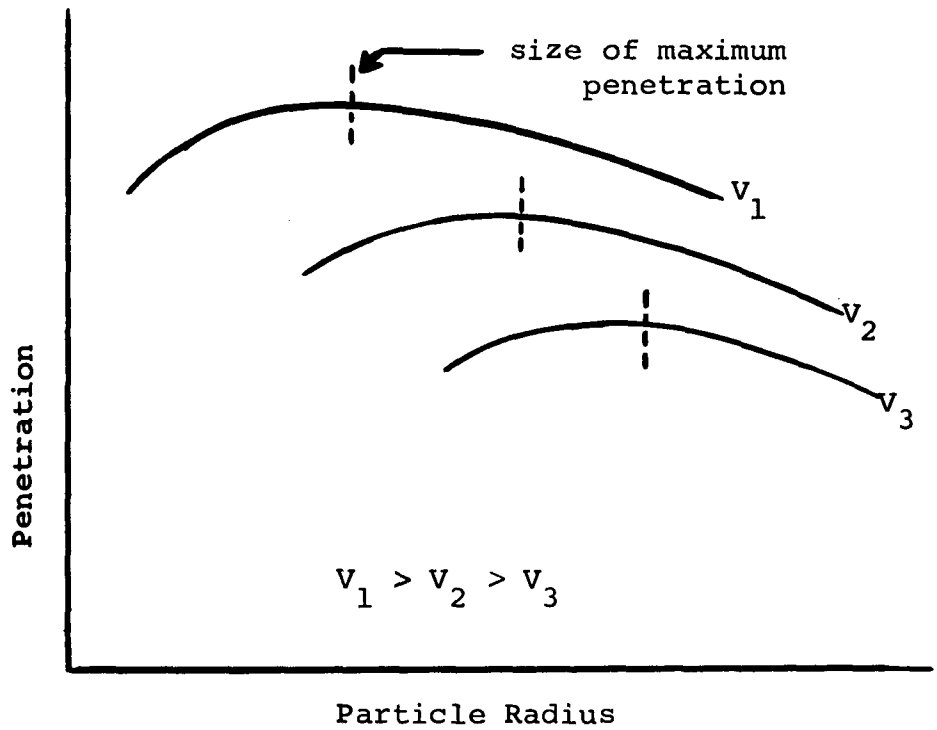

Figure 10. Effect of Velocity on Particle Radius vs Penetration.

Aerosol radius varied from about 0.10 to 1.0 microns. The column height varied from 3 - 8 cm with the sand beds, and over 87 cm with the lead shot beds. Under these conditions, diffusion and gravity settling were the predominant mechanisms of capture, with inertial and direct interception mechanisms having a negligible part. The penetration, which varied with velocity, particle size and sand size, ran from less than one percent to over 75 percent. This was the only work on dilute aerosol penetration of sand beds that the literature disclosed.

5. DEVELOPMENT OF FILTRATION EQUATIONS

One begins by describing the motion of the particles in a fluid. A convenient starting point would be the equation of motion of a particle in a fluid which is moving with velocity $\bar{U}_M$.

$$m_p \frac{d\bar{V}_I}{dt} = \Sigma \bar{F}_I \qquad (10)$$

where

m_p = mass of the aerosol particle

$\bar{V}_I$ = instantaneous particle velocity vector

$\Sigma \bar{F}_I$ = sum of the forces acting on the particle

The instantaneous velocity of the particle can be considered to be composed of two components:

$\bar{V}_B$ = a fluctuating velocity, characterisitic of the Brownian motion of the particle

$\bar{V}_P$ = a non-fluctuating portion, characteristic of the average particle velocity

The forces acting on the particle are as follows:

(i) The resistive forces of the fluid to the Brownian motion of the particle. This is given by Stokes

law of resistance:

$$\bar{R}_B = \frac{6 \pi \mu r_p}{C} (\bar{V}_B - \bar{U}_M)$$

(ii) The resistive force of the fluid to the regular motion of the particle. This is also given by Stokes law of resistance:

$$\bar{R}_P = \frac{6 \pi \mu r_p}{C} (\bar{V}_P - \bar{U}_M)$$

(iii) External forces, such as the force of gravity:

$$m_p \bar{g}$$

(iv) Fluctuating forces which are characteristic of the Brownian motion of the particle:

$$m_p \bar{A}(t)$$

The quantity

$$\frac{C}{6 \pi \mu r_p}$$

is usually called the mobility of the particle. It will be given the symbol B . Using this equation (10) becomes:

$$m_p \frac{d\bar{V}_B}{dt} + m_p \frac{d\bar{V}_P}{dt} = \tag{11}$$

$$- \frac{1}{B} (\bar{V}_B - \bar{U}_M) - \frac{1}{B} (\bar{V}_P - \bar{U}_M) + m_p \bar{g} + m_p \bar{A}(t)$$

The following dimensionless quantities are introduced:

$$\bar{V}_P' = \frac{\bar{V}_P}{U_o} \qquad \bar{g}' = \frac{\bar{g}}{g_o}$$

$$\bar{V}_B' = \frac{\bar{V}_B}{U_o} \qquad t' = \frac{t}{r_c/U_o}$$

$$\bar{U}_M' = \frac{\bar{U}_M}{U_o}$$

where U_o is the free stream velocity.

Substituting into equation (11) and rearranging:

$$\frac{B\, m_p\, U_o}{r_c} \frac{d\bar{V}_B'}{dt'} + \frac{B\, m_p\, U_o}{r_c} \frac{d\bar{V}_P'}{dt'} =$$

$$- (\bar{V}_B' - \bar{U}_M') - (\bar{V}_P' - \bar{U}_M') + \frac{B\, m_p\, g_o}{U_o} \bar{g}' + \frac{B\, m_p}{U_o} \bar{A}(t) \tag{12}$$

The coefficient of the dimensionless acceleration term is the inertial parameter, N_I :

$$N_I = \frac{B\, m_p\, U_o}{r_c}$$

$$= \frac{2}{9}\, \frac{\rho_p\, r_p^{\,2}\, U_o\, C}{\mu\, r_c}$$

and the coefficient of the dimensionless gravity term is the gravity parameter, N_G :

$$N_G = \frac{B\, m_p\, g_o}{U_o}$$

$$= \frac{2}{9}\, \frac{\rho_p\, r_p^{\,2}\, g_o\, C}{\mu\, U_o}$$

$$= N_I\, \frac{r_c}{U_o^{\,2}}\, g_o$$

Thus equation (12) becomes

$$N_I \frac{d\bar{V}_B'}{dt'} + N_I \frac{d\bar{V}_P'}{dt'} = \tag{13}$$

$$(\bar{V}_B' - \bar{U}_M') - (\bar{V}_P' - \bar{U}_M') + N_G\, \bar{g}' + \frac{B\, m_p}{U_o}\, \bar{A}(t)$$

which can be rearranged to

$$\frac{d\bar{V}_B'}{dt'} = -\frac{\bar{V}_B'}{N_I} + \frac{B\, m_p\, A(t)}{U_o\, N_I} + \frac{\bar{U}_M'}{N_I} - \frac{d\bar{V}_P'}{dt'} - \frac{\bar{V}_P' - \bar{U}_M'}{N_I} + \frac{N_G'}{N_I}\bar{g}' \tag{14}$$

The transformation developed by Chandrasekhar (8) is used in a method somewhat similar to that of Friedlander (22) to go from the above equation to the diffusion equation (Appendix A).

$$\frac{\partial n'}{\partial t'} = \frac{2}{Pe}\nabla'^2 n' - \nabla' \cdot (n'\,\bar{U}_M') - \nabla' \cdot n' \left\{ -N_I \frac{d\bar{V}_p'}{dt'} - (\bar{V}_P' - \bar{U}_M') + N_G\,\bar{g}' \right\} \tag{15}$$

where:

$$\nabla' = r_c\,\nabla \qquad n' = \frac{n}{n_o}$$

$$\nabla'^2 = r_c^2 \nabla^2$$

The first two dimensionless quantities are dimensionless operators, the last dimensionless quantity is a dimensionless concentration. A parameter characteristic of the filtration process, the Peclet number ($2\,U_o\,r_c/\Delta$),

also appears in equation (15).

The above transformation applies only if $t >> B m_p$, or in terms of our dimensionless quantities:

$$t' >> N_I$$

In the time scale of the filtration process, on is interested in the flow past the collector. Therefore the dimensionless time, t', is of order unity. Thus the condition for the above transformation becomes

$$N_I << 1$$

If the above condition does not apply, the transformation cannot be made and one must revert to the original force balance relationship. Therefore, neglecting the Brownian velocity and the Brownian resistive forces in equation (11) one has:

$$N_I \frac{d\bar{V}_P'}{dt'} = (\bar{V}_P' - \bar{U}_M') + N_G \bar{g}' \qquad (16)$$

Since the filtration of dilue aerosols is not time dependent, it is customary to use the steady state form of equation (15):

$$0 = \frac{2}{Pe} \nabla'^2 n' - \nabla' \cdot (n' \bar{U}_M') - \nabla' \cdot n' \left\{ - N_I \frac{d\bar{V}_p'}{dt'} - (\bar{V}_p' - \bar{U}_M') + N_G \bar{g}' \right\} \quad (17)$$

Equations (16) and (17) are used to describe the behavior of the particles in the fluid. In the former equation one is looking at changes in the particles trajectory, while in the latter case one is looking at changes in the particle concentration.

However, in order to solve either relationship it is necessary to have the flow pattern of the fluid, $\bar{U}_M'$, around the collector. Various relationships are available. The potential flow or the viscous flow relationships from Lamb (36) are generally used in treating isolated collectors. Other models have been developed, notably the one of Davies (12), but they are more complicated.

In treating a system of collectors, such as a fibrous filter, the current approach is to utilize an expression such as the Kuwabara or Happel velocity fields (44). These relationships have the advantage of describing the flow pattern in the entire system, where the influence of neighboring collectors is included in the velocity field.

In order to obtain solutions of the above equations, suitable boundary and initial conditions must be specified.

The conditions on the diffusion equation are:

(i) Far from the collector the particle concentration is the free stream concentration, $r = \infty$, $n = n_o$

(ii) At the boundary of the collector the particle concentration is zero, $r = r_c$, $n = 0$

(iii) Far from the collector and at time equals zero the particle velocity is the free stream velocity, $t = 0$, $r = \infty$, $\bar{V}_p = \bar{U}_o$

In dimensionless form the above becomes

(i) $r' = \infty$, $n' = 1$

(ii) $r' = 1$, $n' = 0$

(iii) $t' = 0$, $r' = \infty$, $\bar{V}_p' = \bar{U}_o'$

The direct interception effect is included by stipulating the aerosol will be captured when it passes within a distance r_p of the collector surface. Therefore condition (ii) becomes

$$r = r_c + r_p , \quad n = 0$$

or in dimensionless form

$$r' = 1 + R , \quad n' = 0$$

which introduces the direct interception parameter, R.

The solution of equation (17) will enable one to obtain the flux of particles to the surface of the collector.

The solution of the trajectory equation can be more easily obtained by converting it into two first order differential equations:

$$N_I \frac{d\bar{V}_P'}{dt'} = -(\bar{V}_P' - \bar{U}_M') + N_G \bar{g}' \qquad (18a)$$

$$\frac{d\bar{r}'}{dt'} = \bar{V}_P' \qquad (18b)$$

with the conditions

(i) At time equals zero, the velocity of the particle is equal to the free stream velocity, $t = 0$, $\bar{V}_P = \bar{U}_o$

(ii) At time equals zero, an arbitrary position is picked, $t = 0$, $\bar{r} = \bar{r}_o$

or in dimensionless form

(i) $t' = 0$, $\bar{V}_P' = \bar{U}_o'$

(ii) $t' = 0$, $\bar{r}' = \bar{r}_o'$

where $\bar{r}_o$ is the initial position vector of the particle.

Various trajectories are possible, depending on the initial position of the particle. One is interested

in the trajectories of particles that are captured, i.e., that pass the position

$$r = r_c$$

or in dimensionless form:

$$r' = 1$$

The direct interception effect is incorporated into the problem by stipulating that the particle would be collected if it passes within a distance r_p of the collector surface. Thus the condition for capture becomes

$$r = r_c + r_p$$

or in dimensionless form:

$$r' = 1 + R$$

Looking at Figure 1, it can be easily seen that there is a distance above and below the horizontal x axis, y_{crit}, where a particle having a velocity equal to the velocity of the fluid would eventually experience a grazing collision with the collector. The trajectory of this particle is called the critical trajectory. Particles inside this trajectory will be captured, particles outside it will bypass the collector.

The solution of equations (18a) and (18b), as related to the filtration process is to find this

critical trajectory and its accompanying y position, y_{crit}.

The diffusion equation, as presented in equation (17) is too unwieldy to solve. Various simplifications are possible.

(i) The effect of gravity is ignored, and it is assumed that the particle velocity equals the fluid velocity. Thus

$$0 = \frac{2}{Pe} \nabla'^2 n' - \nabla' \cdot (n' \bar{U}_M') + N_I \nabla \cdot \left\{ n' \frac{d\bar{U}_M'}{dt'} \right\} \qquad (19)$$

which is identical to Friedlander's relationship (22).

(ii) The effect of gravity and the inertial term is neglected, thus

$$0 = \frac{2}{Pe} \nabla'^2 n' - \nabla' \cdot (n' \bar{U}_M') + \nabla' \cdot n' (\bar{V}_P' - \bar{U}_M') \qquad (20)$$

which is identical to a relationship obtained by Chen (9) from pure diffusional considerations.

(iii) The effect of gravity and inertia is neglected, and the particle velocity is set equal to the fluid velocity. Thus

$$0 = \frac{2}{Pe} \nabla'^2 n' - \nabla' \cdot (n' \bar{U}_M') \qquad (21)$$

If the fluid is assumed incompressible this equation reduces to:

$$0 = \frac{2}{Pe} \nabla'^2 n' - \bar{U}_M' \cdot \nabla' n' \qquad (22)$$

This simplified relationship is the one generally used to calculate the concentration profile and the particle flux to the collector surface (23,45).

The version of the trajectory equation that is utilized neglects the effect of gravity. Thus

$$N_I \frac{d\bar{V}_P'}{dt} = - (\bar{V}_P' - \bar{U}_M') \qquad (23a)$$

$$\frac{d\bar{r}'}{dt'} = \bar{V}_P' \qquad (23b)$$

In order to obtain the filtration efficiency of a filter composed of many collectors, one starts with the collection efficiency of a single isolated collector.

E^* = single isolated collector particle collection efficiency

$$= \frac{\text{area which remove particles}}{\text{projected area of collector in direction of flow}}$$

$$= \frac{\text{particles removed by collector}}{\text{particles removed if flow was straight}}$$

Consider an arbitrary filter composed of many ideal collectors. Letting

A = area of filter in direction of flow (area)

a_c = projected area of single collector particle (area/particle)

b = thickness of filter (length)

dx = differential thickness of filter (length)

n = concentration of aerosol (particles/volume)

Q = flow rate upstream of filter (volume fluid/time)

s_c = projected area of collector per unit total volume of filter (area/total volume)

V_f = filter velocity (length/time)

V_o = superficial velocity (length/time)

v_c = volume of single collector particle (volume/particle)

ϵ = voidage of filter (free volume of filter/ total volume of filter)

A mass balance on a volume element of the filter is:

$$\left[\begin{array}{c}\text{Particles entering}\\ \text{per unit time}\end{array}\right] - \left[\begin{array}{c}\text{Particles leaving}\\ \text{per unit time}\end{array}\right] = \left[\begin{array}{c}\text{Particles removed}\\ \text{per unit time}\end{array}\right]$$

Now

$$\begin{array}{ll}\text{Particles entering per unit time} & = n V_o A \\ \text{Particles leaving per unit time} & = n V_o A + d(n V_o A) \\ \text{Particles removed per unit time} & = \left[\begin{array}{c}\text{particles/time}\\ \text{unit area in filter}\end{array}\right]\left[\begin{array}{c}\text{area remove}\\ \text{particles in}\\ \text{filter}\end{array}\right] \\ & = (n V_f)(E^* s_c A\, dx)\end{array}$$

Therefore

$$- V_o\, dn = n V_f E^* s_c\, dx$$

but

$$V_o = V_f \epsilon$$

and

$$s_c = \frac{a_c}{v_c}(1 - \epsilon)$$

so

$$\frac{dn}{n} = - E^* \frac{(1 - \epsilon)}{\epsilon} \frac{a_c}{v_c} dx$$

or

$$\frac{n}{n_o} = \exp \left(- E^* \frac{(1 - \epsilon)}{\epsilon} \frac{a_c}{v_c} b \right) \qquad (24)$$

This is the relationship obtained by Chen (9), Davies (13), and others. An alternate form, omitting the voidage in the denominator, had been presented by Wong et al (65), Friedlander (22), Thomas and Lapple (60) and others.

Lapple states that this difference is due to a difference in definition of E^*. However, while the definition of E^* appears to be the same, a more detailed analysis of the term 'particles removed' discloses a possible cause of the variation.

Since

$$E^* = \frac{\text{area which remove particles}}{\text{projected area of collector in direction of flow}}$$

$$s_c = \frac{\text{projected area of collector}}{\text{unit total volume of filter}}$$

Adx = total volume of differential filter element

Then

$$E^* s_c A \, dx = \text{total area from which remove particles}$$

The question is: what is the available area where particles can be removed? Apparently two different areas were chosen.

(i) Chen et al apparently considered the available area for filtration to be the free area, ϵA. Therefore

$$\frac{n Q}{\epsilon A} = \frac{\text{particles/time}}{\text{available area}}$$

so

$$\frac{n Q}{\epsilon A} E^* s_c A \, dx = \text{total particles removed}$$

and from the material balance relationship

$$- Q \, dn = n Q E^* s_c \, dx/\epsilon$$

one obtains equation (24) which was previously derived.

$$\frac{n}{n_o} = \exp \left(- E^* \frac{1 - \epsilon}{\epsilon} \frac{a_c}{v_c} b \right) \qquad (24)$$

(ii) Lapple et al apparently considered the available area for filtration to be the total projected area, A.

Therefore

$$\frac{n\,Q}{A} = \frac{\text{particles/time}}{\text{available area}}$$

so

$$\frac{n\,Q}{A} E^* s_c A\,dx = \text{total particles removed}$$

and from the material balance relationship

$$-Q\,dn = n\,Q\,E^*\,s_c\,dx$$

one obtains the other relationship

$$\frac{n}{n_o} = \exp\left(-E^* (1 - \epsilon) \frac{a_c}{v_c} b \right) \qquad (25)$$

The relationship of Chen, equation (24), will be used exclusively in this work. For the case of fibrous filters, consisting of cylindrical collectors oriented perpendicular to the flow field, one has

$$\frac{a_c}{v_c} = \frac{2}{\pi r_c}$$

and

$$\frac{n}{n_o} = \exp\left(-\frac{2}{\pi} E^* \frac{1 - \epsilon}{\epsilon} \frac{b}{r_c} \right) \qquad (26)$$

For these filters, $\epsilon > 0.90$, hence the actual difference between equations (24) and (25) is generally less than ten percent.

If equation (25) is applied to a sand bed composed of spherical collectors one has:

$$\frac{a_c}{v_c} = \frac{3}{4\, r_c}$$

and

$$\frac{n}{n_o} = \exp\left(-\frac{3}{4} E^* \frac{1 - \epsilon}{\epsilon} \frac{b}{r_c} \right) \qquad (27)$$

If ξ^*, the fractional penetration of the aerosol based on E^* is introduced equation (27) becomes

$$\xi^* = \exp\left(-\frac{3}{4} E^* \frac{1 - \epsilon}{\epsilon} \frac{b}{r_c} \right) \qquad (28)$$

In an actual filter E^*, the isolated single particle collection efficiency, is replaced by E, the single particle collection efficiency of a collector taking into account the presence of neighboring collectors. ξ^* is also replaced by ξ.

Two methods can be used to relate E^* to E. From an historical viewpoint, the first method is that

of Langmuir (37). The velocity profiles of an isolated collector were used to obtain E^*, which was then modified by use of an interference function, Θ, to obtain E:

$$E = \Theta E$$

The interference function was obtained experimentally from pressure drop measurements on the filter.

The alternate approach is to utilize velocity profiles that include the effect of neighboring collectors. This eliminates the need for the interference function, and E and ξ can be obtained directly.

6. EXPERIMENTAL APPARATUS

The sand bed holder required for the dilute aerosol penetration studies was originally designed to be similar to those used by Thomas and Yoder (62,63) and illustrated in their papers. The test section consisted of a 2-inch I.D. plexiglas cylinder of length about 14 inches, with a 3.6 cm sand bed centrally located with respect to the ends, thus providing a sizeable entrance and exit section, a feature which was not present in the work of Thomas and Yoder. The aerosol entered and left through a 3/8 inch opening at the top and the bottom of the cylinder. A second, identical test section was provided as a "blank"; this section was left empty, and penetration measurements for the test section containing the sand was compared with penetration measurements for the blank section. However, experiments using a similar unit, 24 inches long rather than 14 inches, gave different penetration results indicating sizeable entrance and exit losses (Appendix C). These losses were removed by using entrance and exit sections having a small (six degree) taper, and it is this geometry that was finally used in all of the experiments (See Figure 11).

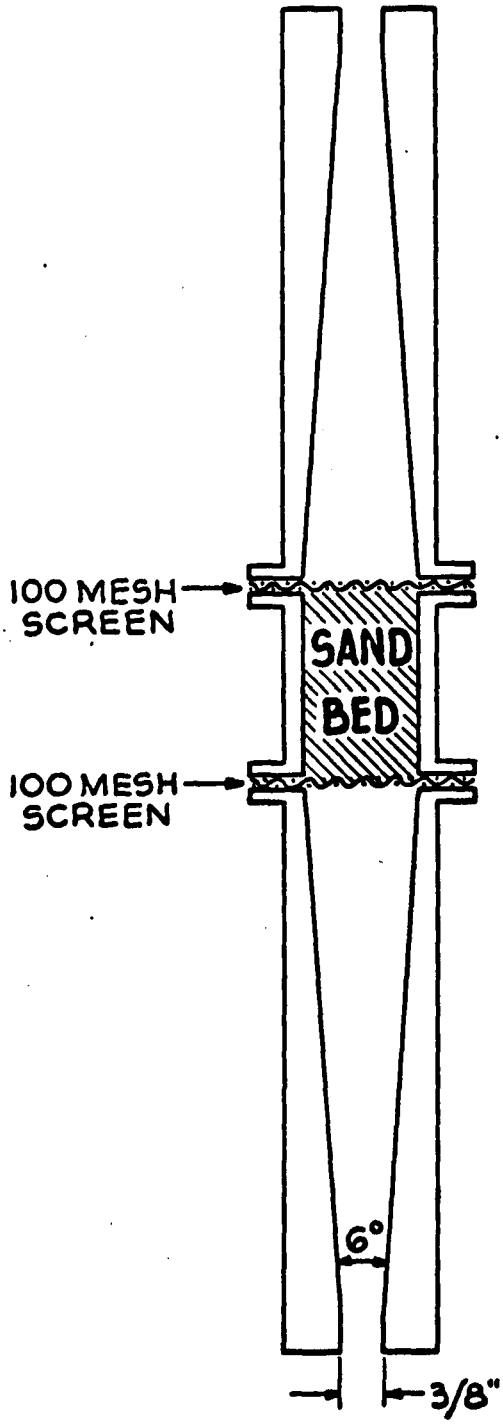

Figure 11. Sand bed test section.

A schematic diagram of the entire experimental apparatus is presented in Figure 12. Compressed air is first passed through an oil, water and dust filter, then over a bed of molecular sieves which reduces the dew point of the air to below -100°F. A 100 millimicron Millipore filter is placed downstream of the pressure regulator to remove any fine dust particles. The flow is monitored at high flow rates by a rotameter, and at low flow rates by measuring the pressure drop across a 3/32 inch diameter capillary tube.

The aerosol, which consists of 1.1 micron diameter polystyrene latex microspheres (Dow Chemical Company), is produced in an AEC-NRL type aerosol generator. This is essentially a metal tube protruding beneath the surface of a 0.5 to 1.0 weight percent suspension of the polystyrene latex microspheres in a 2000 ml wide neck Erlenmeyer flask half-filled with water. In this atomizer type generator high pressure air is forced through four 1/64 inch holes at the bottom of the metal tube, producing bubbles and a mist of aerosols. The aerosols are then mixed with the dry "bypass" air stream where any droplets of water that were produced will evaporate. For low flow rates

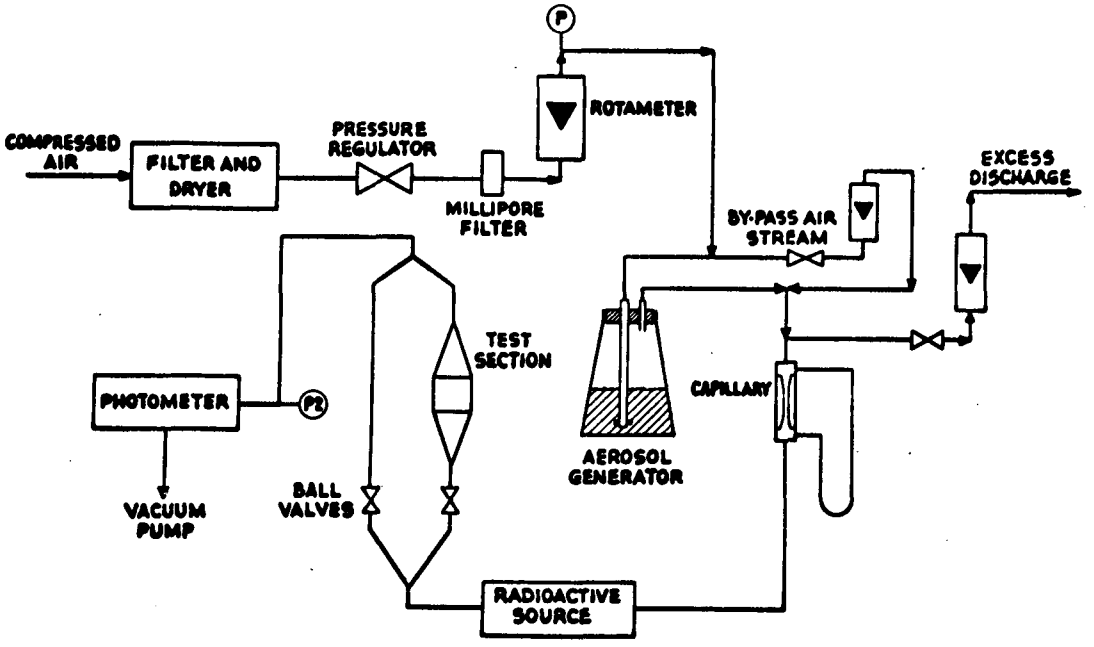

Figure 12. Schematic diagram of the experimental apparatus.

the excess aerosol stream is discharged.

It was found necessary to use a 50 microcurie foil of Am^{241} (Radiation Materials Corporation, model AF.1) to remove electrostatic charges from the aerosol. The presence of the Am^{241} resulted in larger penetrations and decreased fluctuations in the aerosol concentration. After passage over the radioactive source, the aerosol stream is first passed through 3/8 inch Tygon tubing and then the sand bed test section. The aerosol stream then enters the photometer. Appropriate adjustments are made on the system to keep the pressure at the photometer atmospheric.

The aerosol concentration, which was of the order 25 particles/cc , was monitored by a model JM-3000-AL Sinclair-Phoenix photometer. The response was recorded by a Honeywell millivolt recorder fitted with a Disc integrator, so as to eliminate human bias in averaging fluctuations in the aerosol concentration. At approximately 3-10 min intervals (using larger intervals at lower velocities) the aerosol is switched from the test section to a bypass of Tygon tubing. The ratio of the outputs through the test section and through the bypass, as recorded by the photometer, gives after suitable

corrections for losses in a blank test section, the penetration through the sand bed. A more complete description of this procedure is presented in Appendix C.

Two aerosol generators, connected in parallel, were used. One contained the latex suspension mentioned above. The other contained distilled water. The "water" generator was used to produce a "water" aerosol and establish a "zero point"; that is, correct for the presence of any background dust or water droplets in the aerosol stream (Appendix B).

The question of whether the aerosol generated was truly monodispersed and did not contain doublets or even triplets was examined several times using different approaches. Initially a sample of the aerosol stream was collected by placing a 0.45 micron Millipore filter in the Sinclair-Phoenix (Location CFC in Figure B.1, Appendix B). The filter paper was rendered transparent with Cargille immersion oil, Type B, before it was examined under a 970 power optical microscope with an oil immersion objective. The collected aerosol was estimated to be about 90% singlets, with the rest doublets and an occasional triplet. The doublets or triplets could have arisen from particles impinging on one another as they are collected.

This analysis was checked with a Bausch & Lomb Model 40-1 Dust Counter that supposedly could discriminate between particles of diameter 0.5 microns and greater, 1.0 microns and greater, and 2.0 microns and greater. Typical results at a sampling rate of 170 ml/min are listed below:

Diameter	Particles/0.01 ft^3
0.5 microns and greater	2157
1.0 microns and greater	1397
2.0 microns and greater	48

The large difference between the 0.5 micron and the 1.0 micron diameter ranges is easily explained. Rimberg and Thomas (50) evaluated this instrument and found that the response is multivalued for latex particles between 0.65 and 1.2 microns diameter. Therefore a monodispersed aerosol of 1.1 microns diameter would appear heterodispersed.

A similar evaluation was performed on a Royco Particle Counter, Model 220-4 (Appendix D), using a solution about 2 months old. Typical results at a sampling rate of 3 liters/min are listed below:

Diameter	Particles/min
0.5 microns and greater	66,000
1.0 microns and greater	60,000
2.0 microns and greater	8,000

Rimberg and Thomas (51) also evaluated the Royco and found that a monodispersed aerosol can appear as a heterodispersed aerosol, with responses greater than as well as less than the actual size. At worse, about 13 percent of the aerosols are doublets or triplets.

The aerosol suspensions used in the dilute aerosol work were generally replaced after three weeks to a month, while the suspensions used in the fly ash study (Part Two) were kept up to two or three months.

7. EXPERIMENTAL RESULTS

The effect of velocity on penetration was studied in a 10-14 mesh sand bed, using a 1.1 micron polystyrene aerosol. The flow direction was both upshot and downshot, with superficial velocities between 0.3 and 10 cm/sec in a two inch diameter bed. The bed heights examined were 3.7 cm, 8.2 cm, and 19.2 cm. The results of these experiments are illustrated in Figures 13, 14 and 15 respectively. Some sideshot data with screens retaining the vertical sand faces were also obtained in the above velocity range using the 19.2 cm bed (Figure 15). Additional upshot and downshot experiments were performed using a one inch diameter bed, 19.2 cm long, with superficial velocities between 7 and 80 cm/sec, thus extending the velocity range eightfold.

The following results are discernable upon examination of the above data. At superficial velocities less than approximately 20 cm/sec, upshot gave higher penetrations than downshot, with the difference between the two increasing with decreasing velocity. These curves also bracket the sideshot data, but at velocities greater than 30 cm/sec the upshot and downshot curves

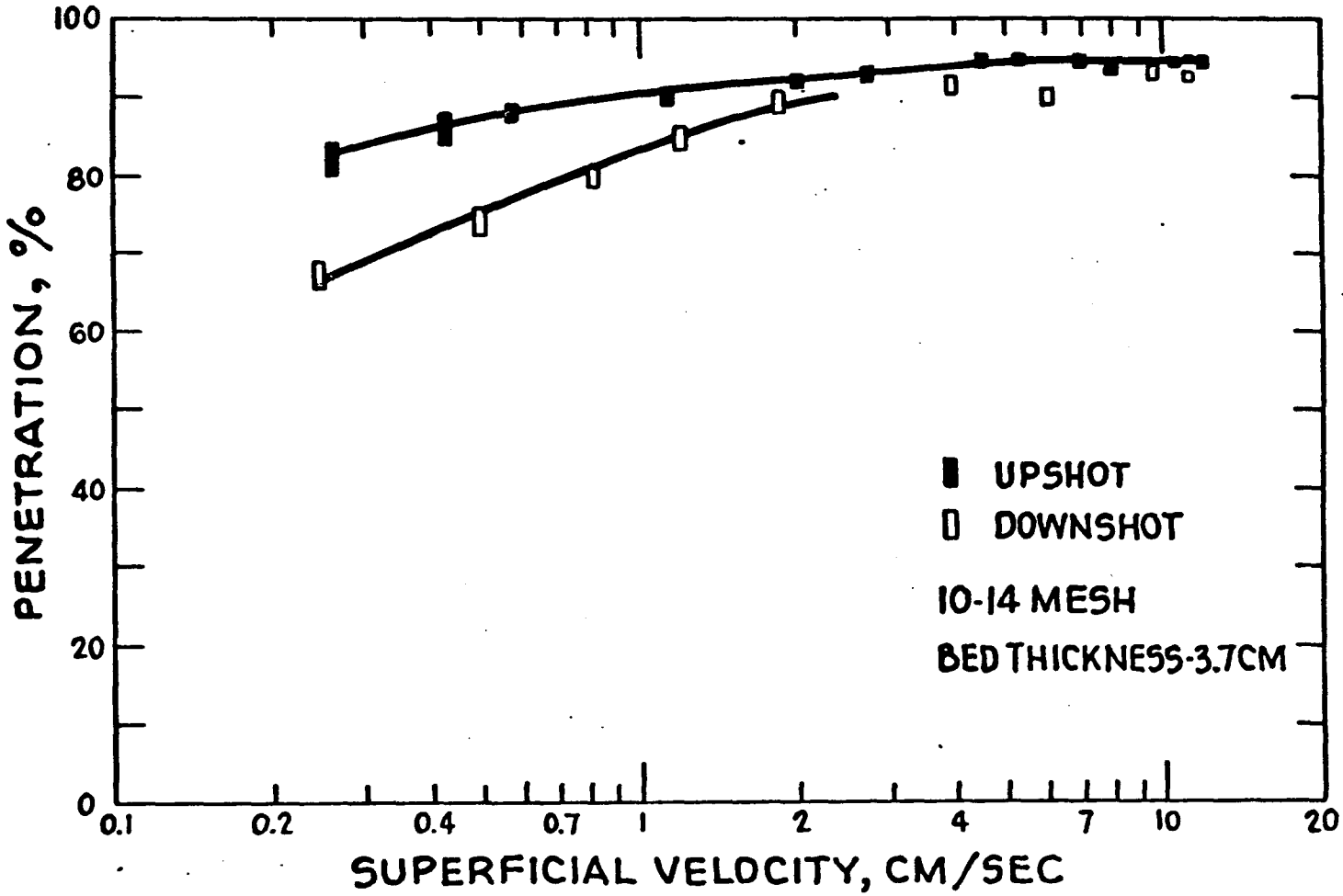

Figure 13. Penetration of a 1.1 micron diameter aerosol as a function of superficial velocity.

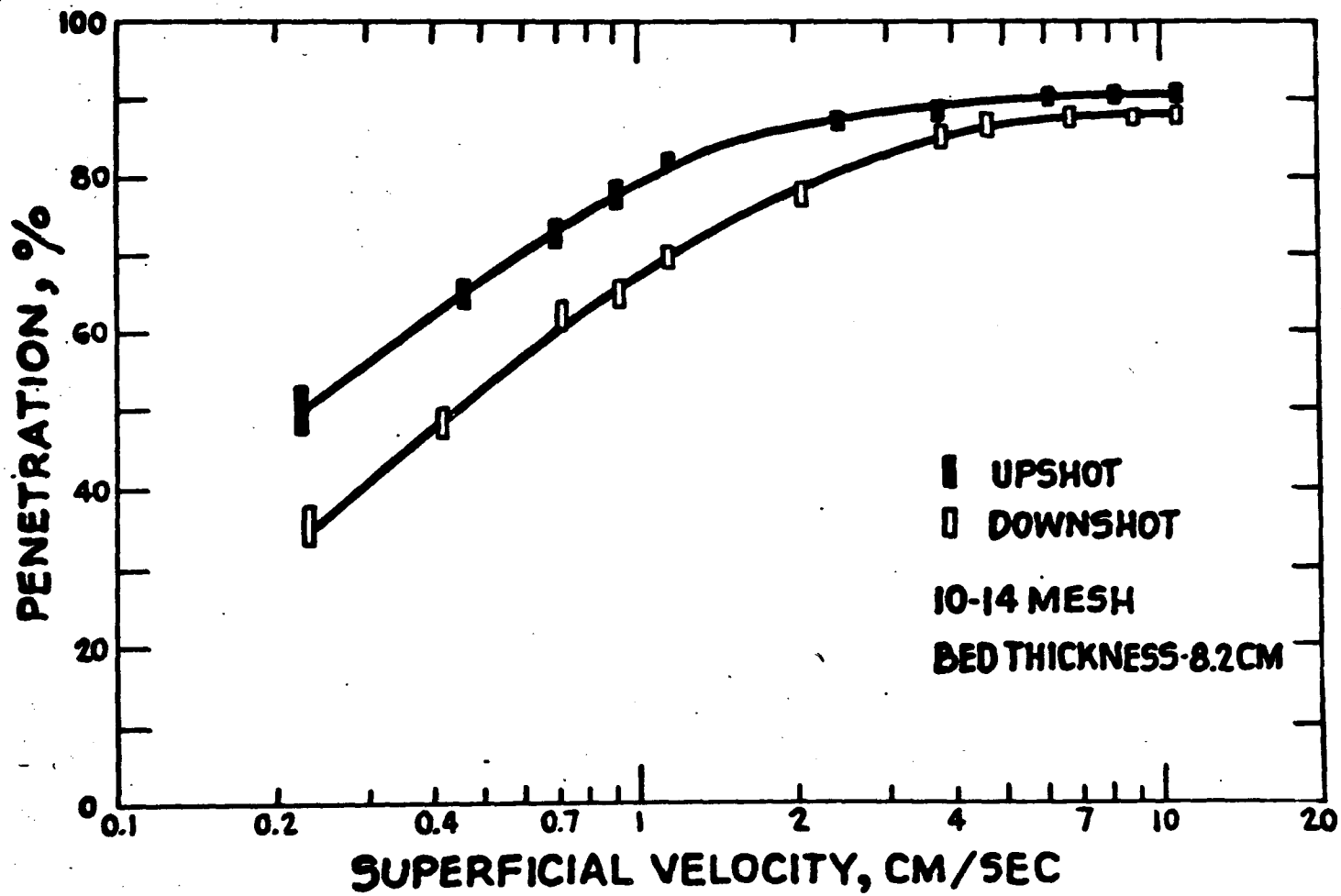

Figure 14. Penetration of a 1.1 micron diameter aerosol as a function of superficial velocity.

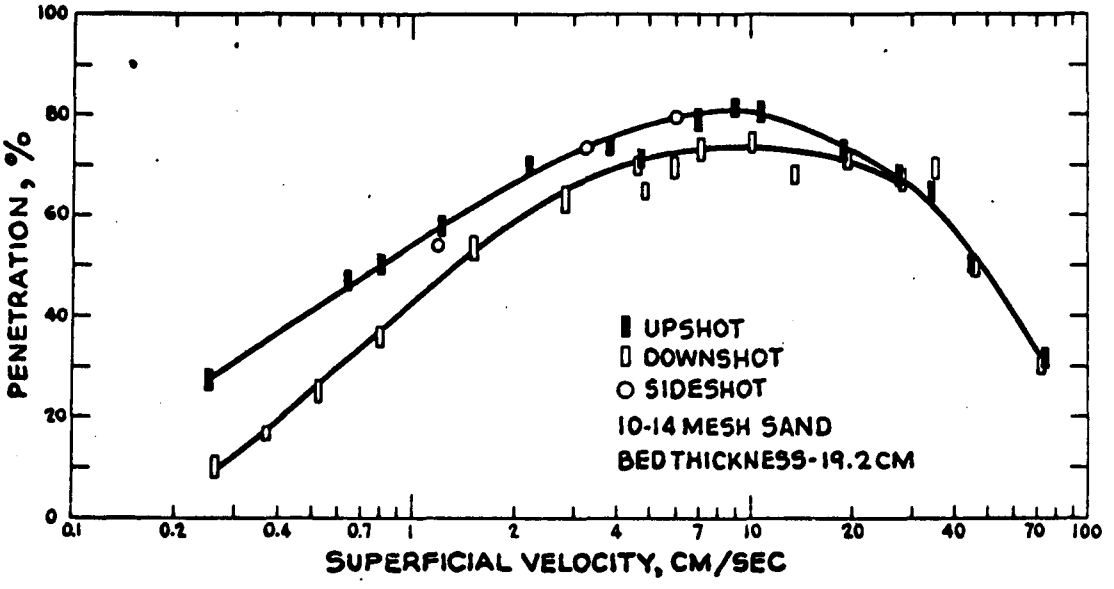

Figure 15. Penetration of a 1.1 micron diameter aerosol as a function of superficial velocity.

merge together. These results indicate that gravity settling contributes to the filtration process but becomes negligible at higher velocities. The existence of a velocity of maximum penetration is also clearly illustrated by the figures. This is not suprising since at low velocities the primary mechanism of aerosol capture is due to Brownian diffusion and gravity settling which decreases with increasing velocity, and at high velocities the primary mechanism of capture is due to inertial impaction which increases with increasing velocity.

Velocity-penetration data were also obtained with a finer sand, 20-30 mesh, again using the 1.1 micron diameter aerosol passed both upshot and downshot. The bed height was 8.2 cm and with the use of both one and two inch diameter beds it was possible to cover the velocity range of 0.3 to 80 cm/sec (see Figure 16). The figure shows the same trends as obtained with the larger 10-14 mesh sand. The penetration at any given velocity, however, was somewhat lower.

In order to compare the experimental data obtained with the experimental data of other investigators, e.g., Thomas and Yoder (62,63) or with theoretical predictions based on simplified mathematical models of

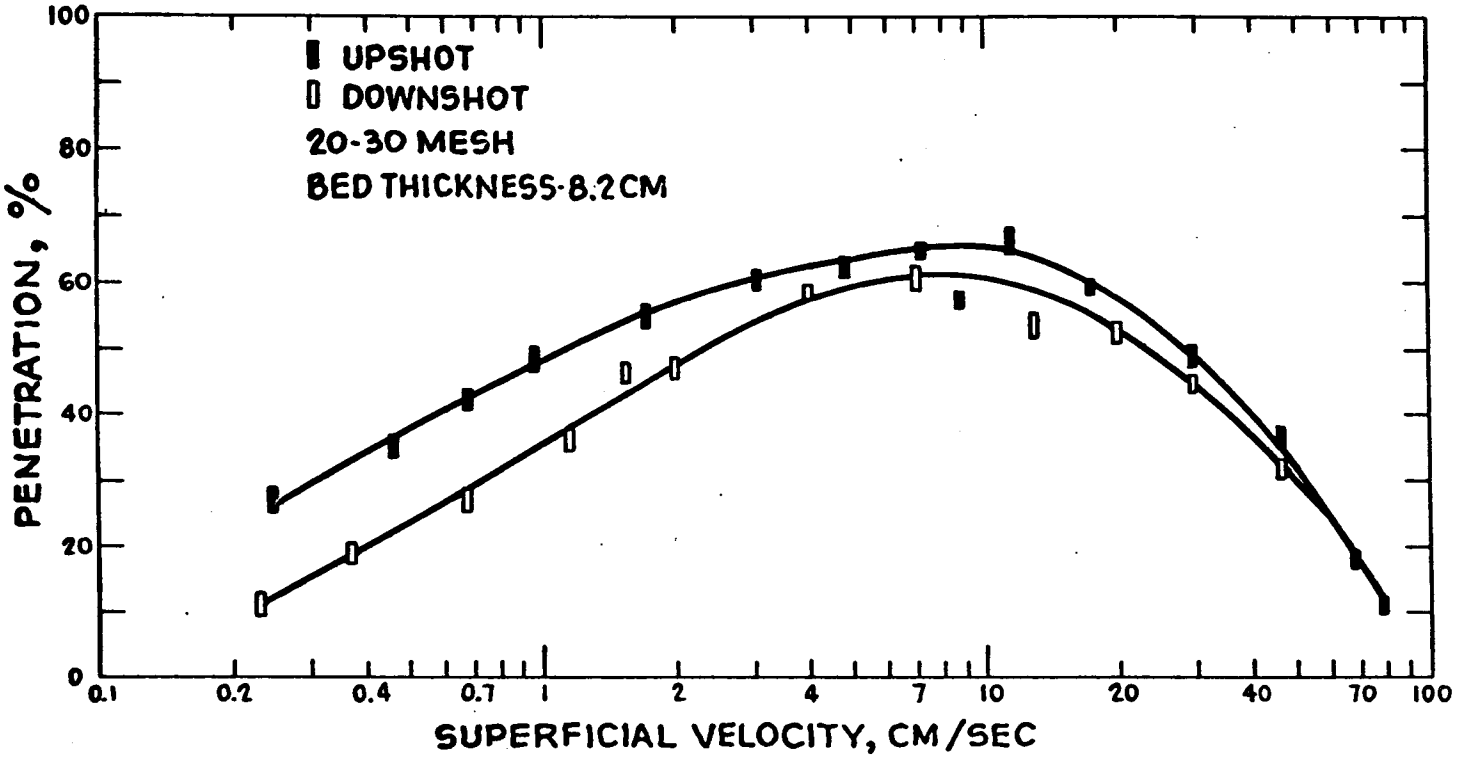

Figure 1 Penetration of a 1.1 micron diameter aerosol as a function of superficial velocity.

the filtration process, it is necessary to reduce the overall penetration data to single particle collection efficiencies through the relationship previously derived (equation (28)):

$$\xi = e^{-\eta b} \tag{29}$$

where

$$\eta = \frac{3}{4} \frac{1 - \epsilon}{\epsilon} \frac{E}{r_c} \tag{30}$$

Figure 17a is a plot of the single particle collection efficiency vs velocity for the three different bed heights of the 10-14 mesh sand. The smooth curves drawn in Figures 13, 14 and 15 were used to generate the data points indicated in Figure 17a. It is noticed that presenting the data in this fashion eliminates the effect of bed height, and shows the parameter η (and therefore E) is independent of bed height. The slight divergence in the upshot 3.7 cm bed height data from the results obtained on the other two bed heights occurred because any aerosol removal affected not by the sand granules (such as collection by the sides of the container), are masked to a greater extent with thicker beds. The smoothed curves for the 10-14 mesh

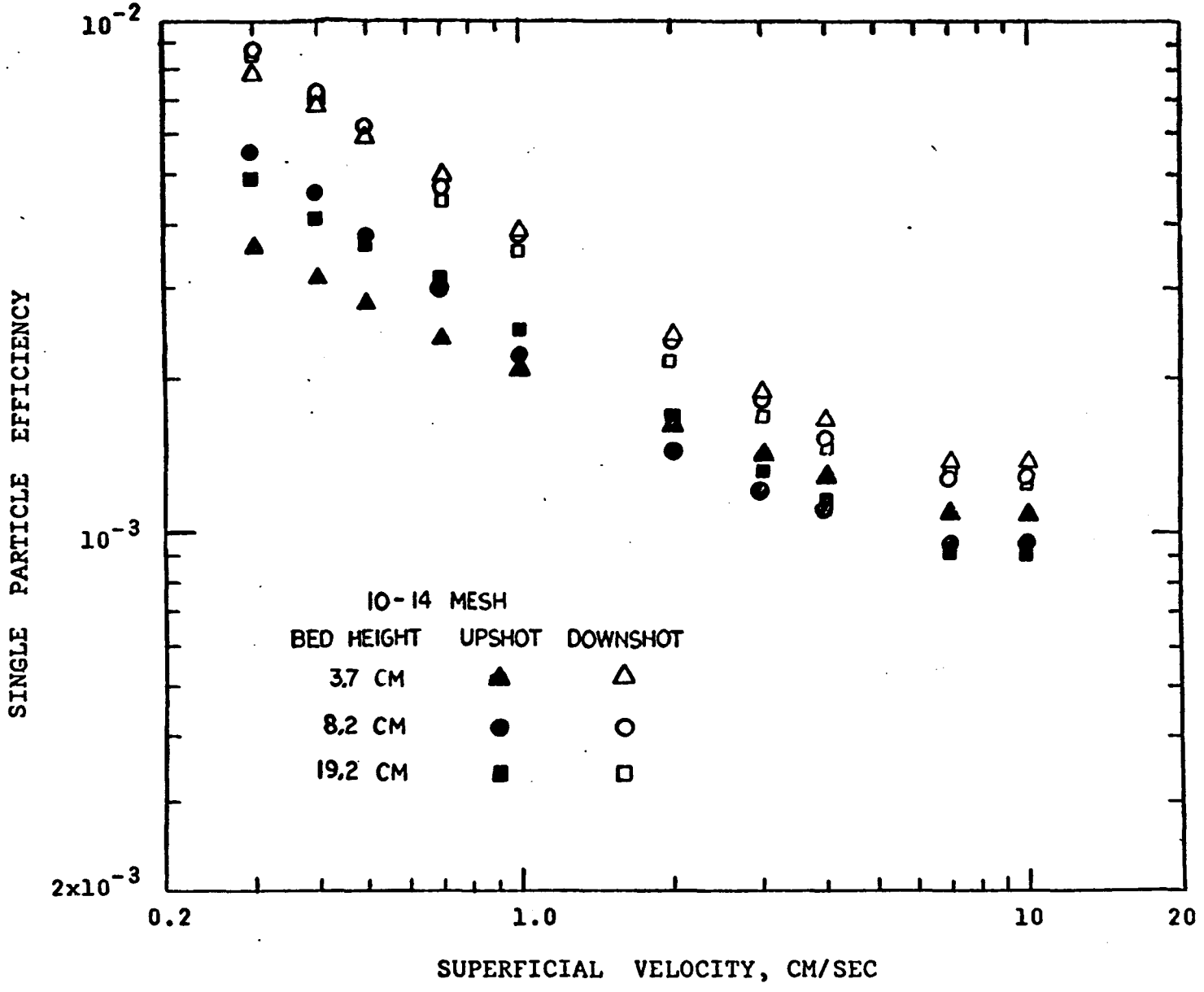

Figure 17a. Single particle efficiency as a function of superficial velocity for three different bed heights.

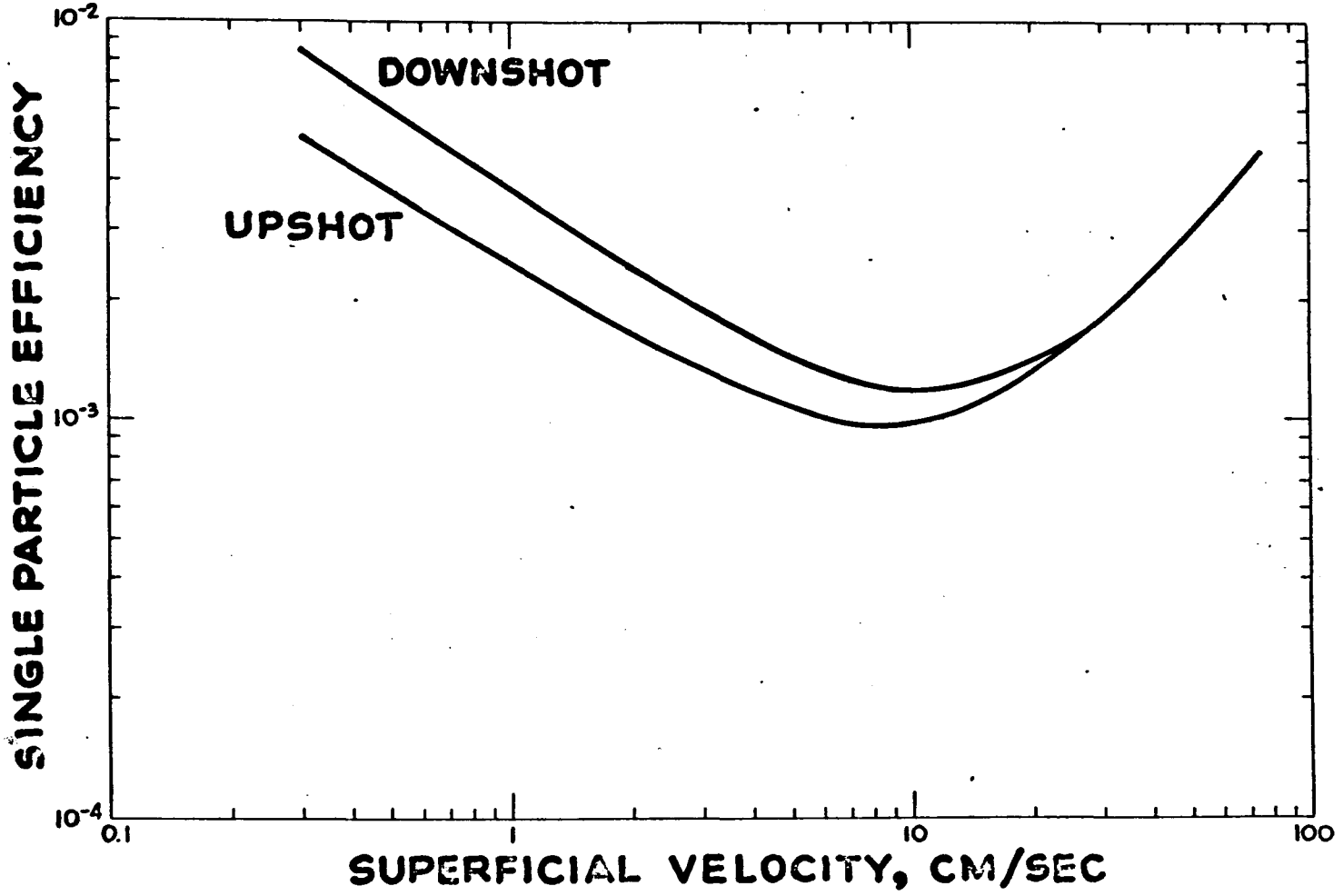

Figure 17b. Single particle efficiency as a function of superficial velocity: 10-14 mesh sand.

sand, covering the entire velocity range, are presented in Figure 17b. The 20-30 mesh data plotted in terms of the single particle efficiency E are shown in Figure 18.

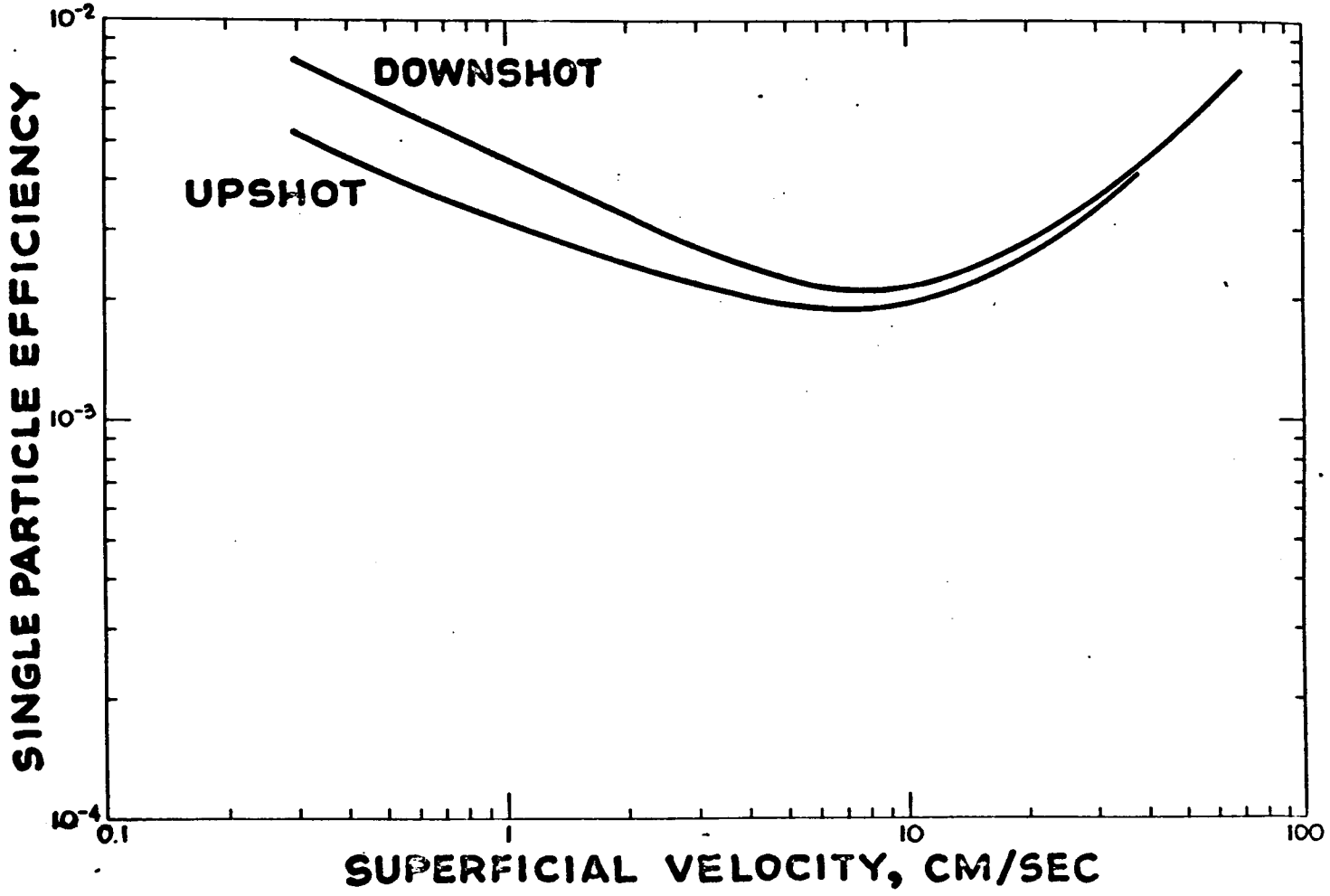

Figure 18. Single particle efficiency as a function of superficial velocity: 20-30 mesh sand.

8. DEVELOPMENT OF FILTRATION MODELS FOR SPHERICAL COLLECTIONS AND APPLICATION TO EXPERIMENTAL DATA

Introduction

Inasmuch as the structure of fibrous filters is radically different from that of granular filters, one cannot simply apply the models developed for fibrous filters to granular filters. A fibrous mat is probably more "ideal" than a sand bed, for the porosity of a fibrous filter is in the neighborhood of 95%, while the porosity of a sand bed is about 40%. In addition, the size of the sand collectors are in excess of several hundred microns, while the fibers are generally about several microns. Thus, anything but the most general inferences concerning the behavior of one media from that of the other would be misleading, as Fuchs (25) pointed out.

Happel's "Free Surface Model" (30) was utilized to obtain analytical expressions that would predict the capture of aerosols by each of the filtration mechanisms in granular beds. The free surface model has been used successfully by Happel and Pfeffer (30,46) to predict sedimentation rates, pressure drop, and heat and mass transfer in packed beds.

The model is developed on the basis that two concentric spheres will describe a typical cell in a random assemblage such as a packed bed of sand particles which can be considered to consist of many cells. Each cell contains a particle surrounded by a fluid envelope and contains the same amount of fluid as the relative volume of fluid to particle volume in the entire assemblage. In an actual packed bed these envelopes will be distorted, but Happel assumed that a typical cell can be taken to be spherical. The outside surface of each cell is assumed to be frictionless or to have a free surface. Thus the entire disturbance due to each particle is confined to the fluid with which it is associated. Figure 19 illustrates the free surface model applied to inertial impaction.

Diffusion

If the conditions are such that only aerosol capture by diffusion is of importance, then the analytical work of Pfeffer (45) based on the free surface model is directly applicable. Pfeffer was able to solve the diffusion equation

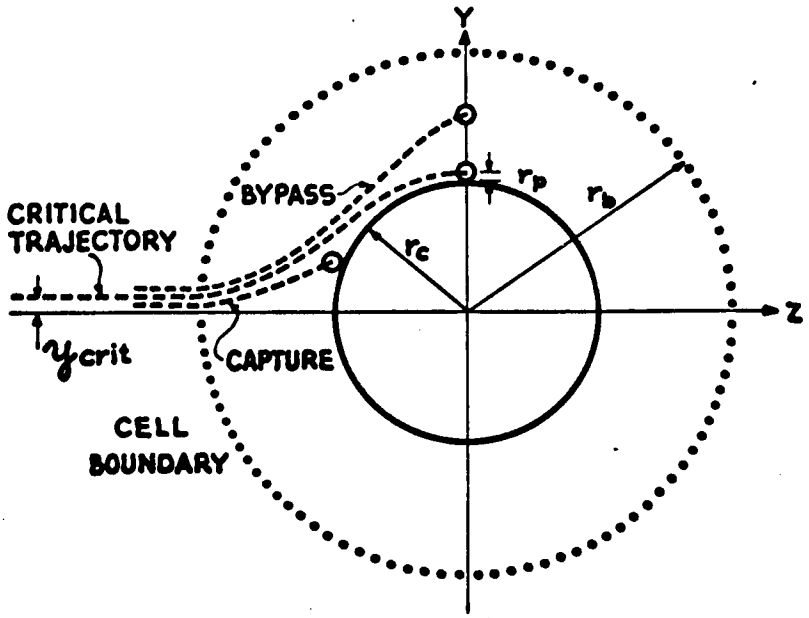

Figure 19. Free surface model applied to inertial impaction.

$$\frac{2}{Pe} \nabla'^2 n' = \bar{U}_M' \cdot \nabla' n' \qquad (22)$$

with the associated boundary conditions

$$n' = 0 \qquad r' = 1 \text{ (at particle surface)}$$

$$n' = 1 \qquad r' = \frac{1}{\gamma} \text{ (at free surface)}$$

The velocity profile associated with the free surface model, given in terms of the stream function was used.

$$\psi = - U_o \sin^2\theta \left(A_\epsilon r^2 + B_\epsilon \frac{r_c^3}{r} + C_\epsilon r_c r + D_\epsilon \frac{r^4}{r_c^2} \right) \qquad (31a)$$

$$U_r = \frac{1}{r^2 \sin\theta} \frac{d\psi}{d\theta} \qquad (31b)$$

$$U_\theta = - \frac{1}{r \sin\theta} \frac{d\psi}{dr} \qquad (31c)$$

The dimensionless constants A_ϵ, B_ϵ, C_ϵ, and D_ϵ are dependent only on the porosity of the bed (see Nomenclature).

Pfeffer obtained an analytical expression for the average Sherwood number (or mass transfer coefficient) around the solid particle as a function of the Peclet

number and bed porosity:

$$Sh_{avg} = 1.26 \left[\rho(\epsilon) \right]^{-1/3} Pe^{1/3} \qquad (32)$$

where $\rho(\epsilon)$ is a complex function of the bed porosity (see Nomenclature). This expression can be readily modified to yield the filtration efficiency of a collector composed of spherical particles such as the sand beds of immediate interest.

The filtration efficiency of a single spherical collector particle in a sand bed of porosity ϵ considering only deposition by diffusion is:

$$E^{*} = \frac{\text{particles removed by collector}}{\text{particles removed if flow is straight}} \qquad (33)$$

The particles removed is equal to the (mass flux to surface) x (area which removes particles). The mass flux is obtained by multiplying the mass transfer coefficient by the concentration in the bulk stream minus the concentration on the surface of the collector (which is assumed to be zero), so that

particles removed by collector

$$= k_c \left(n_{stream} - n_{surface} \right) (4\pi r_c^2)$$

$$= k_c \, n_o \, 4 \, \pi \, r_c^2$$

The denominator of equation (33), or the theoretical number of particles removed is just the free stream flux times the projected area of the collector, so that

particles removed if flow is straight

$$= n_o \, U_o \, (\pi \, r_c^2)$$

Therefore:

$$E_D^* = \frac{4 \, k_c}{U_o} \tag{34}$$

But the Sherwood number was obtained through consideration of the influence of neighboring particles. Thus E^* becomes E, and equation (32) combined with equation (34) yields

$$E_D = 5.04 \, \rho(\varepsilon)^{-1/3} \, Pe^{-2/3} \tag{35}$$

Since the Peclet number is directly proportional to the sand size and the superficial velocity, equation (35)

indicates that the single particle efficiency by diffusion decreases as the collector particle size and the superficial velocity increases. The single particle efficiency also increases as the filter bed becomes more concentrated since $\rho(\epsilon)^{-1/3}$ becomes larger as ϵ decreases.

Furthermore, as $\epsilon \to 1$, $\rho(\epsilon) \to 2$, $\rho(\epsilon)^{-1/3} \to 0.8$ and the single particle collection efficiency approaches the value predicted for a single isolated collector, i.e.,

$$E_D^* = 3.99\ Pe^{-2/3}$$

obtained by using the Levich-Lighthill solution

$$Sh = 0.997\ Pe^{1/3}$$

for a single particle in an infinite fluid.

A plot of the single particle efficiency vs the Peclet number for low Peclet numbers where diffusion is the dominant mechanism of aerosol capture is shown in Figure 20. The experimental data as well as data of Thomas and Yoder (62,63) are also presented as a comparison. It is seen that as the Peclet number, and hence, the velocity decreases, the agreement with the experimental data increases. Deviations may be attributed

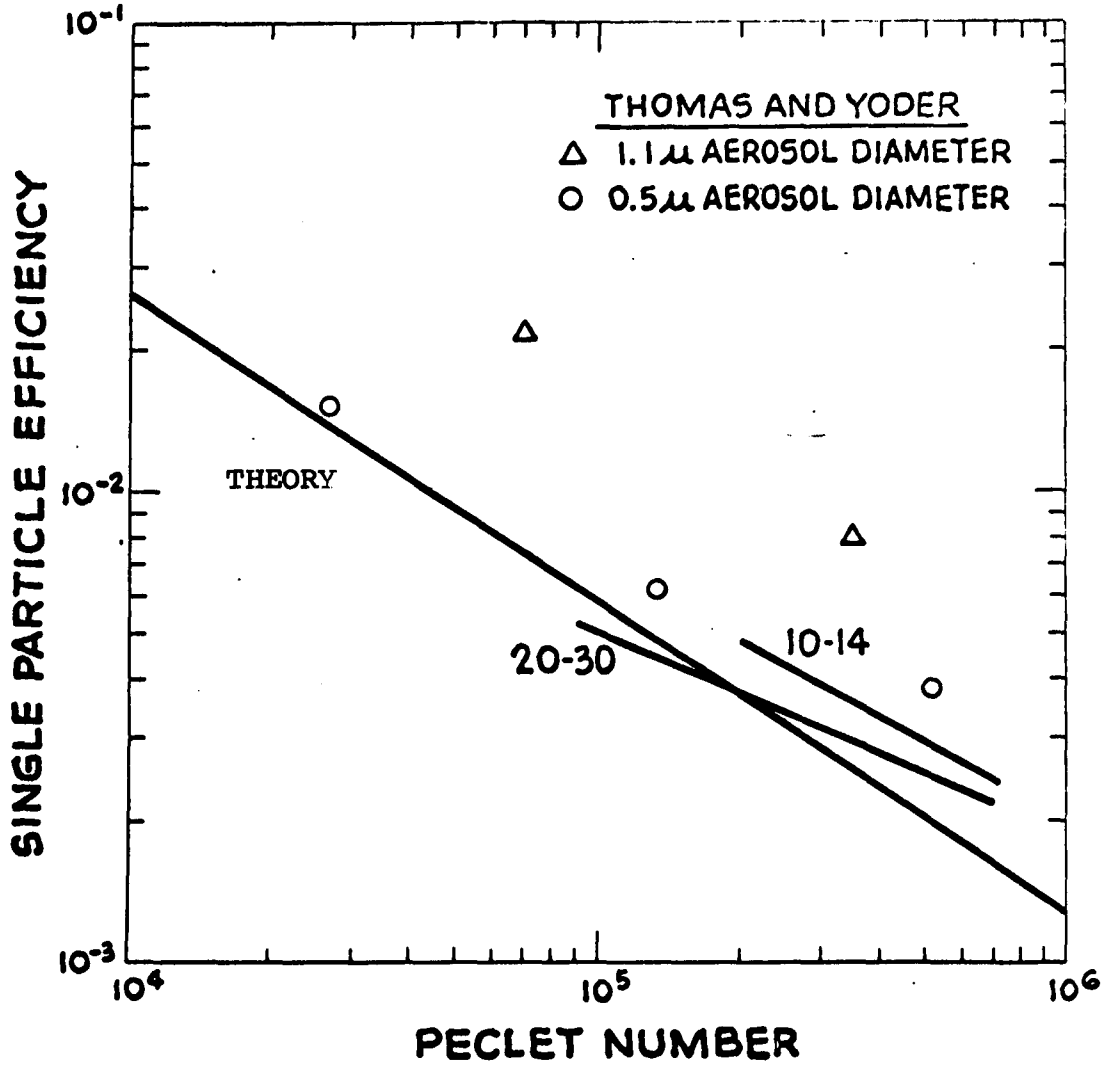

Figure 20. Comparison of the theoretical and experimental (upshot) single particle efficiency due to Brownian diffusion.

to the lack of appropriate entrance and exit sections or to gravity effects. With the smaller particles (0.5 microns diameter), the effect of inertial effects in sharp entrance and exit sections and the effect of gravity is not as important as with the larger particles (1.1 microns diameter).

Direct Interception

Particles captured by the mechanism of direct interception are assumed to follow the streamlines of the fluid and are removed only if they pass within a distance r_p of the collector surface measured at the angle $\theta = 90^o$ with respect to the direction of flow. Therefore, the single particle collection efficiency by direct interception is given by

$$E_{DI}^{*} = \frac{n_o \int_{r=r_c}^{r=r_c+r_p} U_\theta\big|_{\theta=90^o} \; 2\pi r \, dr}{n_o U_o \pi r_c^2} \qquad (36)$$

Using the free surface model to represent the bed of sand particles, the dimensionless velocity U_θ' can be obtained from equation (31).

$$U_\theta' = \left(2 A_\epsilon - \frac{B_\epsilon}{r'^3} + \frac{C_\epsilon}{r'} + 4 D_\epsilon r'^2 \right) \sin\theta \quad (37)$$

Since the velocity profile used accounts for the presence of neighboring spheres, E^* is replacad by E. Substituting equation (37) into equation (36) one has

$$E_{DI} = 2\int_{r'=1}^{r'=1+R} \left(2 A_\epsilon - \frac{B_\epsilon}{r'^3} + \frac{C_\epsilon}{r'} + 4 D_\epsilon r'^2 \right) r'dr'$$

$$= \frac{3 R^2}{W}\left[(1 - \gamma^5) - R(1 + 4\gamma^5) + R^2(1 - \gamma^5) \right]$$

or since

$$\rho(\epsilon) = \frac{W}{1 - \gamma^5}$$

$$E_{DI} = \frac{3 R^2}{\rho(\epsilon)} \left[1 - R(1 + 5 \gamma^5 \rho(\epsilon)) + R^2 \right] \quad (38)$$

Neglecting terms of order R and higher (for the spherical collectors in this work $R<<1$), one obtains

$$E_{DI} = 3 R^2 \rho(\epsilon)^{-1} \tag{39}$$

The efficiency increases as ϵ decreases, and as $\epsilon \rightarrow 1$, $\rho(\epsilon) \rightarrow 2$, and the efficiency approaches the value predicted for a single isolated spherical collector.

$$E_{DI}^{*} = \frac{3}{2} R^2 \tag{40}$$

Thus capture by direct interception is independent of velocity and particle density and depends only on particle and collector size and the porosity of the collecting particles.

In this study this effect is small and is only about 4% of the total single particle efficiency by all the mechanisms together.

Inertial Impaction

The "free surface" model can also be used to predict capture by inertial impaction. This is accomplished by computing the trajectory of the aerosol particle as the fluid flows around the inner sphere (the collector) in the concentric sphere model. The

flow field in spherical coordinates is two dimensional with respect to r and Θ, and symmetric with respect to φ. The velocity profile of a single particle may therefore be described in a two-dimensional rectangular coordinate system (see Figure 19). The single particle inertial impaction efficiency, E_I^*, is defined on the basis of the starting point of the critical trajectory (see page 48) at the cell boundary. It can be easily seen that using equation (33):

$$E_I^* = \frac{n_o U_o \pi (y_{crit})^2}{n_o U_o \pi (r_c)^2}$$

so that

$$E_I^* = \left(\frac{y_{crit}}{r_c}\right)^2 \qquad (41)$$

The critical trajectory is defined as the trajectory of an aerosol particle starting at the cell boundary and just missing capture by the collector as it flows around it. As before, since the model accounts for neighboring particles, E^* is replaced by E.

The starting point in this analysis is the trajectory equations which have previously been developed:

$$N_I \frac{d\bar{V}_P'}{dt'} = - (\bar{V}_P' - \bar{U}_M') \tag{23a}$$

$$\frac{d\bar{r}'}{dt'} = \bar{V}_P' \tag{23b}$$

It is assumed that the particle is a point mass which does not affect the fluid flow field, but experiences a resistive force due to the relative velocity of the particle with respect to the velocity of the fluid. It is also assumed that the particle is traveling in the z direction with the undisturbed stream velocity at the cell boundary.

In a two-dimensional rectangular coordinate system the above equations become

$$N_I \frac{dV_{P_y}'}{dt'} = - V_{P_y}' + U_{M_y}' \tag{42a}$$

$$N_I \frac{dV_{P_z}'}{dt'} = - V_{P_z}' + U_{M_z}' \tag{42b}$$

$$\frac{dy'}{dt'} = V_{P_y}' \tag{42c}$$

$$\frac{dz'}{dt'} = V_{P_z}' \tag{42d}$$

with the initial conditions

$$V_{P_y}' = 0 \quad \text{at} \quad t' = 0$$

$$V_{P_z}' = 1 \quad \text{at} \quad t' = 0$$

$$y' = y_o' \quad \text{at} \quad t' = 0$$

$$z' = z_o' \quad \text{at} \quad t' = 0$$

where y_o' and z_o' are the dimensionless initial positions of the particle at the cell boundary.

The fluid velocities are based on the free surface model (equation (31)) and in the two-dimensional system used are:

$$U_{M_y}' = -\frac{2y'z'}{r'^2}\left[A_\epsilon + \frac{B_\epsilon}{r'^3} + \frac{C_\epsilon}{r'} + D_\epsilon r'^2\right] + \frac{y'z'}{r'^2}\left[2A_\epsilon - \frac{B_\epsilon}{r'^3} + \frac{C_\epsilon}{r'} + 4D_\epsilon r'^2\right] \tag{43a}$$

and

$$U_{M_z}' = -\frac{2z'^2}{r'^2}\left[A_\epsilon + \frac{B_\epsilon}{r'^3} + \frac{C_\epsilon}{r'} + D_\epsilon r'^2\right] - \frac{y'^2}{r'^2}\left[2A_\epsilon - \frac{B_\epsilon}{r'^3} + \frac{C_\epsilon}{r'} + 4D_\epsilon r'^2\right] \tag{43b}$$

with

$$r'^2 = y'^2 + z'^2 \tag{43c}$$

Equation set (42) is solved numerically by using a fourth order Runge-Kutta forward integration method. An initial position y_o' for the particle at the outer cell is first chosen. The Runge-Kutta calculation proceeds - generating the particle's trajectory at succeeding time intervals - until the particle is either captured or bypasses the collector. The initial guess on y_o' is then updated, and the calculation is repeated, until the critical initial position is obtained.

The single particle efficiency, E_I, as obtained from equation (41) is plotted against the inertial parameter, N_I, for three values of the bed porosity, $\epsilon = 0.39$, $\epsilon = 0.43$, and $\epsilon = 0.49$ in Figure 21. This porosity range was chosen as typical for the sand beds which were studied experimentally. Results for $\epsilon = 0.66$ and $\epsilon = 1$ (a single spherical collector) have also been obtained and are included in the figure. The numerical results for a single spherical collector ($\epsilon = 1.0$) are in excellent agreement with those obtained previously by Herne (33) - thus presenting a reasonable check on the validity of the numerical calculations. As can be seen in the figure the shape of the curves for the five different values of ϵ are

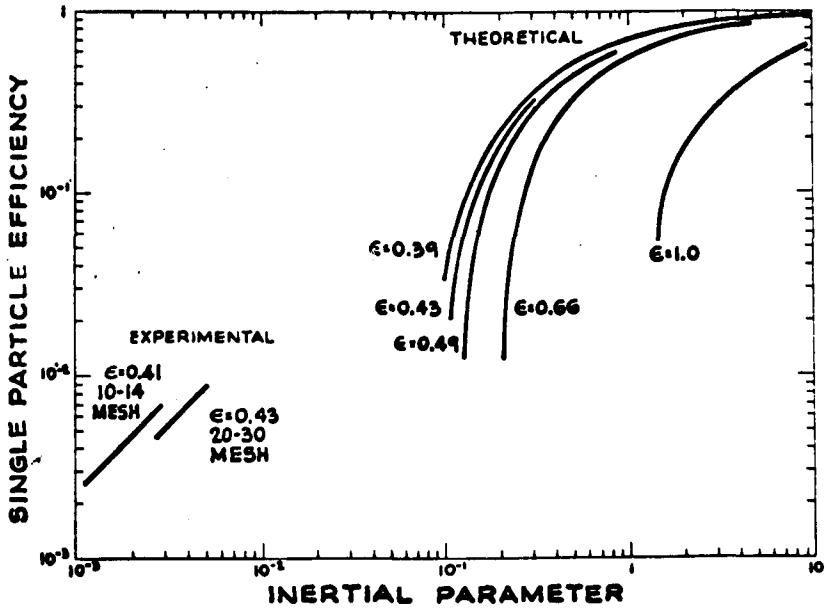

Figure 21. Comparison of the theoretical and experimental single particle efficiency due to inertial impaction.

quite similar, with E_I approaching unity as N_I goes to infinity, as expected. For the single collector, Herne found that there is a limiting value of the inertial parameter equal to 1.212 (for viscous flow) below which there is no deposition due to inertial impaction. For the beds of porosity $\epsilon = 0.39$ to $\epsilon = 0.49$ there also appears to be a limiting value of the inertial parameter although this value is about ten times smaller than for a single particle collector. The figure also shows that decreasing the porosity will increase the efficiency at a given value of N_I indicating that a bed of particles is more effective in capturing aerosols by inertial impaction than a single particle.

It should be noted that several numerical computations were performed to include the direct interception effect. That is, the critical trajectory was the trajectory that passed within a distance of the collector equal to the radius of the aerosol particle. Because the value of R in the system of interest, 1.1 micron diameter aerosols and sand sizes from 10-30 mesh, are less than 2×10^{-3}, no significant difference was observed by increasing the radius of the collector by an amount equal to the radius of the aerosol.

The experimental results given in Figures 17 and 18 have shown that the single particle efficiency goes through a minimum with respect to velocity and then rises again as the velocity is increased. The increase in filtration efficiency at the higher face velocities (above 25 cm/sec) was thought to be due to capture by inertial impaction. The rising portion of the curves in Figures 17 and 18 were replotted in Figure 21 as a function of the inertial parameter N_I (this is directly proportional to the face velocity since all the other terms in N_I were held constant in the experiments). The experimental data were all taken at much lower values of the inertial parameter, N_I, than the critical value of N_I predicted by the "free surface" model. In other words, the model predicts that at low values of N_I at which the experimental data were obtained, there should be no capture whatsoever due to inertial impaction and, therefore, there should be no increase in the single particle efficiency as the velocity is increased in the velocity range of the experiments.

Since the theoretical model does not fit the experimental data it is left to empirical means to correlate the data in the inertial impaction regime. An

enlarged plot of E vs N_I for the rising portion of the velocity-penetration curve is presented in Figure 22. The relationships for the individual sand sizes are:

10-14 mesh

$$E_I = 2.5\, N_I^{1.13} \tag{44a}$$

20-30 mesh

$$E_I = 0.78\, N_I^{0.98} \tag{44b}$$

Friedlander and Pasceri (24), in their compilation of data other investigators obtained on fibrous filters got the expression

$$E_I = 0.075\, N_I^{6/5} \tag{45}$$

for the range $0.8 < N_I < 2$. This correlation is presented in Figure 23. The large difference in the coefficient of the inertial parameter, which depends on the porosity of the filter medium, is probably due to the great difference between a fibrous filter with a fiber diameter of the order of a few microns and a sand bed with a particle diameter of several hundred microns. Friedlander states that the large amount of scatter in the data for $N_I < 0.5$ (Figure 23) is due

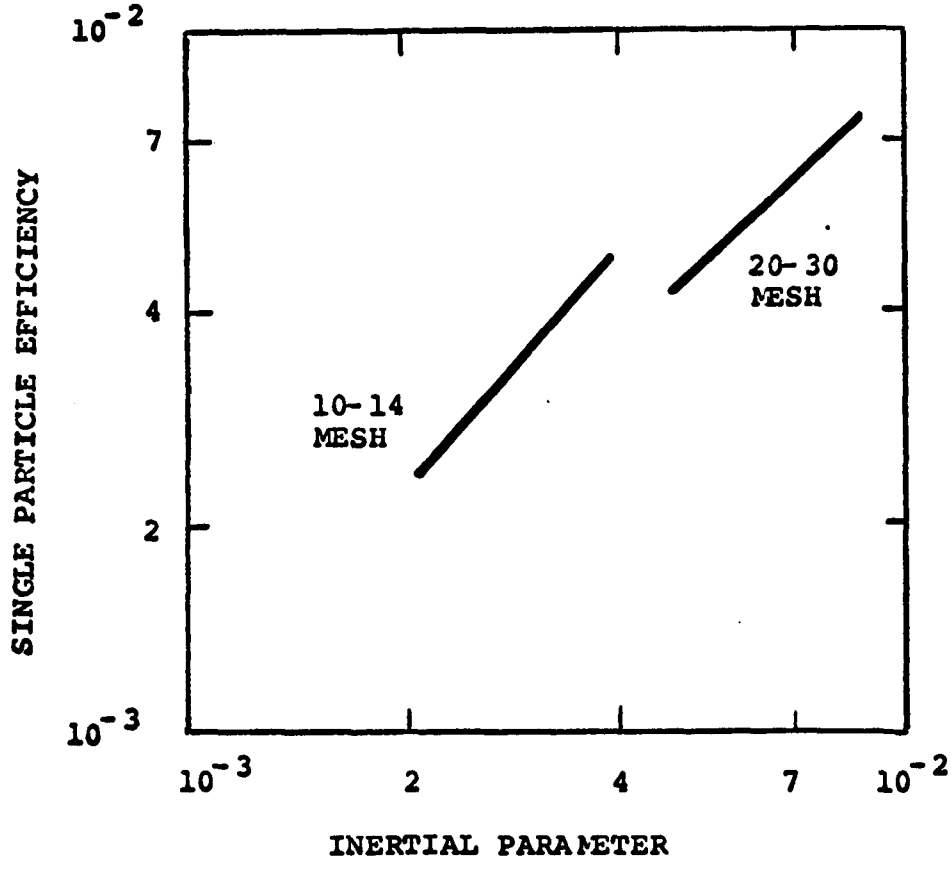

Figure 22. Experimental single particle collection efficiency from the inertial impaction regime.

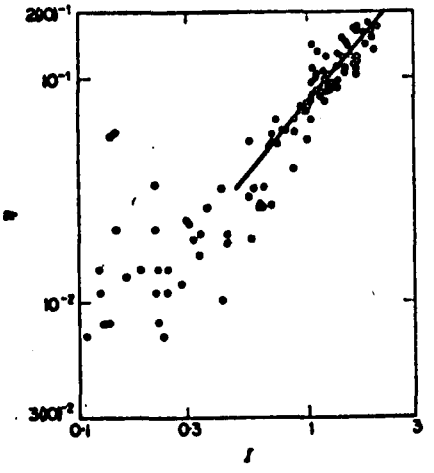

FIG. 5. Correlation of data for fiber efficiency in impaction range. Equation of line: $\eta = 0.075\, I^{3/2}$.

Figure 23. Friedlander and Pasceri's compilation of the single particle collection efficiency in the inertial impaction range for fibrous filters (24).

I = Inertial Parameter (N_I)

η = single particle efficiency (E)

to the emergence of direct interception as the controlling mechanism. While this may be the case for fibrous filters, it is clearly not true here. It should be noted that it is not too difficult to draw a curve through Friedlander's correlation with a slope of 0.98. In addition, the solid fraction of a fibrous filter is about 0.04, while the solid fraction for a sand bed is about 0.60. The ratio of the solid fraction of a fibrous filter to the solid fraction of a sand bed is about 0.067 (i.e., 0.04/0.60). This ratio is fairly close to the ratio of the respective numerical coefficients of equations (44a) and (44b) (2.5 and 0.78) with the numerical coefficient of equation (45) (0.075). That is 0.075/2.5 = 0.030, and 0.075/0.78 = 0.096.

Contrary to the experimental data in this work, it is very tempting to say that the use of the inertial parameter removes the effect of collector size on the single particle efficiency. First of all, the free surface model indicates that collector size is not required as an additional factor to correlate single particle collection efficiency in the inertial impaction regime. In addition, Friedlander and Pasceri (24) showed that the use of N_I alone is

sufficient. Thirdly, the experimental difference is probably due to either the average sand grain diameter not being the average of the mesh cuts, or a variation in the sand roughness between the two sand sizes. Thomas and Yoder (62) found that the difference in collection efficiency between rough, irregular sand and smooth, fine sand of the same mesh size can be about 50% (see Figure 24). Porosity differences alone cannot account for this large spread. Fibrous filters are generally all very smooth, thus the effect of roughness would not appear in fibrous data.

With this in mind, it would be beneficial to present a relationship that combines the data from the two sand sizes. The best overall fit of the data for the two sand sizes, trying to keep the power on N_I as a fraction, is:

$$E_I = 2.0\ N_I^{9/8} \tag{46}$$

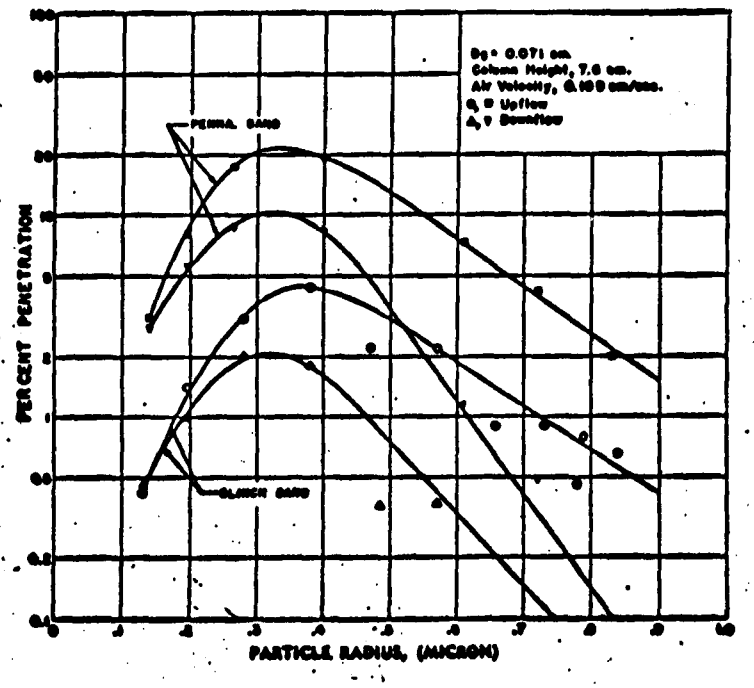

Fig. 4. — Penetration of homogeneous DOP aerosol through Clinch River and Pennsylvania glass sand (20-30 mesh sand, $D_g = 0.071$ cm.).

Figure 24. Data from Thomas and Yoder illustrating effect of coarseness of sand on penetration (62).

Pennsylvania sand: smooth
porosity = 0.41

Clinch River sand: rough, irregular
porosity = 0.38

Gravity Settling

The fourth mechanism of aerosol capture which will be discussed is that of gravity settling. As had been previously mentioned, gravity settling is treated as being superimposed on other filtration mechanisms.

Deposition by gravity settling occurs because the gaseous boundary layer surrounding the collector surface is effectively at rest. Particles of negligible inertia will settle onto the collector while falling vertically at their sedimentation velocity, V_s . The single particle collection efficiency due to gravity settling or sedimentation is defined as (9):

$$E_G^* = \frac{\text{particles removed by collector}}{\text{particles removed if flow was straight}}$$

$$= \frac{n_o V_s \pi r_c^2}{n_o U_o \pi r_c^2}$$

$$= \frac{V_s}{U_o}$$

$$E_G^* = N_G \qquad (47)$$

From Figures 17 and 18 it is seen that the total collection efficiency for downshot flow $E_T(\downarrow)$ is greater than that for upshot flow $E_T(\uparrow)$. The same phenomena

was observed by Thomas and Yoder (62,63). This occurrence can be understood by examining the collection process around a collector particle, as illustrated below.

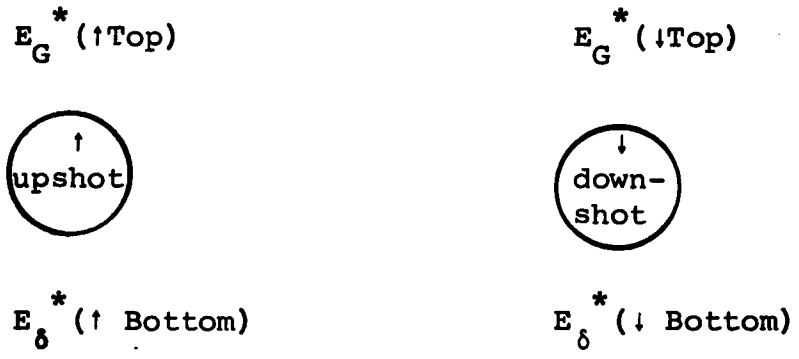

Consider initially the top surface of the collector. Here particles are collected by sedimentation, with a collection efficiency of E_G^* (↑ Top) for upshot flow and E_G^* (↓ Top) for downshot flow. Because of boundary layer separation and the existence of a wake downstream of the collector (when the collector Reynolds number is greater than one), E_G^* (↓ Top) > E_G^* (↑ Top).

On the bottom face we effectively have the opposite condition. Here particles that would be deposited by other mechanisms are carried back into the main stream by sedimentation. In other words, on the bottom face sedimentation impedes deposition by other mechanisms. The only mechanism which collects particles

on the downstream surface of the collector other than sedimentation is Brownian diffusion. Since more particles are deposited by Brownian diffusion on the upstream face of the collector, due to a greater concentration gradient, it follows that the loss in collection efficiency for upshot flow $E_\delta^*(\uparrow \text{Bottom})$, is greater than that for downshot flow $E_\delta^*(\downarrow \text{Bottom})$. This term is defined so that $E_\delta^* > 0$.

Therefore, for upshot flow the total effect by sedimentation on the collection efficiency is

$$E_G^*(\uparrow) = E_G^*(\uparrow \text{Top}) - E_\delta^*(\uparrow \text{Bottom}) \qquad (48)$$

and for downshot flow

$$E_G^*(\downarrow) = E_G^*(\downarrow \text{Top}) - E_\delta^*(\downarrow \text{Bottom}) \qquad (49)$$

Since

$$E_G^*(\downarrow \text{Top}) > E_G^*(\uparrow \text{Top})$$

and

$$E_\delta^*(\uparrow \text{Bottom}) > E_\delta^*(\downarrow \text{Bottom})$$

it follows that

$$E_G^*(\downarrow) > E_G^*(\uparrow)$$

Following the assumption that the effect of sedimentation can be superimposed on the other filtration mechanisms, the difference between the total collection efficiency for downshot flow and the total collection efficiency for upshot flow is

$$\Delta E_T^* = E_T^*(\downarrow) - E_T(\uparrow) \tag{50}$$

Therefore

$$\Delta E_T^* = E_G^*(\downarrow) - E_G^*(\uparrow) \tag{51}$$

and substituting from equations (48) and (49)

$$\begin{aligned} \Delta E_T^* = & \left[E_G^*(\downarrow \text{Top}) - E_G^*(\uparrow \text{Top}) \right] \\ & - \left[E_\delta^*(\downarrow \text{Bottom}) - E_\delta^*(\uparrow \text{Bottom}) \right] \end{aligned} \tag{52}$$

The above analysis also applies to a bed of actual collectors, therefore the isolated single particle efficiencies (the * terms, i.e., ΔE_T^*) can be replaced with the single particle efficiencies of the collectors in an actual bed (i.e., ΔE_T).

A plot of ΔE_T vs N_G is presented in

Figure 25 using the data obtained in this work. Here the aerosol particle size was held constant (at 1.1 micron diameter) and the face velocity was varied. It is seen that the difference ΔE_T is independent of collector size.

Data from the work of Thomas and Yoder (62,63) are also presented in this figure. In their work the aerosol particle size was varied at constant face velocity (Figures 24 and 26). Excellent agreement is obtained with their data acquired at a face velocity of 0.109 cm/sec, with slight divergences appearing with their data acquired at face velocities of 0.745 and 1.49 cm/sec. This discrepancy at the higher velocities may be attributed to the lack of suitable entrance and exit sections, as discussed previously.

From Figure 25 the differences between the upshot and downshot single particle collection efficiency can be related to the gravity settling parameter by the empirical relation

$$\Delta E_T = 8.4 \times 10^{-2} N_G^{0.78} \qquad (53)$$

The remaining task is to establish the actual contribution due to gravity settling. No definite

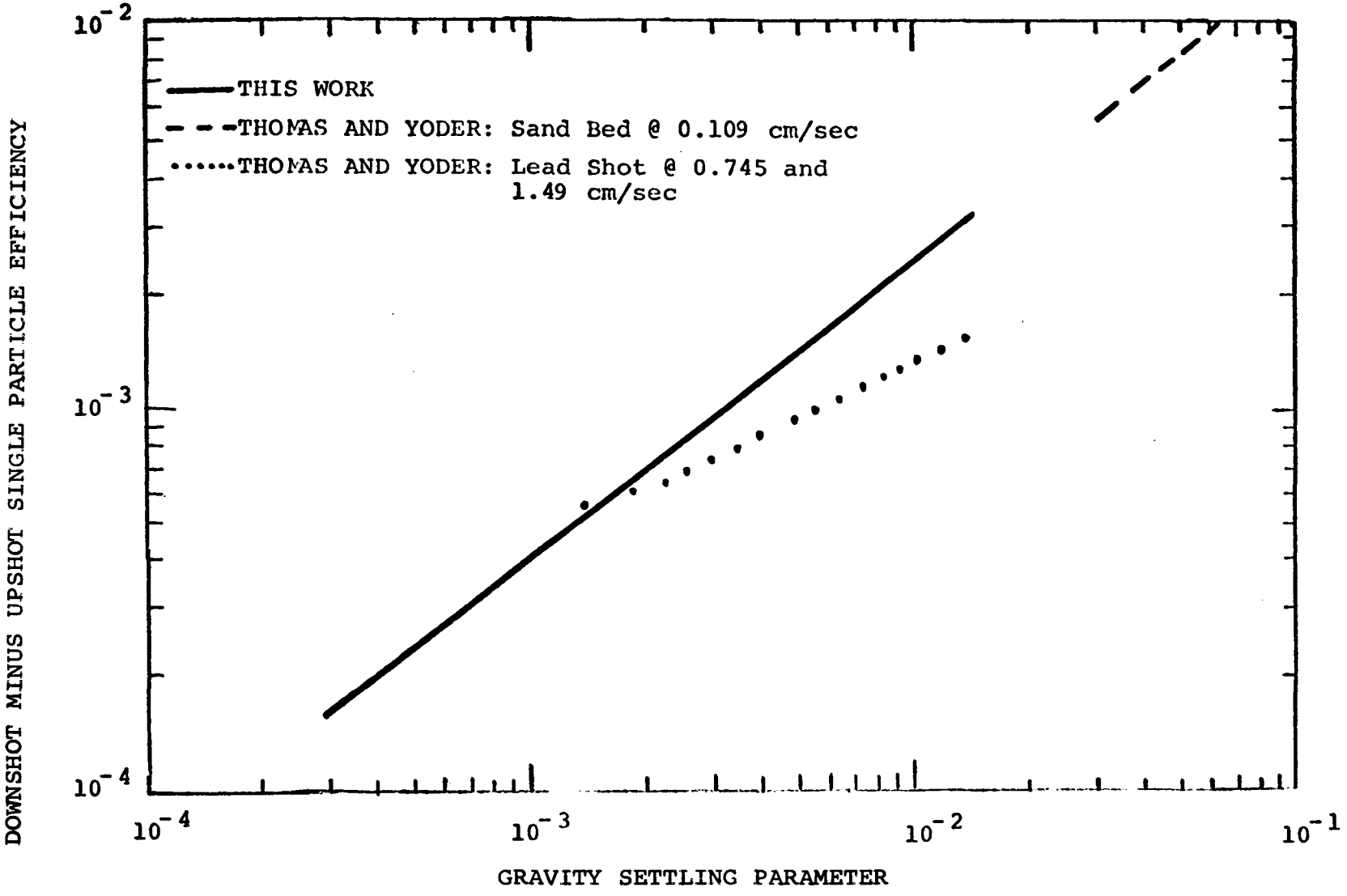

Figure 25. Difference between downshot and upshot single particle collection efficiency vs Gravity Settling Parameter.

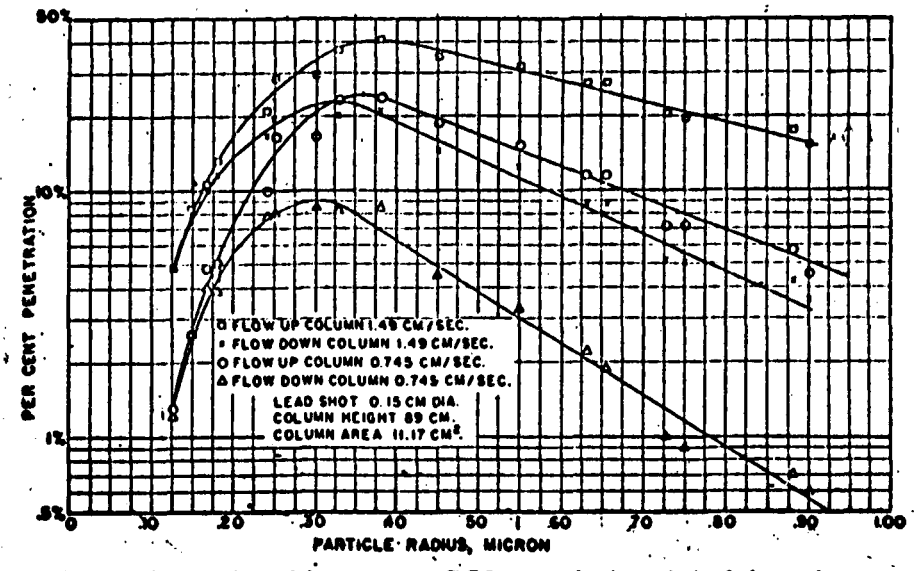

Fig. 3.—Penetration of homogeneous DOP aerosols through lead-shot column.

Figure 26. Data from Thomas and Yoder (63).

information can be obtained from this work, for in the range of variables investigated diffusion and gravity settling acted simultaneously and in the same direction. That is, an increase in velocity produced a decrease in both collection by diffusion and gravity settling, and it was impossible to ascertain the individual contributions. Rather, it is necessary to resort to the work of Thomas and Yoder (62,63).

Thomas and Yoder varied the aerosol size at constant velocity, as indicated in Figures 24 and 26. The rising portion of the curves are due solely to diffusion, and the falling portions are caused by gravity settling.

The lead shot data (Figure 26) will be utilized to obtain the effect of gravity, because as the bed gets longer a greater fraction of the aerosol is filtered by the collectors, thus diminishing the relative effect of the entrance and exit losses.

Using the data from the 1.49 cm/sec run, where the collection efficiency can be assumed to be due only to gravity settling the empirical relationship

$$E_G(\uparrow) = 1.5 \times 10^{-2} N_G^{1/2} \qquad (54)$$

is suggested for the upshot collection efficiency due to gravity settling.

The downshot single particle collection efficiency due to gravity settling can then be obtained as the sum of equations (53) and (54), or

$$E_G(\downarrow) = E_G(\uparrow) + \Delta E_T$$

$$E_G(\downarrow) = 1.5\times10^{-2}\, N_G^{1/2} + 8.4\times10^{-2}\, N_G^{0.78} \qquad (55)$$

9. TOTAL FILTRATION PROCESS

Unfortunately, in an actual filter one has several filtration mechanisms acting simultaneously. The simplest approach is to assume the effect of each of the collection mechanisms is additive in terms of the penetration. That is

$$\xi_T = \sum_i (\exp - \eta_i b) \tag{56}$$

and assuming that only diffusion, gravity settling, direct interception and inertial impaction are present:

$$\xi_T = \exp(- \eta_D b) + \exp(- \eta_G b) + \exp(- \eta_{DI} b) + \exp(- \eta_I b) \tag{57}$$

Fuchs (25) criticized this approach, for it is possible to have $\xi_T > 1$.

Dorman suggested that the total penetration can be expressed as

$$\xi_T = \exp - (\eta_D + \eta_G + \eta_{DI} + \eta_I) b \tag{58}$$

with (see equation (30))

$$\eta_i = \frac{3}{4} \frac{1 - \epsilon}{\epsilon} \frac{E_i}{r_c}$$

This removes the problem of having $\xi_T > 1$.

It has been shown in the previous chapter that the single particle collection efficiencies for diffusion, gravity settling (upshot), inertial impaction, and direct interception obtained either from theory or empirical correlation of data are:

$$E_D = 5.04\ \rho(\epsilon)^{-1/3}\ Pe^{-2/3} \qquad \text{(Theory)} \qquad (35)$$

$$E_G(\uparrow) = 1.5 \times 10^{-2}\ N_G^{1/2} \qquad \text{(Empirical)} \qquad (53)$$

$$E_I = 2.0\ N_I^{9/8} \qquad \text{(Empirical)} \qquad (46)$$

$$E_{DI} = 3\ \rho(\epsilon)^{-1}\ R^2 \qquad \text{(Theory)} \qquad (39)$$

Since

$$E_T(\uparrow) = E_D + E_G(\uparrow) + E_I + E_{DI} \qquad (59)$$

the overall theoretical-empirical model for dilute aerosol filtration by sand beds is

$$E_T(\uparrow) = 5.04\ \rho(\mathbf{c})^{-1/3}\ Pe^{-2/3} + 1.5x10^{-2}\ N_G^{1/2} + 2.0\ N_I^{9/8} + 3\ \rho(\mathbf{c})^{-1}\ R^2 \quad (60)$$

Dorman's curve fitting method (Chapter 4) will be used to check the value of the coefficients in the above expression. The experimental data on the 10-14 mesh sand (upshot) will be used as an illustration. (For convenience the suffix (↑) will be omitted in the following analysis.)

Since the velocity was varied in this work (as with Ramskill and Anderson (47)), one expresses each of the filtration mechanisms as a function of velocity (here aerosol particle velocity equals fluid velocity):

$$E_T = D\ V^{-2/3} + G\ V^{-1/2} + A\ V^{9/8} + I \quad (61)$$

where D, G, A, and I are numerical coefficients to be evaluated.

At the velocity of maximum penetration (minumum single particle collection efficiency), which is read from Figure 17b as 8.5 cm/sec:

$$\left.\frac{dE_T}{dV}\right|_{V=V_{max}} = 0$$

then, using equation (61):

$$A = \frac{\frac{2}{3} V_{max}^{-2/3} D + \frac{1}{2} V_{max}^{-1/2} G}{\frac{9}{8} V_{max}^{9/8}} \qquad (62)$$

Substituting for A and collecting terms:

$$E_T = D V_{max}^{-2/3}\left[\left(\frac{V}{V_{max}}\right)^{-2/3} + \frac{16}{27}\left(\frac{V}{V_{max}}\right)^{9/8}\right] + I + G V_{max}^{-1/2}\left[\left(\frac{V}{V_{max}}\right)^{-1/2} + \frac{4}{9}\left(\frac{V}{V_{max}}\right)^{9/8}\right] \qquad (63)$$

In Dorman's curve fitting analysis of Chapter 4 gravity settling was not present as a collection mechanism, hence $G = 0$. Therefore Dorman would have plotted E_T vs $\left(\frac{V}{V_{max}}\right)^{-2/3} + \frac{16}{27}\left(\frac{V}{V_{max}}\right)^{9/8}$ and obtained D and I from the slope and intercept of the resultant straight line. In this work collection by direct interception is negligible. The working equation (equation (63)) becomes

$$E_T = D\,V_{max}^{-2/3}\left[\left(\frac{V}{V_{max}}\right)^{-2/3} + \frac{16}{27}\left(\frac{V}{V_{max}}\right)^{9/8}\right] + G\,V_{max}^{-1/2}\left[\left(\frac{V}{V_{max}}\right)^{-1/2} + \frac{4}{9}\left(\frac{V}{V_{max}}\right)^{9/8}\right] \quad (64)$$

It is possible to divide through by either of the bracketed terms, say $\left(\frac{V}{V_{max}}\right)^{-1/2} + \frac{4}{9}\left(\frac{V}{V_{max}}\right)^{9/8}$, and obtain D and G from the slope and intercept of the resultant plot. However, since diffusion and gravity settling both act in the same direction (decreasing in importance with increasing velocity), this approach is unsuitable. At higher velocities (in the inertial impaction regime) the ratios are very sensitive to slight changes in the velocity.

However, it is clear that at low velocities ($V < \approx 2$ cm/sec, for example), collection is governed only by gravity settling and diffusion. Therefore, neglecting inertial impaction

$$E_T = D\,V^{-2/3} + G\,V^{-1/2}$$

$$= D\,V_{max}^{-2/3}\left(\frac{V}{V_{max}}\right)^{-2/3} + G\,V_{max}^{-1/2}\left(\frac{V}{V_{max}}\right)^{-1/2}$$

or

$$\frac{E_T}{\left(\frac{V}{V_{max}}\right)^{-1/2}} = D\, V_{max}^{-2/3}\left(\frac{V}{V_{max}}\right)^{-1/6} + G\, V_{max}^{-1/6} \tag{65}$$

If the previous assumptions are correct, a plot of $\frac{E_T}{\left(\frac{V}{V_{max}}\right)^{-1/2}}$ vs $\left(\frac{V}{V_{max}}\right)^{-1/6}$ should generate a straight line. This in fact is the case, as seen in Figure 27 for the 10-14 mesh data. D and G, obtained from the slope and intercept of the line, are:

$$D = 1.4 \times 10^{-3}$$

$$G = 1.2 \times 10^{-3}$$

These values are substituted into equation (62), and A is obtained as

$$A = 3.4 \times 10^{-4}$$

The complete filtration equation suggested by

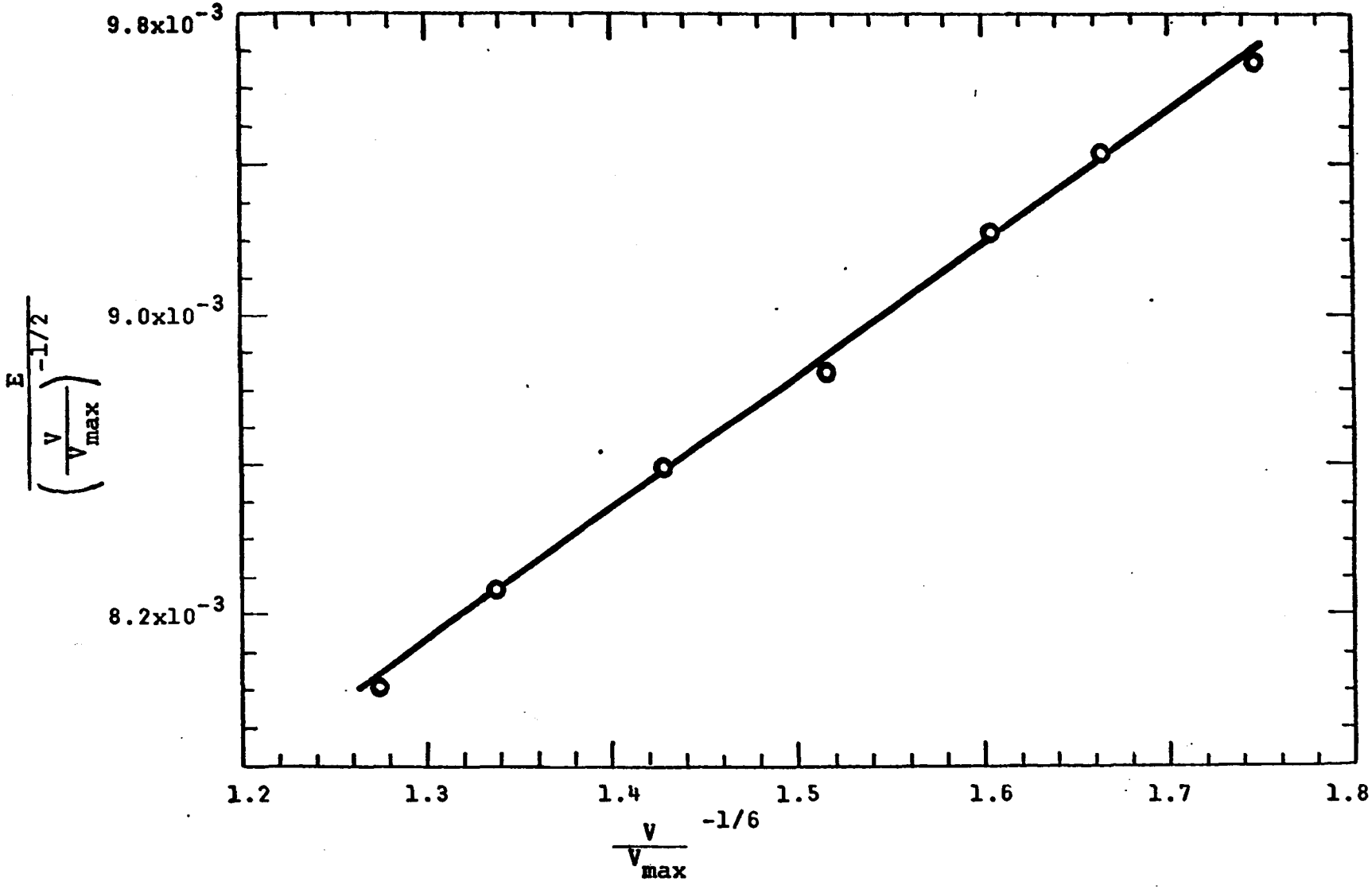

Figure 27. Calculation of constants in filtration equation using experimental data in low velocity regime (0.3 to 2.0 cm/sec).

this curve fitting technique, a la Dorman, is therefore

$$E_T = 1.4\times10^{-3}\ V^{-2/3} + 1.2\times10^{-3}\ V^{-1/2} + 3.4\times10^{-3}\ V^{9/8} \quad (66)$$

or in terms of dimensionless groups

$$E_T = 11\ Pe^{-2/3} + 1.8\times10^{-2}\ N_G^{1/2} + 2.2\ N_I^{9/8} \quad (67)$$

This compares quite favorably with the theoretical-empirical filtration model (equation (60)), which can be written as (since $\epsilon = 0.43$)

$$E_T = 15\ Pe^{-2/3} + 1.5\times10^{-2}\ N_G^{1/2} + 2.0\ N_I^{9/8} \quad (68)$$

A comparison of the above relationships with the experimental data is presented in Figure 28. It is seen that the agreement between the experimental data and the two models (equations (67) and (68)) is quite good.

It is useful to develop a curve fitting approach that can be used for the data of Thomas and Yoder (62,63). Gravity settling and diffusion were the only filtration

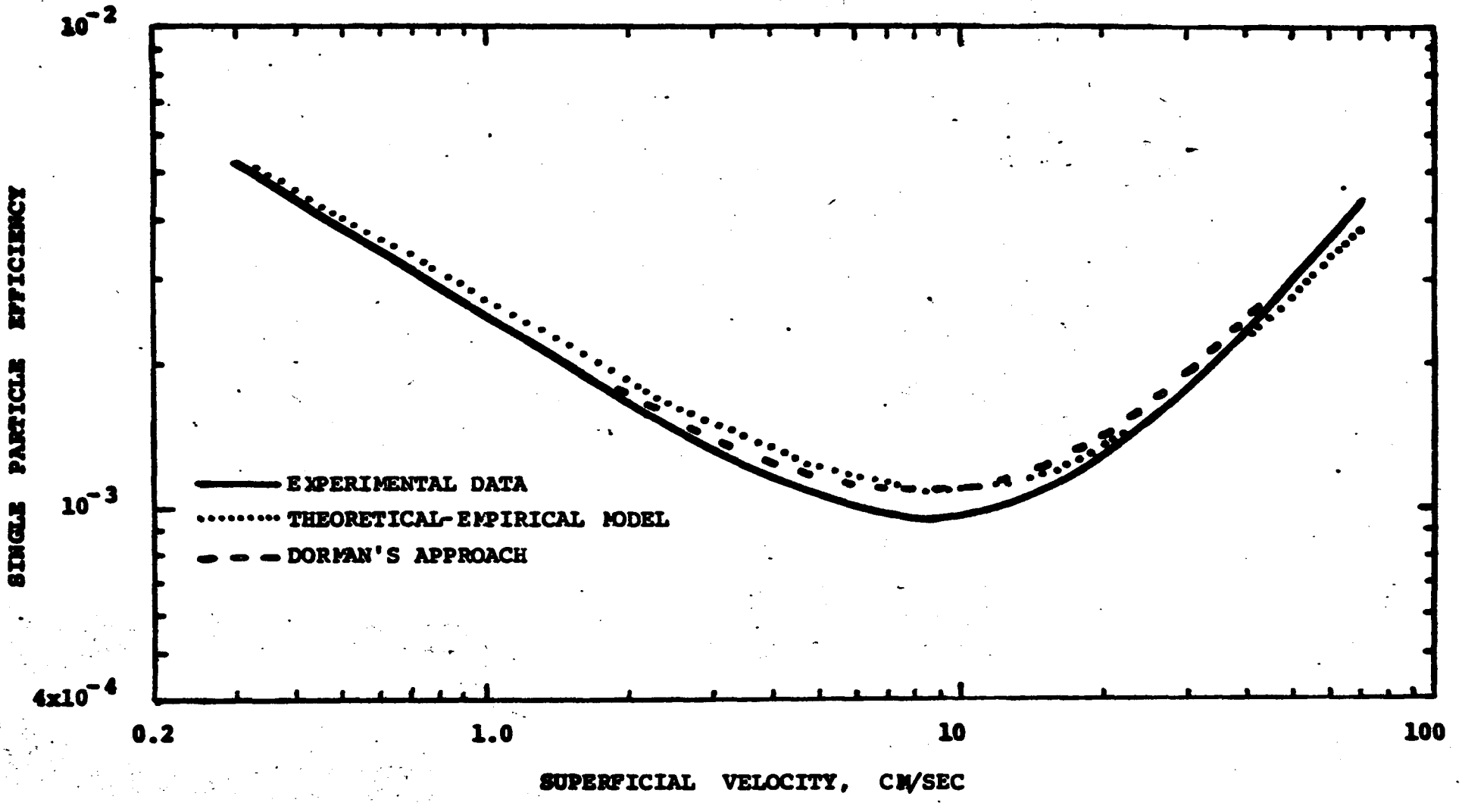

Figure 28. Comparison of experimental data with different models (10-14 mesh sand, upshot flow).

mechanisms prevalent in their work. Since they studied the effect of aerosol diameter on the penetration, the filtration equation becomes

$$E_T = E_D + E_G(\uparrow)$$

$$= D_1 \Delta^{2/3} + G_1 (r_p^2 C)^{1/2} \qquad (69)$$

where Δ is the diffusion coefficient and C is the Cunningham correction, both of which are functions of the aerosol size, r_p. The expression becomes too cumbersome if written solely in terms of r_p, so it is left as is.

At the particle size of maximum penetration

$$\left.\frac{dE_T}{dr_p}\right|_{r_{p_{max}}} = 0$$

so

$$\frac{dE_T}{dr_p} = D_1 \frac{2}{3}(\Delta^{-1/3}) \frac{d\Delta}{dr_p} + G_1 \frac{1}{2}(r_p^2 C)^{-1/2} \frac{d(r_p^2 C)}{dr_p}$$

but

$$C = 1 + \frac{\Theta}{r_p}$$

and

$$\Delta = \frac{\varphi C}{r_p}$$

with Θ and φ being independent of r_p. Setting the derivative equal to zero at $r_{p_{max}}$ and solving for G_1 gives

$$G_1 = D_1 \frac{4}{3} \frac{\Delta^{2/3}}{(r_p{}^2 C)^{1/2}} \frac{(2C - 1)}{(C + 1)} \Bigg|_{r_{p_{max}}} \tag{70}$$

$$= D_1 K$$

where K is a function of $r_{p_{max}}$ only.

Substituting for G_1 in equation (69) yields

$$E_T = D_1 \left[\Delta^{2/3} + K (r_p{}^2 C)^{1/2} \right]$$

or

$$D_1 = \frac{E_T}{\left[\Delta^{2/3} + K (r_p{}^2 C)^{1/2} \right]} \tag{71}$$

The experimental values of E_T are divided by $[\Delta^{2/3} + K(r_p^2 C)^{1/2}]$ at various values of r_p. The average of these ratios gives D_l. G_l is then obtained from equation (70).

The above modification of Dorman's curve fitting technique was applied to some of the data of Thomas and Yoder (62), obtained with a face velocity of 0.545 cm/sec and a bed height of 3.6 cm. Two sand sizes were used, 8-20 mesh and 40-50 mesh. The original data are presented in Figure 29. The equations obtained were compared with the theoretical-empirical model developed in this work. The relationships are:

***8-20 mesh

Dorman's curve fitting technique

$$E_T = 12\ Pe^{-2/3} + 6.1\times10^{-2}\ N_G^{1/2} \qquad (72)$$

Theoretical-empirical model

$$E_T = 14\ Pe^{-2/3} + 1.5\times10^{-2}\ N_G^{1/2} \qquad (73)$$

***40-50 mesh

Dorman's curve fitting technique

$$E_T = 9.8\ Pe^{-2/3} + 1.3\times10^{-1}\ N_G^{1/2} \qquad (74)$$

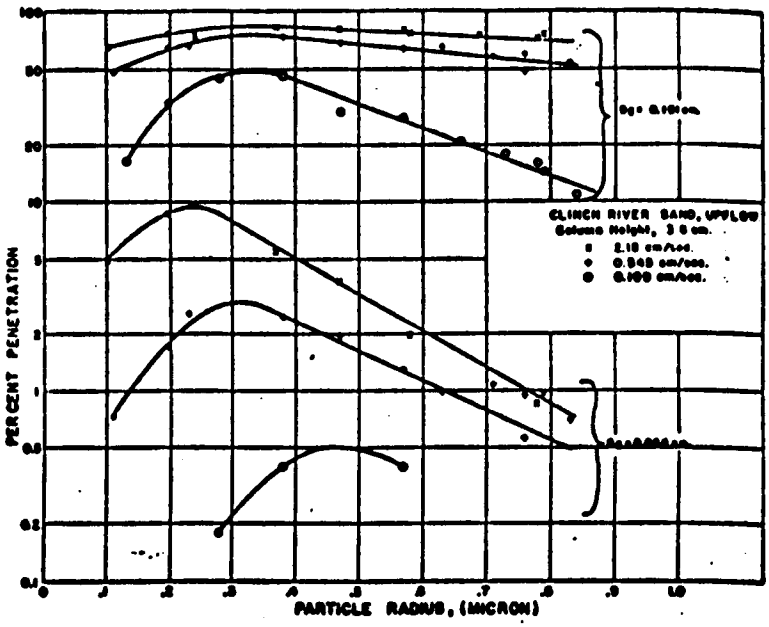

Fig. 3.—Penetration of homogeneous DOP aerosols through two size-fractions of Clinch River sand (8-20 mesh, D_g = 0.161 cm.; 40-50 mesh, D_g = 0.036 cm.).

Figure 29. Data from Thomas and Yoder (62) used to test filtration model.

Theoretical-empirical model

$$E_T = 14\ Pe^{-2/3} + 1.5x10^{-2}\ N_G^{1/2} \qquad (75)$$

The curves suggested by the above expressions and the experimental data are presented in Figure 30. Both models (Dorman's curve fitting technique and the theoretical-empirical model) show excellent agreement in the diffusion regime. However, the theoretical-empirical model indicates poor correspondence with the experimental data in the gravity settling regime. Even Dorman's curve fitting approach, which essentially forces an expression to fit experimental data, shows mediocre agreement with the experimental data in the gravity settling regime for the 40-50 mesh sand.

The penetration data of Thomas and Yoder, when expressed in terms of E, show an extremely sharp transition from one regime to the other. This was characteristic of most of their data. This contrasts with the smooth transition obtained with the experimental data of this investigation. This phenomena, and the poor agreement with the data in this work at higher values of r_p, lends credence to the possibility that the lack of suitable entrance and exit sections caused

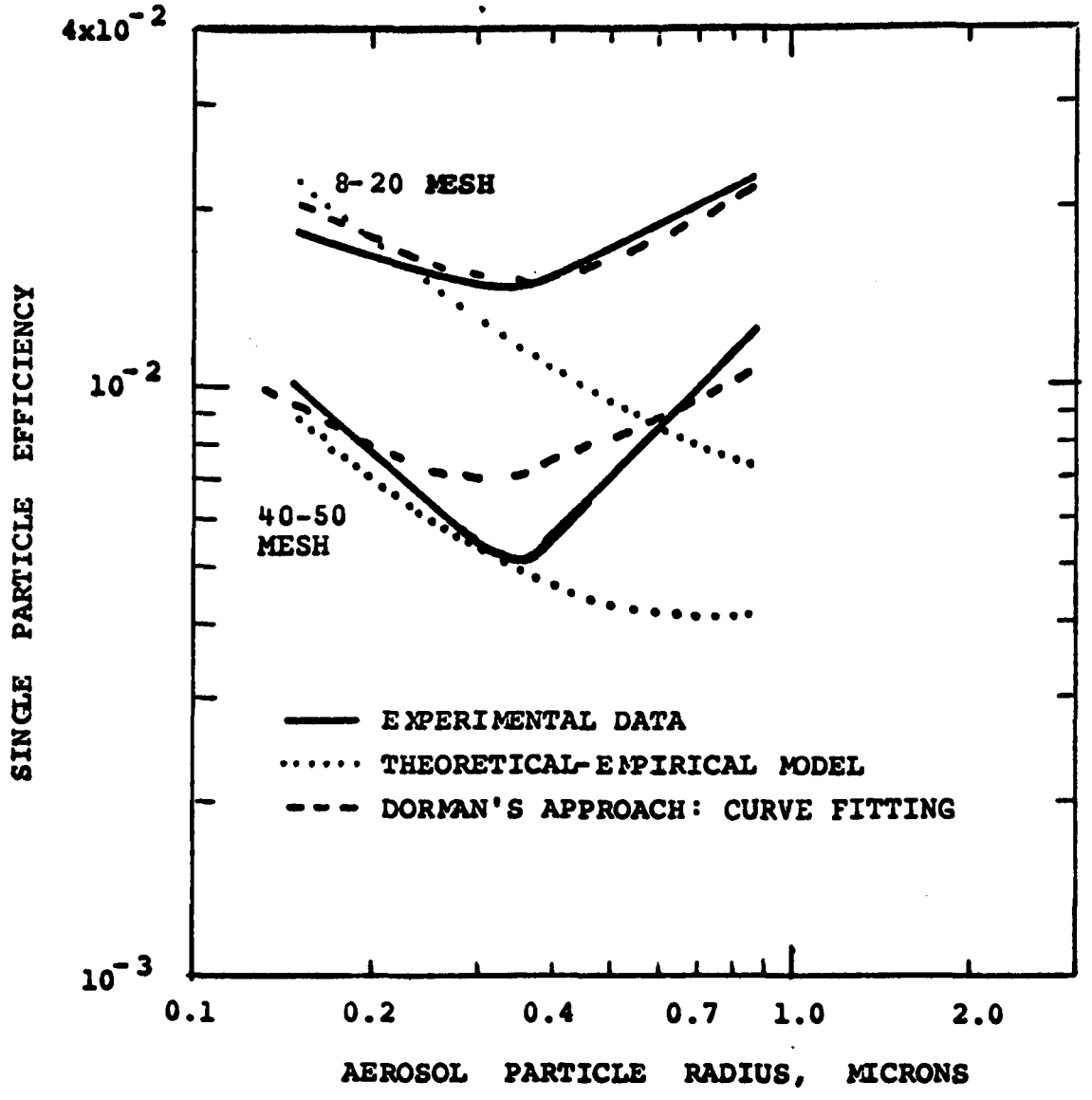

Figure 30. Comparison of experimental data of Thomas and Yoder (62) presented in Figure 29 with different models.

Superficial velocity = 0.545 cm/sec
Bed height = 3.6 cm

the difference, for as r_p increases, the effect of inertia increases.

10. DISCUSSION

Since the results have been discussed as they were presented, this section is confined to some general comments.

The deviation between theory and experiment, in diffusion for example, is not as serious as it appears if one takes into account that a relatively small error in ξ can cause a large error in E.

Equation (28) is the relationship used to reduce the overall penetration through the sand bed (ξ) to the single particle collection efficiency (E). Thus

$$\xi = \exp - \frac{3}{4} \frac{1 - \epsilon}{\epsilon} E \frac{b}{r_c}$$

or, upon rearranging

$$E = - (\ln \xi) \frac{4}{3} \frac{\epsilon}{1 - \epsilon} \frac{r_c}{b}$$

The standard error in E is obtained by computing the variance of E. Thus

$$(\delta E)^2 = \left(\frac{\delta E}{\delta \xi}\,\delta\xi\right)^2 + \left(\frac{\delta E}{\delta \epsilon}\,\delta\epsilon\right)^2 + \left(\frac{\delta E}{\delta r_c}\,\delta r_c\right)^2 + \left(\frac{\delta E}{\delta b}\,\delta b\right)^2 \tag{76}$$

or

$$(\delta E)^2 = \left(\frac{E}{\ln\xi}\,\frac{\delta\xi}{\xi}\right)^2 + \left(\frac{E}{1-\epsilon}\,\frac{\delta\epsilon}{\epsilon}\right)^2 + \left(E\,\frac{\delta r_c}{r_c}\right)^2 + \left(E\,\frac{\delta b}{b}\right)^2 \tag{77}$$

The standard deviation is just the square root of the variance. If the standard deviation is divided by the value of E of interest, the relative error in E can be computed. Thus

$$\frac{\delta E}{E} = \left[\left(\frac{1}{\ln\xi}\,\frac{\delta\xi}{\xi}\right)^2 + \left(\frac{1}{1-\epsilon}\,\frac{\delta\epsilon}{\epsilon}\right)^2 + \left(\frac{\delta r_c}{r_c}\right)^2 + \left(\frac{\delta b}{b}\right)^2\right]^{1/2} \tag{78}$$

Each of the constituent terms of the above expression will be considered separately. The

contribution from ξ is not linear, and will depend on the value of ξ . ξ values of 0.80 and 0.20 will be taken to be representative of this work. The average experimental variation was of the order $\delta\xi = \pm 0.03$ for the velocity vs penetration data. For the purpose of comparison, the same approximate order of experimental variation will be assigned to the data of Thomas and Yoder (62,63), i.e., 10%. It appears that only one measurement was made for each of their data points, while in this work at least ten and often as many as twenty measurements were performed to get a data point on the velocity-penetration curve. A representative value of the penetration for the work of Thomas and Yoder is of the order 0.02 .

The average value of the porosity was 0.42, and it is not unreasonable to assume that there was at least a $\pm$ 0.02 variation in ϵ .

Focusing attention now on r_c , the radius of the sand grains, the average of the two mesh cuts was taken as its value. The sand cuts used in this work were 10-14 and 20-30 mesh. Looking at the table below:

Mesh Size	Opening (cm)	Average (cm)
10	0.200	0.17
14	0.141	
20	0.084	0.071
30	0.059	

it is perfectly possible to have as much as a 15% deviation from the average. A variation of 5% will be assigned to the variation in r_c .

The contribution from b would depend on the bed thickness. Taking 1/2 of the smallest calibrated division on the ruler as the error, or ± 0.05 cm, the error would be less than one percent with a 8.2 cm bed and can be considered to be negligible.

The following table can be constructed:

Percentage Error in E due only to	Term	Value of Penetration 0.80	0.20	0.02
ξ	$\frac{1}{\ln \xi} \frac{\delta \xi}{\xi}$	17	10	3
ϵ	$\frac{\epsilon}{1 - \epsilon} \frac{\delta \epsilon}{\epsilon}$	8	8	8
r_c	$\frac{\delta r_c}{r_c}$	5	5	5
Total Variation in E		21	16	13

On the basis of the above table, the agreement between theory and experiment appears quite good.

Thomas and Yoder (62) demonstrated that two different sands, one coarse and one fine, with the same mesh cuts and with only a 0.03 difference in the porosity can have as much as a four-fold difference in the penetration (Figure 24). This difference (ξ = 0.20 and ξ = 0.05) translates into a two-fold difference in the single particle collection efficiency.

The question of whether a critical value of N_I exists warrants further comment. Recall that the theoretical model has shown that there is a value of N_I below which no capture by inertial impaction occurs. This directly conflicts with the experimental observations. The free surface model does not allow, for example, for deposition on the back of the collector. Zimon (68) indicates that with high velocities, eddies are created, and particles can be deposited on the back.

Davies (14) asserts that when a particle is approaching the collector the inertial parameter alone is no longer a sufficient method of characterizing collection because the Brownian motion of the particle becomes significant. He further criticizes the

treatment whereby the flow around the particle is entirely neglected and the particle is considered as a point except for its drag and its interception by the collector. Both of the above criticisms apply to the inertial impaction model used in this work.

Table 5 lists the values of the dimensionless parameters typical of this work.

Table 5. Representative Values of Parameters in This Work

	Superficial Velocity (cm/sec)			
	0.3	1.0	10	70
Peclet Number				
10-14 mesh	2.0×10^{-7}	6.8×10^{-7}	6.8×10^{-6}	4.8×10^{-5}
20-30 mesh	8.5×10^{-8}	2.8×10^{-7}	2.8×10^{-6}	2.0×10^{-5}
Inertial Parameter				
10-14 mesh	1.5×10^{-5}	5.1×10^{-5}	5.1×10^{-4}	3.5×10^{-3}
20-30 mesh	3.7×10^{-5}	1.2×10^{-4}	1.2×10^{-3}	8.6×10^{-3}
Gravity Settling Parameter				
Independent of sand size	1.4×10^{-2}	4.3×10^{-3}	4.3×10^{-4}	6.2×10^{-5}
Direct Interception Parameter				
10-14 mesh		6.5×10^{-4}	Independent of Velocity	
20-30 mesh		1.6×10^{-3}		
Reynolds Number (Particle)				
Independent of sand size	2.2×10^{-4}	7.3×10^{-4}	7.3×10^{-3}	5.1×10^{-2}
Reynolds Number (Collector)				
10-14 mesh	3.4×10^{-1}	1.1×10^{0}	1.1×10^{1}	7.9×10^{1}
20-30 mesh	1.4×10^{-1}	4.7×10^{-1}	4.7×10^{0}	3.3×10^{1}

11. CONCLUSIONS

The experimental results show that a velocity of maximum penetration exists. Reduction of the aerosol filtration data to single particle collection efficiencies indicates that there is no effect of bed height on the single particle collection efficiency. It is also noted that the experimental single particle collection efficiencies are larger for the finer sand in the velocity range investigated.

At low velocities the primary means of capture is by diffusion and gravity settling, the influence of which decreases as the velocity increases. The "free surface" model predicts that collection by Brownian diffusion depends only on the dimensionless Peclet number and a complex function of the bed porosity. The theoretical expression correlates the experimental data fairly well.

The effect of gravity settling can be considered to be superimposed on the other mechanisms. Gravity settling is an appreciable effect at velocities less than 10 cm/sec for the 1.1 micron diameter polystyrene aerosol, but its influence decreases with increasing velocity. Gravity settling is responsible for the

differences between the upshot and downshot efficiencies. This difference can be correlated solely in terms of the dimensionless gravity settling parameter. Data from other investigators also appear to follow this correlation.

Filtration efficiencies of aerosols by direct interception can also be predicted using the free surface model. The influence of direct interception is independent of velocity and depends only on aerosol and collector size. In the experiments performed here, however, this effect is negligibly small.

Prediction of single particle efficiencies by inertial impaction using the free surface model confirms the existence of a critical value of the inertial parameter, predicted earlier for a single target sphere, and is in agreement with the value reported in the literature for a voidage of 1.0 (single collector). The critical value was much higher than the values of the inertial parameter for which data were obtained in these experiments, indicating that either impaction was not a significant means of capture or that the theoretical model was not correct. An empirical correlation for collection by inertial impaction was presented.

The methodology of Dorman, the addition of

the individual collection efficiency for each mechanism to obtain the overall collection efficiency of a system, appears to be reasonable for correlating the experimental data.

The relationship for the single particle collection efficiency for upshot flow is:

$$E_T(\uparrow) = 5.04\ \rho(\epsilon)^{-1/3}\ Pe^{-2/3} + 1.5\times10^{-2}\ N_G^{1/2} + 2.0\ N_I^{9/8} + 3\ \rho(\epsilon)^{-1}\ R^2$$

In order to obtain the single particle efficiencies for downshot flow it is only necessary to add the term

$$8.4\times10^{-2}\ N_G^{0.78}$$

which accounts for the difference between upshot and downshot single particle collection efficiencies.

12. RECOMMENDATIONS FOR FURTHER WORK

The discrepancy between the calculated and the experimental results in the inertial impaction regime is quite large and therefore further work is in order. It is quite possible there may be errors in the experimental data, but this is unlikely in view of the fact that the exponent on the inertial parameter in this work was 9/8, and Friedlander's correlation on fibrous filters gave an exponent of 6/5. It may be necessary to call into question the classical procedure of estimating collection efficiencies by summing the independent effects of the several collection mechanisms. In an analysis which simultaneously considers inertial impaction together with the other mechanisms, the critical value of N_I may turn out to be below the values indicated in the calculations.

The first obvious step is to increase the velocity range investigated, so as to have values of the inertial parameter in the region where the model predicts collection by inertial impaction goes to zero.

The variation of aerosol particle size (about

six fold) in the work of Thomas and Yoder should be extended, using tapered entrance and exit sections. This should help clear up the uncertainty with which the gravity settling calculations were performed. In this way the effect of gravity settling could be totally isolated from diffusion.

The effect of sand size on the collection efficiency should also be investigated to a greater extent. The use of a very small grain size would increase the value of the direct interception parameter and increase collection by this mechanism.

With a wide range of data on sand size and aerosol size an analysis of the Dorman type could be performed on the experimental data, and a complete test of the filtration model could be performed.

PART TWO: FLY ASH STUDIES

13. BACKGROUND

Introduction

The conventional method of removing fly ash from the stack gases of a coal-fired power plant is electrostatic precipitation. In theory, an electrostatic precipitator can afford an efficiency approaching 100 percent. In practice, consistently high efficiencies are difficult to achieve. The precipitator can only collect dusts of high electrical resistance. Upon cleaning the electrodes the dust aggregates should fall into the dust bunker; however, detached or loosened dust sometimes escapes and is re-dispersed in the cleaned gas. Brandt (6) enumerates many of the shortcomings of electrostatic precipitators. Slight changes in operating conditions, such as a 12 to 18 percent increase in the gas flow can double dust emissions. Different fuel compositions also alter the operating conditions.

Clearly, an effort to find a new method for cleaning the stack gas of a power station of fly ash

would be worthwhile. If, in addition to dealing with particulate matter, the new method could also remove SO_2 , all the more reason to pursue its development.

Development of Granular Gas Treating Devices

Squires and Pfeffer (55) have summarized the development of granular bed filters. The use of a bed of granular solids to treat a gas can be traced to the Deacon Process Reactor of the last quarter of the 19th century (41). The bed illustrated in Figure 31 is held in place by louvered walls which resemble venetian blinds. This unit provided a quick way to dump the short-lived Deacon catalyst, clay soaked with copper chloride, a portion at a time without having to shut down completely and cool the reactor. Additional virtues of this unit were its low pressure drop and high gas-treating capacity. This reactor was used until about 1910, when the Deacon technique was replaced by the electrolytic process.

Baggaley in 1903 (4) proposed that a device similar to the one in Figure 31 be charged either with an alkaline solid or with charcoal to remove SO_2 in the offgas from the smelting of sulfide ores. Baggaley's

method offers a way to eliminate the power station's electrostatic precipitator and replace it with a unit that can deal with SO_2 and fly ash simultaneously. Candidate solids for use in the panel for simultaneous removal of these pollutants are the alkalized alumina developed by the U.S. Bureau of Mines, copper oxide, and half-calcined dolomite.

Modes of Operations of Panels

Spent catalyst was withdrawn from the bottom of the Deacon reactor. An extensive patent literature has arisen disclosing panel bed devices with bottom take off of spent solid.

Several methods have been disclosed in the patent literature for removing filter cake and spent solid from the gas-entry surfaces of the panel. Each gas-entry surface is a free, loose surface of the filter solid, inclined at its angle of repose and resting upon a louver.

Fiechter (19) and Gavett (26), in devices for gas and liquid filtration respectively, would provide plows which travel horizontally along the gas-entry face of the panel, one plow for each fluid-entry surface to

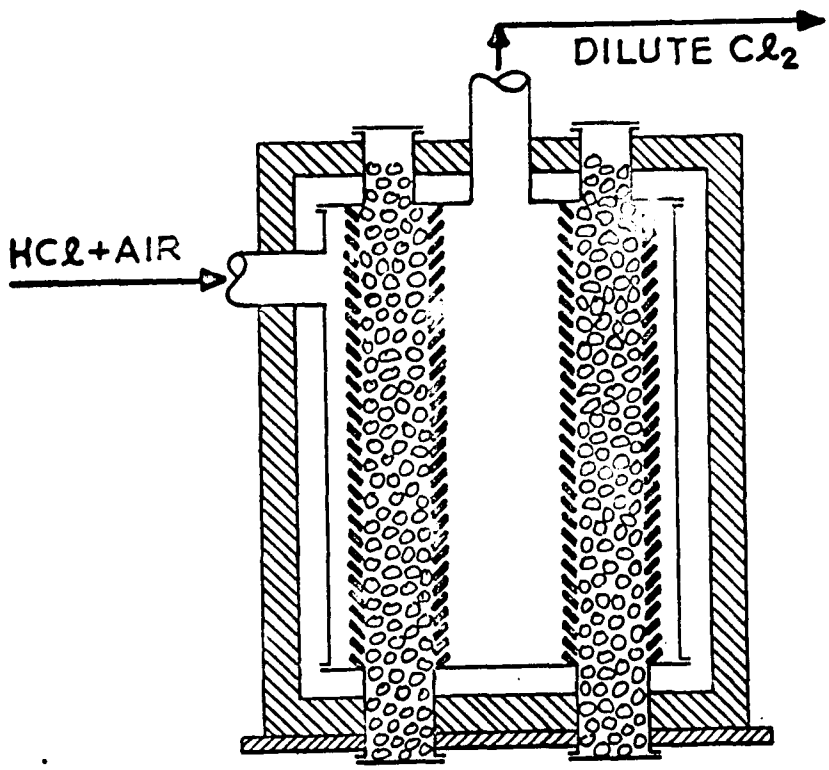

DEACON PROCESS REACTOR

Figure 31. Panel Bed Reactor for Deacon Process. The twelve-sided, nearly circular panel was housed in a circular steel shell within a brick furnace. The catalyst space was three feet across, and both outer diameter and height were about 15 feet. The catalyst space was divided by partitions into six segments, one of which was dumped and renewed each fortnight [ ].

scrape away a layer of filter solid together with accumulated filter cake. Fournier (21) would provide louvers which pivot about their inner edges, so that filter solid may be spilled from the gas-entry face. A patent by Rigg (49) did not disclose a panel bed device, but does suggest that another satisfactory alternative would be to induce an inward motion of the louvers which support the gas-entry surfaces. Squires (53) discovered that filter cake and a controlled amount of filter solid can be removed from each gas-entry surface by applying a surge backflow of gas from the clean side of the panel.

Panels have been disclosed employing screens to retain free surfaces of filter solid, yet permitting removal of filter cake by a blowback technique (31,67). These devices would not seem well suited for simultaneous removal of fly ash and SO_2 .

The use of panels with side take-off of spent solid and Squires' surge-backflow technique seems to be the most promising for simultaneous removal of fly ash and SO_2 .

Selection of Operating Conditions

Some idea of the performance to be expected from a panel bed device can be gleaned from the few practical results to be found in the literature.

Fairs and Godfrey (18) described a panel filter used in a contact acid plant burning sulfur. Granite chips, probably all between about 1/8 and 1/2 inch were held in a panel much like that seen in Figure 31. The panel was one foot across in the narrow direction and 12 feet tall. The face velocity was about 125 ft/min. Filtration efficiency was said to be 96% for a dust smaller than 76 microns (65% under 53 microns, 24% under 26, and 5% under 13). Dust loading was 0.006 grams/m^3 . Pressure loss was 0.8 inches water for the clean filter, rising to 6 inches water when the filter was taken out of service for cleaning. The service life was not given, but was undoubtedly many days or even weeks.

The preceding two panels were dumped intermittently. M. I. Dorfan (1) built four units with continuous downward movement of the column of solid. Each handled 17,000 ft^3/min. They collected asbestos rock dust which was all smaller than 100 mesh and

60% smaller than 10 microns. Loading was 14 grams/m^3, and collection efficiency was said to be 96.7%. Collecting granules were 1/2x1-1/2 inches.

Strauss and Thring (58) conducted field tests of a horizontal filter on fumes from an oxygen-laced open-hearth furnace. Gas flow was downshot at superficial velocities between 50 and 200 ft/min. The filter bed was comprised of crushed brick between about 0.1 and 0.3 inches. Loading varied widely, from about 0.11 to nearly 11 grams/m^3. Collection efficiencies in 9 and 10-1/2 inch beds generally fell between about 85 and 95%.

The only granular bed device that apparently achieved considerable acceptance for dust filtration is Lurgi's "gravel bed filter," described by Englebrecht (17). The filter is horizontal, and is held on a sieve plate. The gravel used has a diameter of about 3-16 mesh. The gas flow was upshot, at superficial velocities of about 50-160 ft/min. The pressure loss ranged from 2-6 inches water. Collection efficiencies for dust reached over 99% at loadings of 5 to 14 grams/m^3. Periodically, the flow of dirty gas was interrupted, and the bed was shaken to cause the collected dust to fall from the bed

into a hopper below. There was a flexible seal between the bed and the side of the walls of the containing box, so that the bed could be vibrated independently of the remaining structure. The flexible seal put an operating temperature limit on its use.

Brandt (6) criticized the Lurgi bed, for the wear and tear on the seal and its temperature limitation. Finer sand could not be used to achieve a higher efficiency without a reduction in throughput or failure on account of fluidization of the sand. This device has been withdrawn from the market by Lurgi and replaced with a newer unit.

The panels developed by Squires (53,54) overcome the above difficulties. The simplicity of the design and the lack of any mechanical seal removes the temperature limitations of the Lurgi design.

It is doubtful that the power industry would welcome a new device to collect fly ash which falls short of 99% collection efficiency. The foregoing data from the literature leads one to consider much lower face velocities and smaller collecting solids so a stable filter cake can form. The presence of a cake resting upon the free surface of sand across which the dirty

gas enters the bed will enhance the filtration efficiency of the unit (55).

Studies of Filter Cake Formation

A synopsis of the formation of dusts of various types on fabric filter media was made by First and Silverman (20). It was mentioned that the efficiency of deposition of particles increases with time of operation, for the particles initially retained on the fibers act as secondary collectors, presenting additional targets for the impinging dusts. This surface dust is important in the retention of the fines, for the efficiency of cake filtration is greater than that of media filtration. As the efficiency increases, the resistance to flow also increases, and a means of cleaning the filter elements must be devised. After a number of cleanings following periods of filtration, the cleaned filter "initial" resistance (the resistance just after cleaning) no longer increases. The filter is then considered to be "loaded" and the peak initial efficiency is obtained. This behavior permits one to distinguish between permanent and removable dust. The most advantaneous method for cleaning the filter medium is to impart a

shock to the filter, i.e., mechanical shaking or intermittent pulses of reverse air flow. A steady reverse flow does not accomplish any cleaning.

First and Silverman (20) reported, for example, that flocking a bag filter with asbestos floats, to the extent of 0.0135 grams/cm^2, raised the collection efficiency for 1.2 micron oil smoke from 20.3 to 99.9%. Fuchs (25) reviewed work by Eliseev on the formation of deposits of fine powders on metal gauze. The deposits were said to have a solid volume fraction of only 6%, yet were "impervious" to the lead and zinc oxide smokes from which the deposits had been made.

These considerations give confidence that a panel bed operating in a cyclic manner allowing a filter cake to form will provide collection efficiencies higher than 99%.

Borgwardt, Harrington and Spaite (5) reported the filtering characteristics of fly ash filtered from the flue gas of a pulverized coal fired power plant. The fly ash was collected on fabric filters in a baghouse. The characteristics of the filter cake, (i.e., its specific resistance) varied with the operating conditions

under which it was formed. The pressure loss through the filter and the cake was reported in the form:

$$\text{Filter Drag} = \frac{\Delta P\ A}{Q} = R_s\ w + S_R \qquad (79)$$

where:

ΔP = pressure drop across filter (inches water)

Q = gas flow rate (ft^3/min)

A = filter area(ft^2)

R_s = specific resistance of dust [inches water/(ft/min velocity-lbs dust/ft^2)]

w = dust mass on filter (lbs dust/ft^2)

S_R = residual drag of filter media (fiber plus unremoved dust present after cleaning) (inches water/ft/min velocity)

The factor R_s varied with the filtration velocity, as illustrated in Figure 32, and type of filter media used. The value of R_s, which ranged from about 7 to 16, first increased and then decreased as the velocity increased. The velocity ranged from about 1 - 5 ft/min, and the dust loading was about 4.6 grams/m^3. Collection efficiencies were not reported. Noteworthy was the fact that power

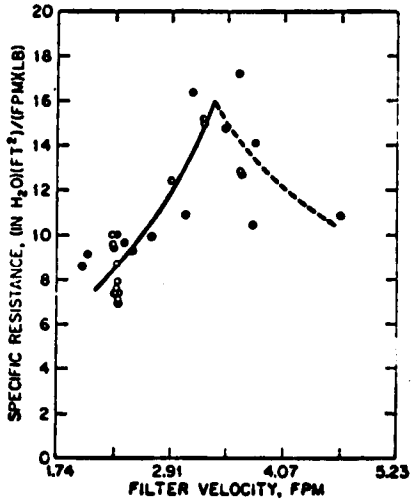

Fig. 2. Effect of filtration rate on specific resistance of fly ash. (Mercer field tests.)

Figure 32. Data from Borgwardt et al (5) indicating variation of specific resistance of filter cake with velocity.

station fly ash redispersed in the laboratory gave the same specific resistance values for the dust as did field tests.

A recent study by Taub (59) demonstrated the mechanism whereby fly ash is collected at velocities much higher and with sand particles much larger than those used in this work (0.5 to about 1.5 mm in diameter and 60 to 240 ft/min). A cone of fly ash, deposited primarily by inertial impaction, would form on the upstream face of each of the collector particles. Once a particular layer of sand was saturated with fly ash, the fly ash cones would develop on subsequent layers. When all the layers of the bed were saturated with the cones of ash, the filtration efficiency of the bed would go to zero.

Tests on Panel Bed Filters

Three panel bed filters were constructed by Squires (55). The salient results of tests on these filters will be reported.

(a) Test of Unit LS-1

The LS-1 panel, illustrated in Figure 33, was 1-3/8 inches wide in the horizontal direction parallel to the

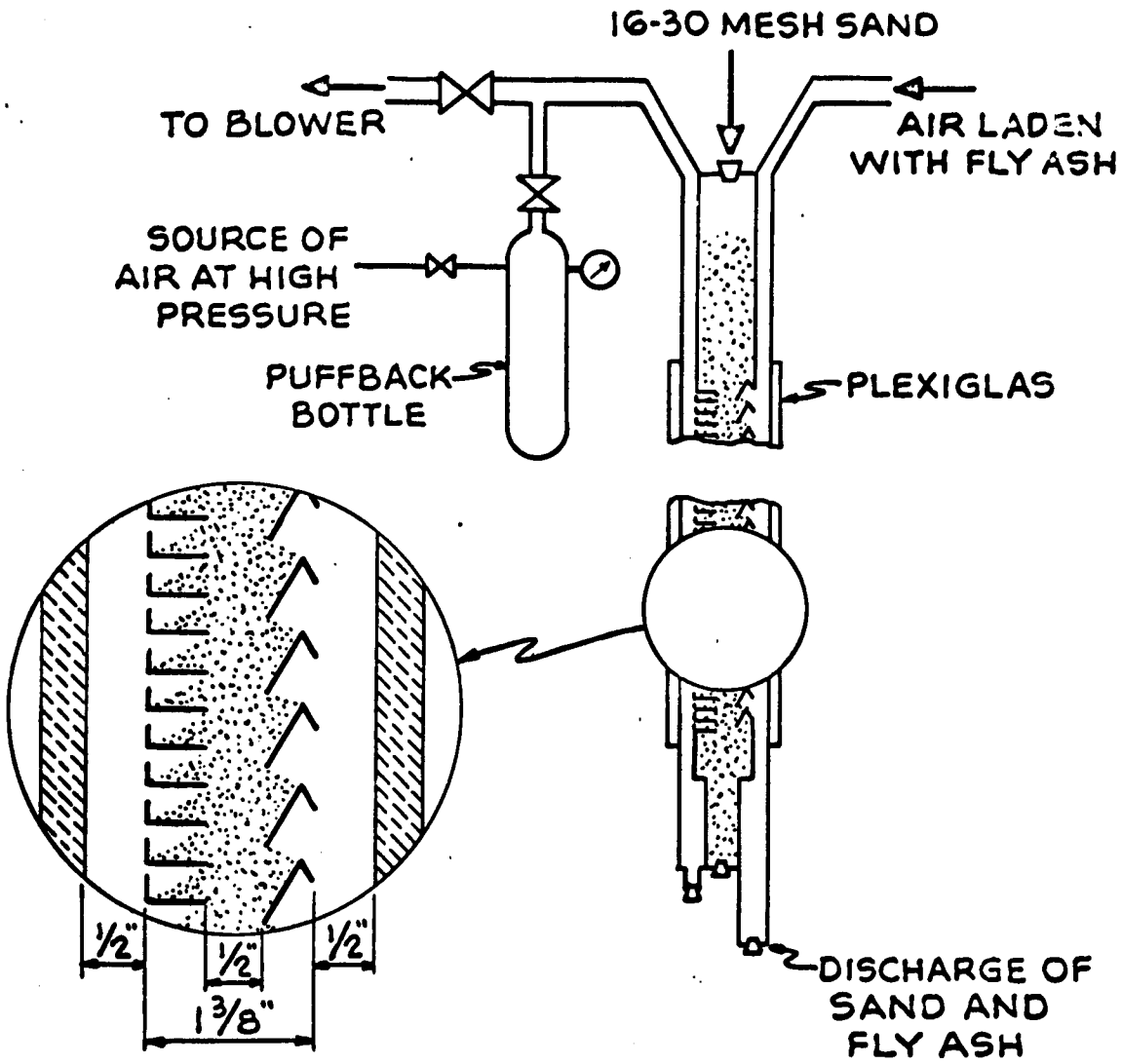

Figure 33. Arrangement of Unit LS-1 (55).

gas flow across the bed, 12 inches wide in the horizontal direction perpendicular to the gas flow, and 58 inches in height. Dirty gas flowed downshot in a space 1/2 inch wide adjacent to the "dirty" face of the panel, and clean gas flowed upshot in a similar space next to the "clean" face. Fly ash was dispersed into air from a fluidized bed, and drawn through the panel by a blower and passed through paper filters. No tests were conducted to determine the effectiveness of the dispersion technique. Collection efficiencies were judged from the weight increase upon the filters. The initial pressure loss across the bed at 12 ft/min was about 0.1 inches of water; a run was terminated when the pressure loss reached about 0.6 inches water.

The panel was cleaned by applying Squires' surge blowback or "puffback" technique, and the pressure drop was consistently restored to the initial value after a puffback.

Table 6 summarizes the main features of the results obtained from the tests conducted on this unit. The results appear highly encouraging.

This work demonstrated that filter sand need not be rendered free of ultra-fine particles when cleaned

Table 6. Summary of Tests on Unit LS-1 (from 55)

Air throughput	=	60 ft^3/min
	=	12 ft/min based upon panel area*
Loading of fly ash in dirty air	=	2 to 4 grains/ft^3 (4.6 to 9.2 grams/m^3)
Duration of run	=	30 to 50 minutes
Quantity of fly ash collected in a run	=	10 to 15 ounces (283 to 425 grams)
	=	2 to 3 oz/ft^2 (0.06 to 0.09 grams/cm^2) based upon panel area*
Pressure drop at start of run	=	0.1 inches water
Increase in pressure drop due to formation of fly ash filter cake	=	about 0.5 inches water
Crude filtration efficiency	=	99.7 to 99.9 percent
Puffback bottle volume	=	315 in^3
Puffback valve area	=	0.625 in^2
Puffback pressure	=	40 psig
Weight ratio of sand to fly ash in dumped material after puffback	=	about 2.5

*Area = 4.83 ft^2 = projected area of the panel. Notice this is not the area of the sand surface, used as basis for expressing results "per unit area" for ash and sand quantities in Chapters 14-18.

up for re-use in the panel. Sand used in the tests was merely screened for re-use and was not especially clean. It was coated with a floury material which dusted badly whenever the sand was poured. A test in which clean air was passed through the panel for 15 minutes showed negligible pick-up of the dust. This is understandable in light of the well-known difficulty of blowing a fine dust from a solid surface (10,11).

(b) Tests of Unit LS-2

This unit (Figure 34) was constructed entirely of plexiglas in order that the motion of the sand during puffback could be seen.

The effect of puffback is to cause the sand to move as a "plug" toward each fly ash bearing surface, throughout the panel from top to bottom. As illustrated in Figure 35 the pluglike character of the sand motion lifts each gas-entry surface and causes both fly ash and a thin layer of sand to spill from each surface. The precision of this phenomenon may be appreciated from the fact that the average sand spill achieved during operation of unit LS-1 amounted to removing a layer of sand having a depth approximately equal to the width of two average grains of sand.

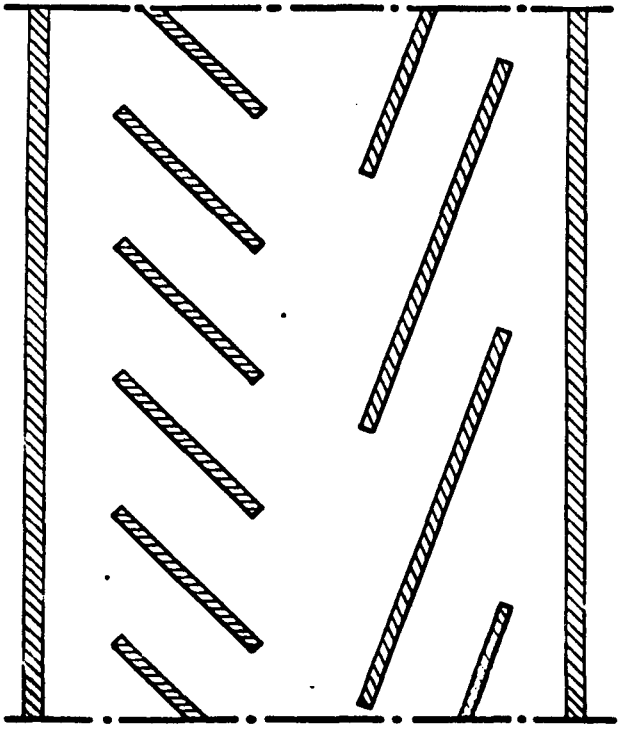

Figure 34. Cross-section of panel of Unit LS-2, fabricated entirely of plexiglas.

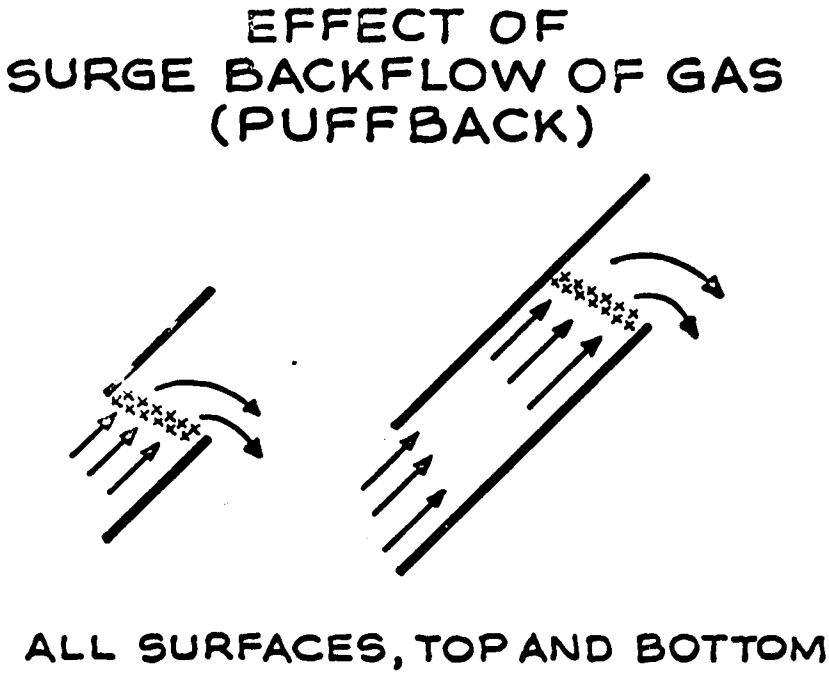

Figure 35. A surge backflow of gas (puffback) of sufficient intensity produces a plug-like movement of sand toward gas-entry surfaces (55).

Unit LS-2 was operated solely to study puffback, and no filtration efficiencies were measured.

All attempts to clean the LS-2 panel from either side by means of a steady backflow of gas failed. Any spilled sand arises from a narrow zone along the inner edge of the upper slat; the spilled sand originating from deep within the panel (Figure 36). The spilled sand contained no detectable quantity of fly ash.

Shock cleaning of fabric filters is fairly common. Smith (52) discovered that an explosive shock could dislodge the filter cake without disturbing the filter medium. The work on the LS panels is apparently the first demonstration that shock cleaning can both clean filter cake from a filter having many loose, renewable surfaces and also renew each surface without undue loss of filter solid.

(c) Test of Unit GSC-1

Figure 37 is a cross-section (to scale) of Unit GSC-1. The author of this dissertation participated in design and fabrication of this unit. The GSC-1 was designed to provide counter-current contacting of a gas and a solid within the panel. Dirty gas enters the panel from the right, and must flow upward through

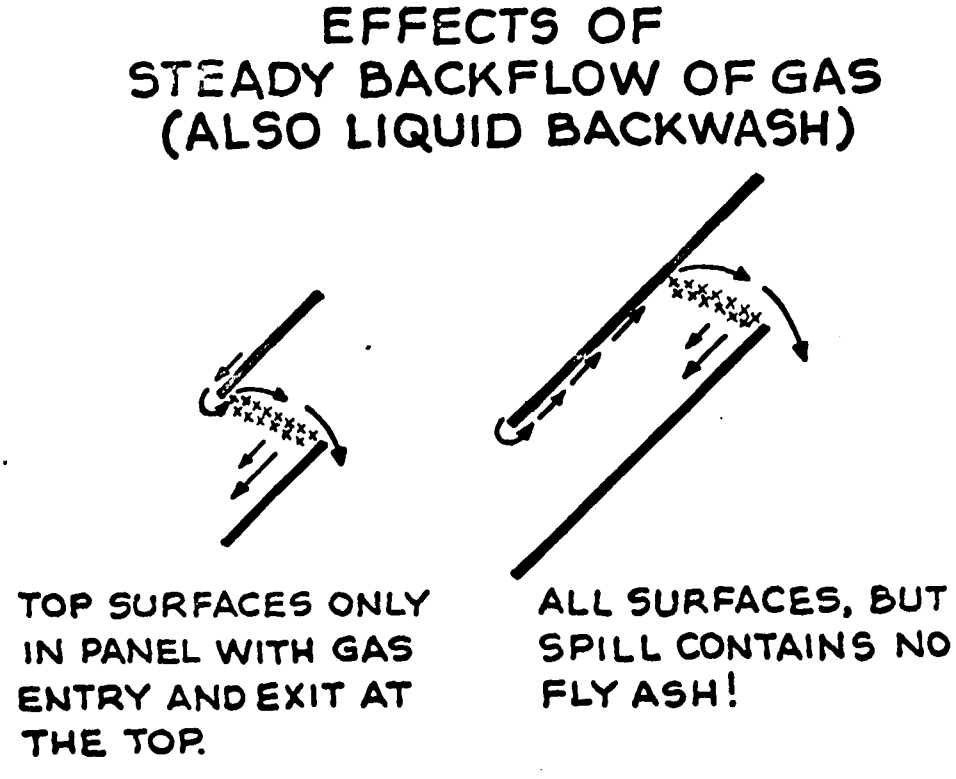

Figure 36. A steady backflow of gas produces a useless flow of sand from within the bed (55).

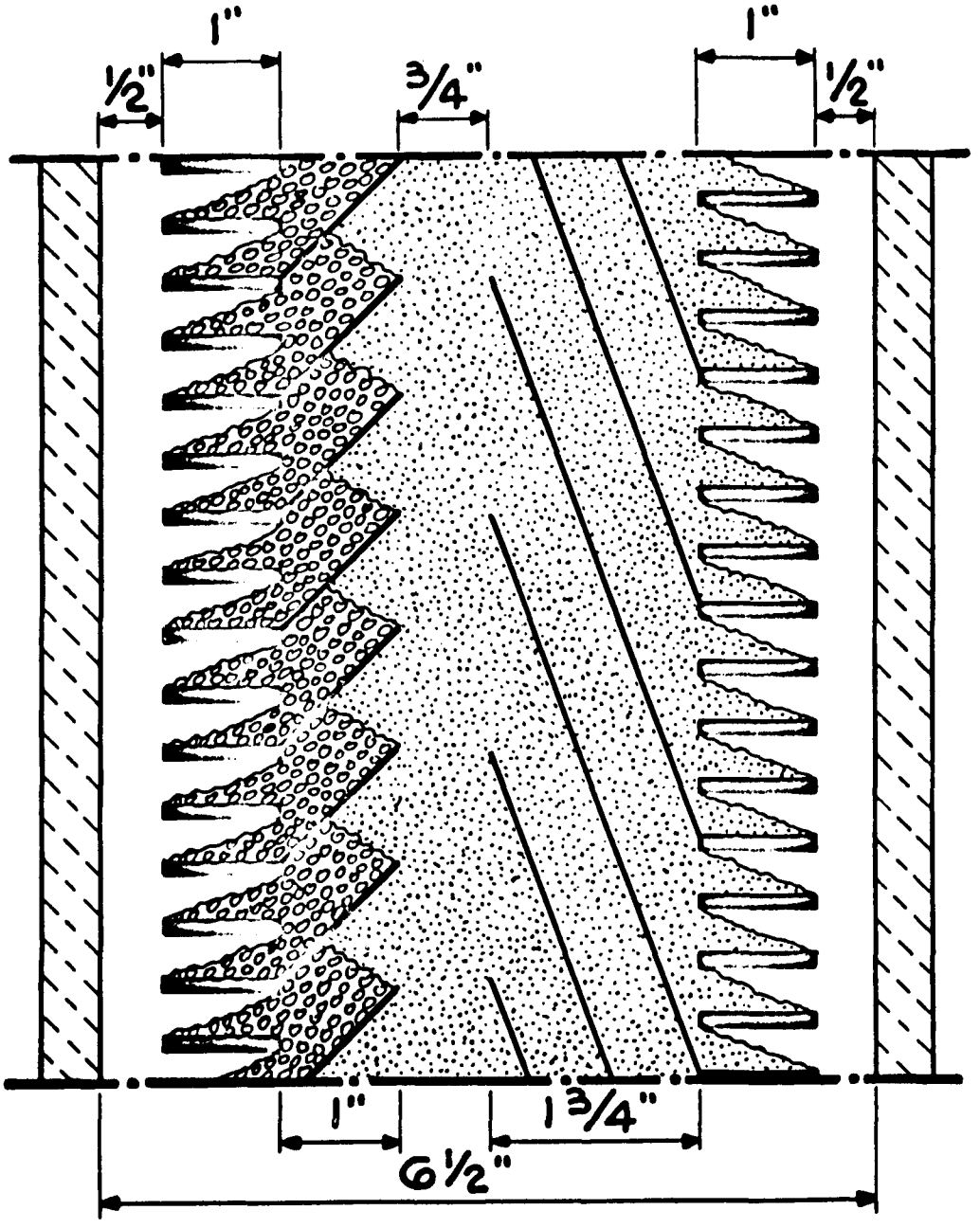

Figure 37. Cross-section of panel of Unit GSC-1. Flow of dirty gas is from left to right. The steeply inclined louvers define treating spaces which afford counter-current contacting of filtering granules and gas. The coarser solid at the left provides insurance against a spill from the clean face of the panel (55).

"gas treating spaces" lying between the steep louvers. When filter cake and spent treating solid are discharged from the gas-entry surfaces at the right of the panel, fresh solid enters each gas-treating space from above.

At the left of the panel, louvers are provided to retain a "sealing solid" of larger grain size. The presence of a coarser solid at the gas-exit face of the panel will permit higher face velocities without danger of a disastrous spill of treating solid from the clean face. The use of a sealing solid of high density would appear to be particularly important in conjuction with a treating solid of low density, such as alkalized alumina. The treating solid was 20-30 mesh sand and the sealing solid was 10-14 mesh sand.

Figure 38 shows the arrangement of the GSC-1 unit. The active portion of the panel was 15 inches wide and 26 inches tall. The entire unit was fabricated of plexiglas except for the inclined louvers, which were of brass. The flow of the dirty air was upshot in a 1/2 inch space at the right of the panel, and the flow of the cleaned air was upshot in a similar space at the left. Air entered or left via a horizontal slot, 1/4 inch wide and 13-1/2 inches in length.

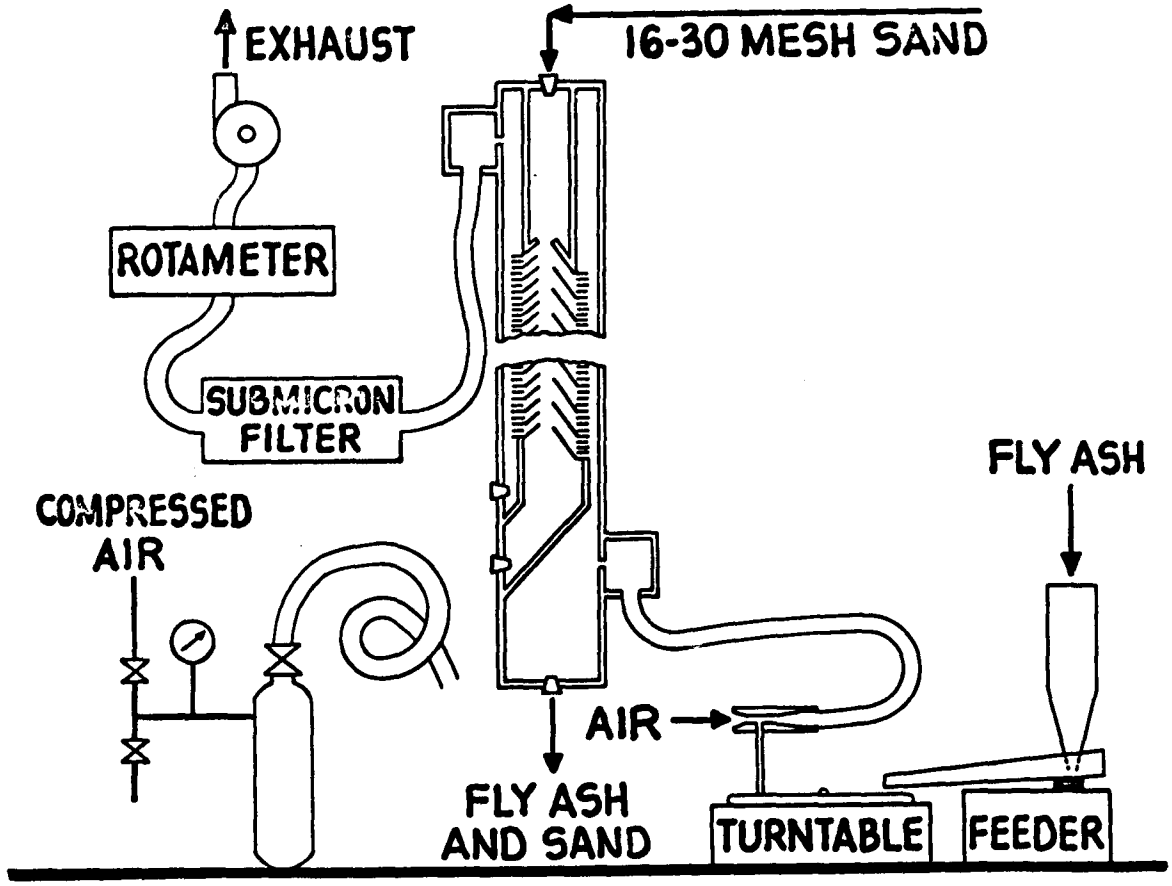

Figure 38. Arrangement of Unit GSC-1.

Fly ash was delivered through the use of a modified Harvard Feeder (56). A vibratory feeder delivered fly ash to a rotating turntable where it was picked up by a tube connected to the throat of a venturi. Air, which entered the system upstream of the venturi, was pulled through the unit by a blower.

The unit was cleaned by puffback, and the efficiency of the unit was obtained by measuring the weight change of filter cartridges placed downstream of the panel.

The initial pressure loss across the unit was about 2 inches of water, the final about 2.5 inches water at a face velocity of about 12 ft/min. The fly ash loading was of the order 4.6 grams/m^3. The crude filtration efficiencies were quite encouraging, in excess of 99.3%. However, the ash-to-sand ratio in the spent solid was somewhat low, about 4 grams of ash to 30 grams of sand.

A defect in the design was revealed by a slow leakage of individual grains of the 20-30 mesh sand from the clean face of the panel. These grains had evidently worked their way through the bed of sealing solid. The distance of the shortest path for flow of

gas through the bed of sealing solid was evidently too small, and much of the gas flow was concentrated along this path. Moreover, passages between the 10-14 mesh sand grains of the sealing solid lying against a flat louver were appreciably larger than passages between similar grains in the middle of the bed. A vertical, louvered space should be provided between the inclined louvers and the horizontal elements which retain the bed of sealing solid. In commercial practice, it would probably be necessary to provide for drainage of the sealing solid from time to time.

Experimental Plan

In light of the results obtained from the tests on the panels discussed in this chapter, it was felt that a more detailed understanding of the operation of a panel bed filter could be obtained from experiments performed on a small representative section of the panel.

Such experiments were undertaken, the plan being to obtain two kinds of information: (1) efficiency of filtration of fly ash from air passed across the

representative section of the panel, and (2) penetration of a monodispersed aerosol of 1.1 micron diameter polystyrene latex microspheres across the panel after a filter cake of fly ash had been deposited during the course of a filtration test. During the course of the work, need was felt for data on aerosol filtration through a filter cake of fly ash carefully deposited upon a horizontal sand surface, and such data were also obtained.

14. EQUIPMENT AND PROCEDURES

Horizontal Sand Bed

Figures 39 and 40 illustrate the horizontal sand bed with its accompanying equipment. The aerosol generator system and the 2 inch tapered sand bed unit from the dilute aerosol studies (see Chapter 6) were also used here.

Fly ash was deposited onto the sand surface in increments of from about 0.25 grams of ash to about 0.75 grams of ash. This is equivalent to a weight of ash deposited per unit area of sand bed between 0.0118 grams/cm^2 and 0.0352 grams/cm^2. The ash was introduced through the top of the tapered section, about 26 inches from the sand surface. After each incremental addition of fly ash, the pressure loss across the unit and the penetration of the test aerosol of 1.1 micron diameter Dow microspheres through the sand bed and filter cake were measured. The inlet aerosol concentration was of the order of 10^{-5} grams/m^3 (about 50 particles/cm^3).

The effects of variations in the method of adding the increments of fly ash on the structure of

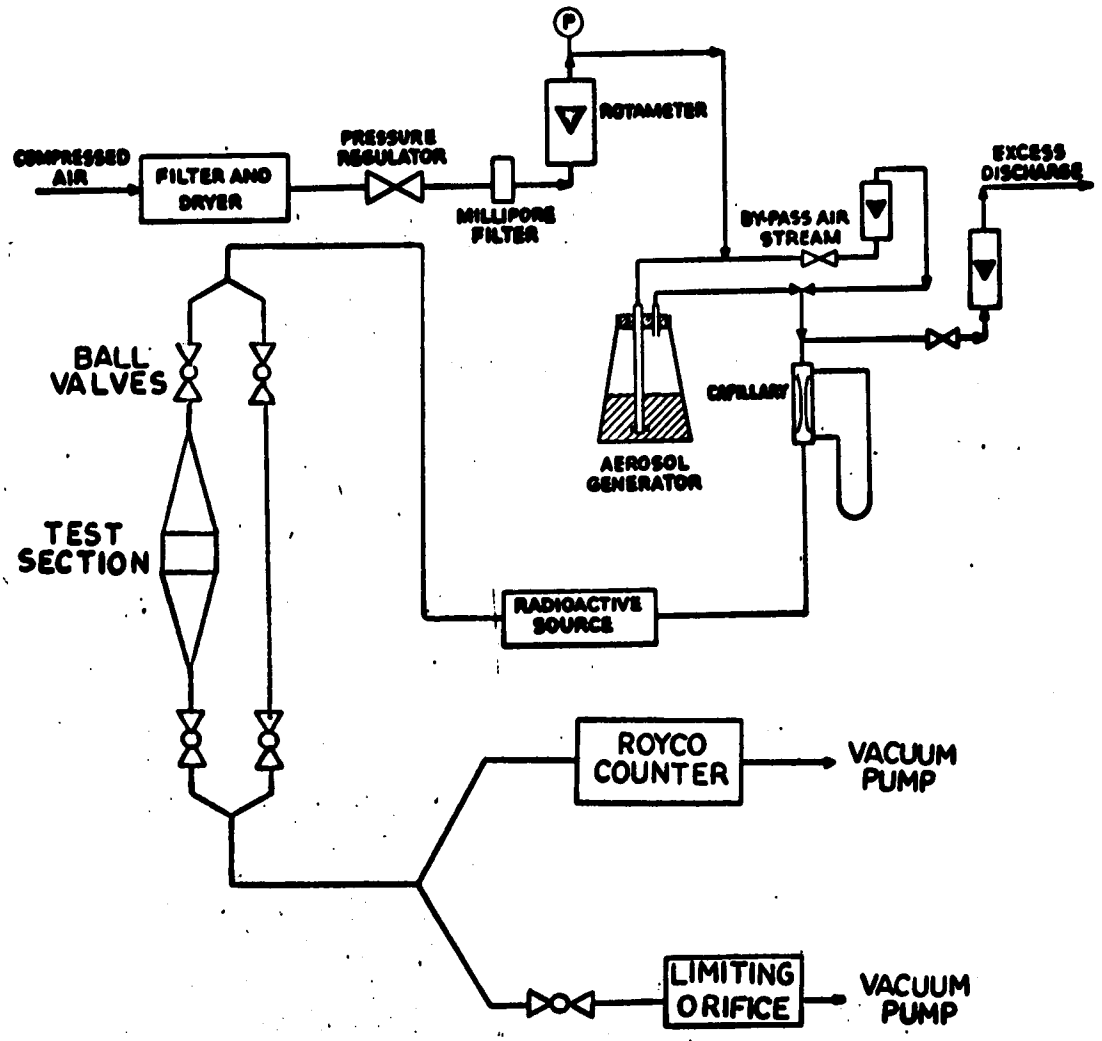

Figure 39. Schematic of horizontal bed experimental apparatus.

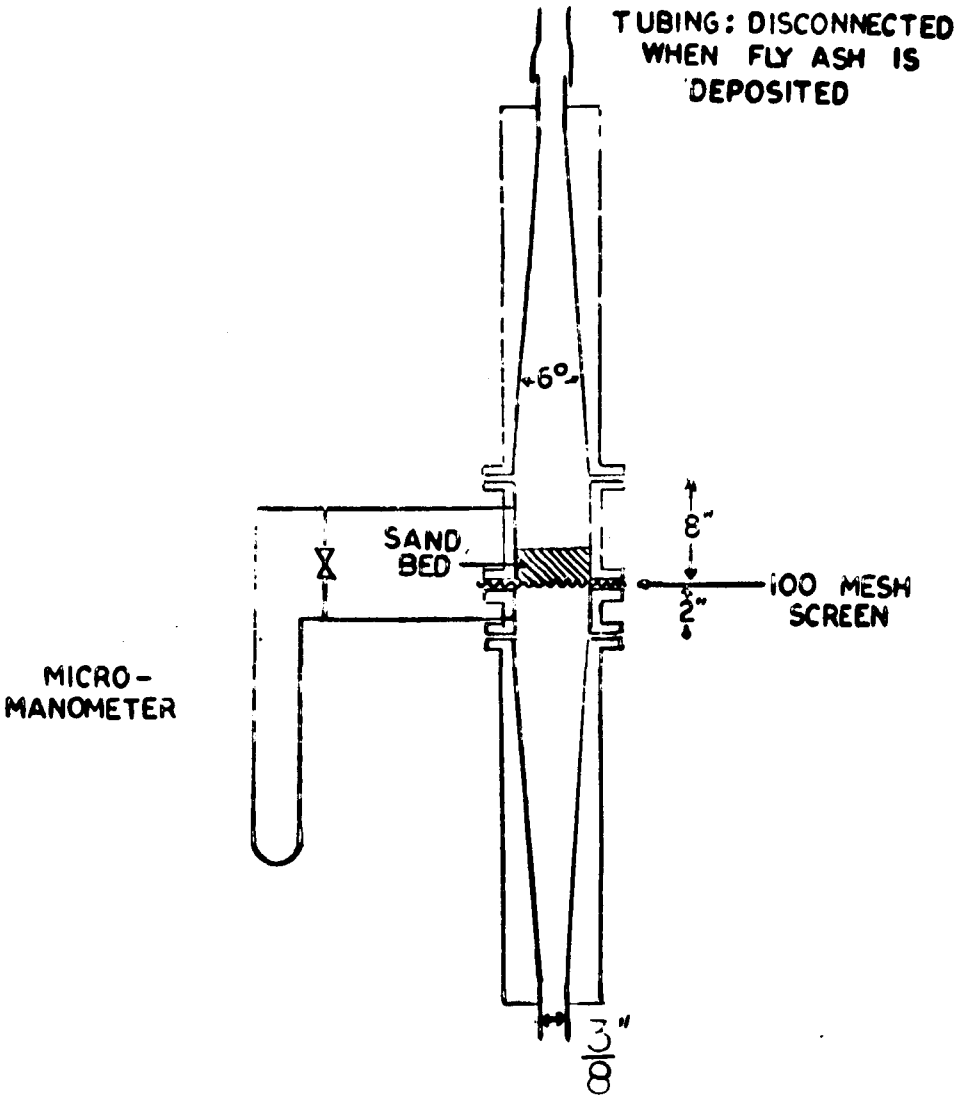

Figure 40. Horizontal sand bed test section.

the filter cake were explored.

----The fly ash was allowed to fall freely onto the sand surface by sedimentation. This method will be referred to as "Zero Velocity Deposition". After the fly ash had settled pressure drop measurements were made on the resultant filter cake.

----The fly ash was allowed to fall onto the sand surface with the assistance of room air that was passed through the bed at a flow rate equal to the flow rate at which pressure loss and aerosol penetration measurements were to be performed.

----The fly ash was passed through a 100 mesh wire screen which was placed on top of the tapered section. The use of the wire screen produced a finer (more dispersed) deposit.

----The rate at which each increment of fly ash was added was varied. This rate will be characterized by the term "Intensity of Deposition" (weight ash added per unit time). A low intensity of deposition would indicate a slow addition of each increment, while a

high intensity would signify the increment was added rapidly.

For a particular run on the horizontal sand bed the method of addition of the fly ash and the size of the increments were kept constant. Runs were performed at face velocities from about 1 to 12 cm/sec. This face velocity, unless otherwise mentioned, is the velocity at which the pressure loss and test aerosol penetration measurements were performed.

The aerosol concentration was monitored with a Royco Model 220-4 sensor with a Model 263 digital display. Since the pump on the Royco operated at only one flow rate (about 2.7 liters/min), it was necessary to divide the bed or bypass effluent stream into two portions in order to investigate higher flow rates. All penetration measurements were made, as with the dilute aerosol studies reported in Part One, with the bypass Tygon tube as a standard. First, the test aerosol penetration with respect to the Tygon was obtained on a clean bed. After an increment of ash had been added, the test aerosol measurement was repeated, again with respect to the Tygon. The

ratio of the two resultant measurements gives the fraction of the aerosol stream that was removed by the fly ash filter cake.

A 0.45 micron Millipore filter placed in a limiting orifice unit was installed as indicated in Figure 39. This was a simply way to maintain a constant flow rate through the horizontal test section, and to obtain the overall fly ash collection efficiency of the sand bed.

A bed height of about 7.9 cm (3.1 inches) was used in the two inch diameter plexiglas tube. The sand used was 20-30 mesh.

Description of Panel

A flow sheet for the panel is presented in Figure 41. A more detailed diagram of the panel is illustrated in Figure 42. Compressed air is supplied by a two-state, two horsepower, Kellogg-American compressor with a capacity of about 5 scfm. Three consecutive combination oil-water-dust filters preceed the two driers. A 0.45 micron Millipore filter is used to remove residual dust from the air stream. The flow rate is monitored with a rotameter

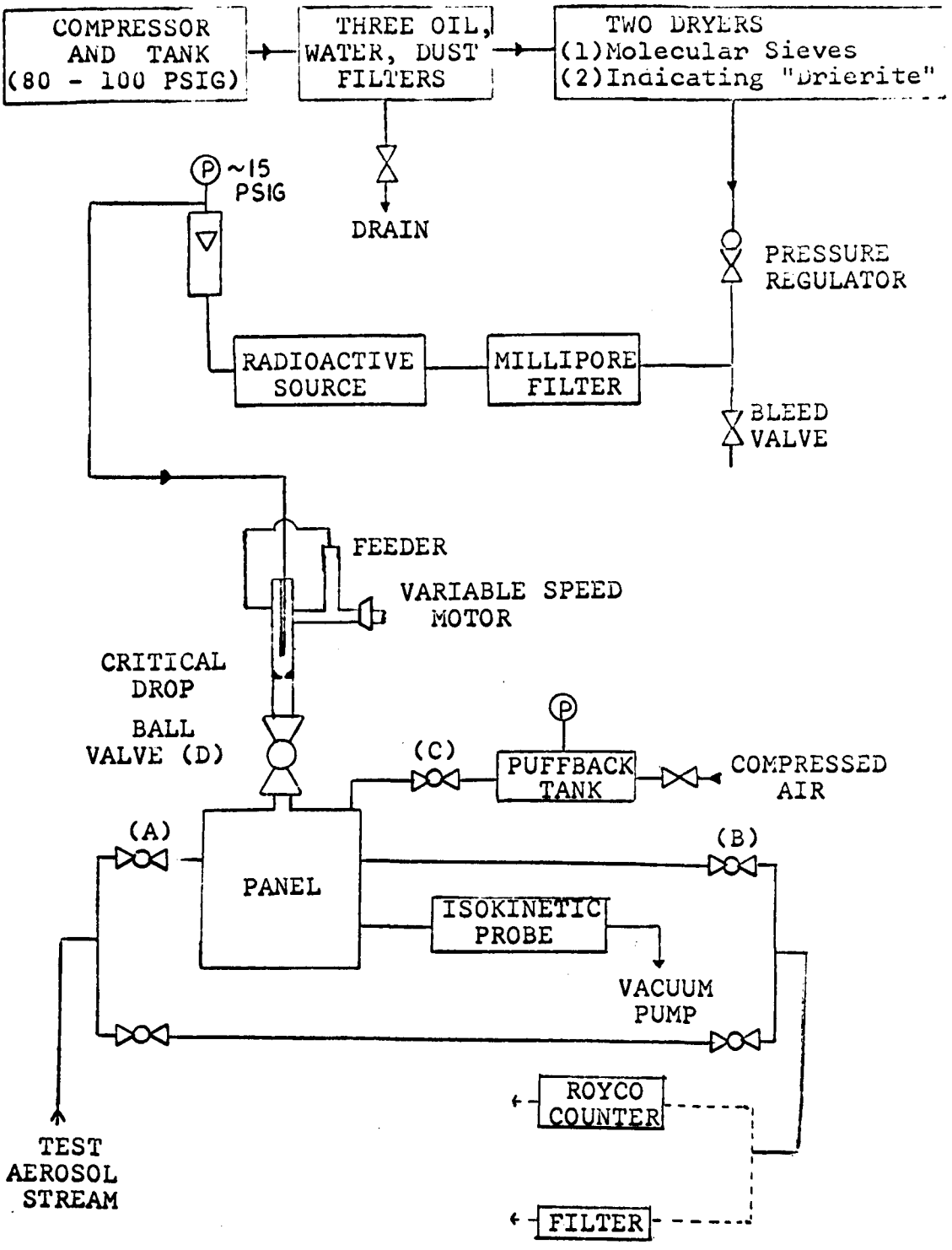

Figure 41. Schematic of panel bed experimental apparatus

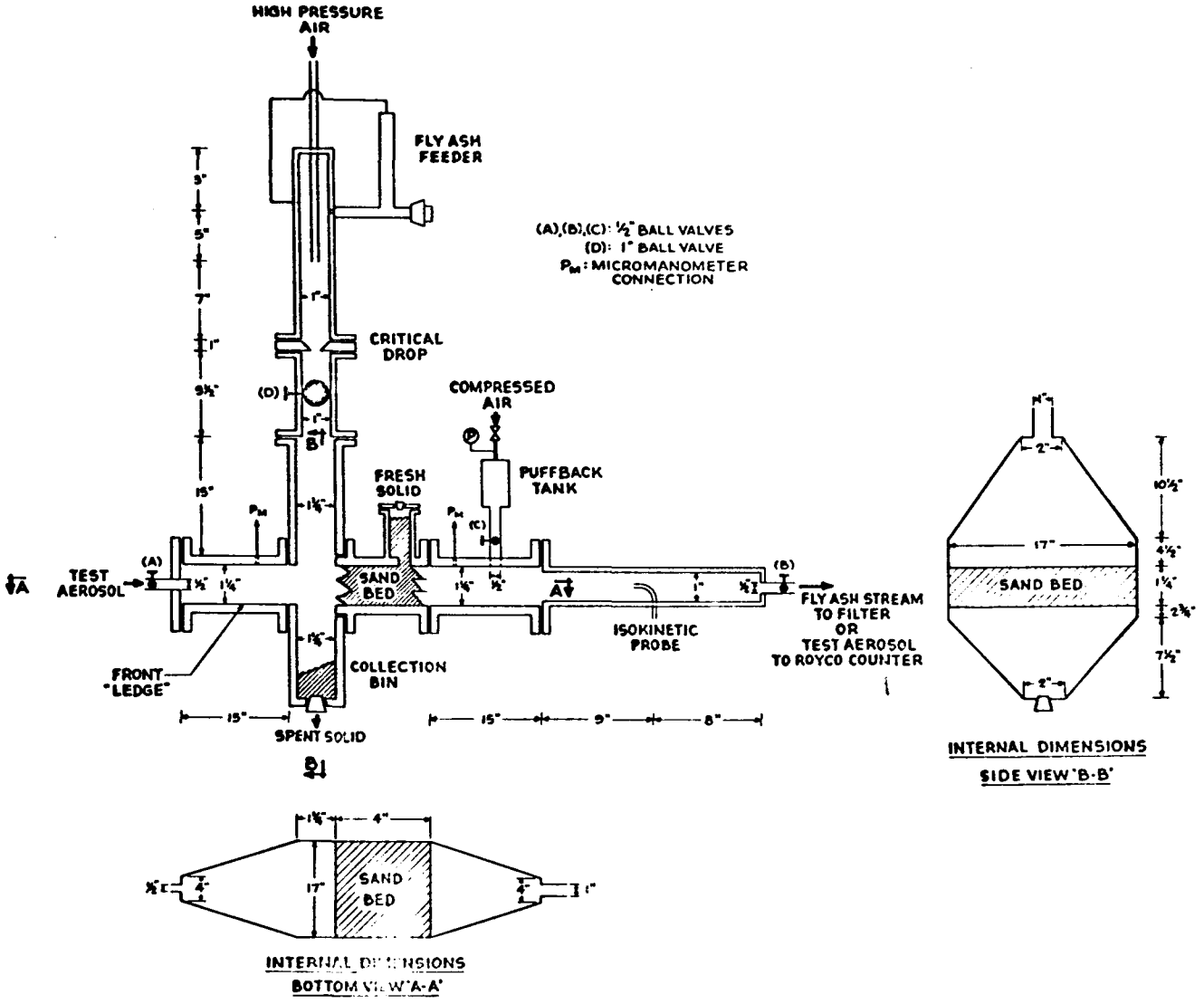

Figure 42. Panel bed filter and auxiliary equipment

before the air stream passes to the panel.

Compressed air enters the panel section through a 3/8 inch copper tube concentrically located in a 1 inch I.D. plexiglas tube (Figure 42 and 43). The air is at a pressure of about 15 psig. This high pressure air stream enters the plexiglas tube downstream of the feeder (Figure 43). Attempts to feed the fly ash against a high pressure air stream (air entering upstream of the feeder inlet) were unsuccessful.

The feeder itself (Figure 43) is similar to one developed by the U.S. Bureau of Mines (39), but modified so as to be able to feed fly ash against a static pressure head. A 1/4 horsepower motor with an RPM range of 80-1360 and a torque of 224 inch-ounces was used with a variable speed controller to rotate the drill bit.

The fly ash is dispersed upstream of the sand bed by passing it through a critical drop created by a sharp edged venturi. The fly ash particles are then carried downwards by the air stream until they enter the typical cross section of the panel bed.

The granular bed, illustrated in Figure 44, is 1-1/4 inches high by 17 inches wide, with an average

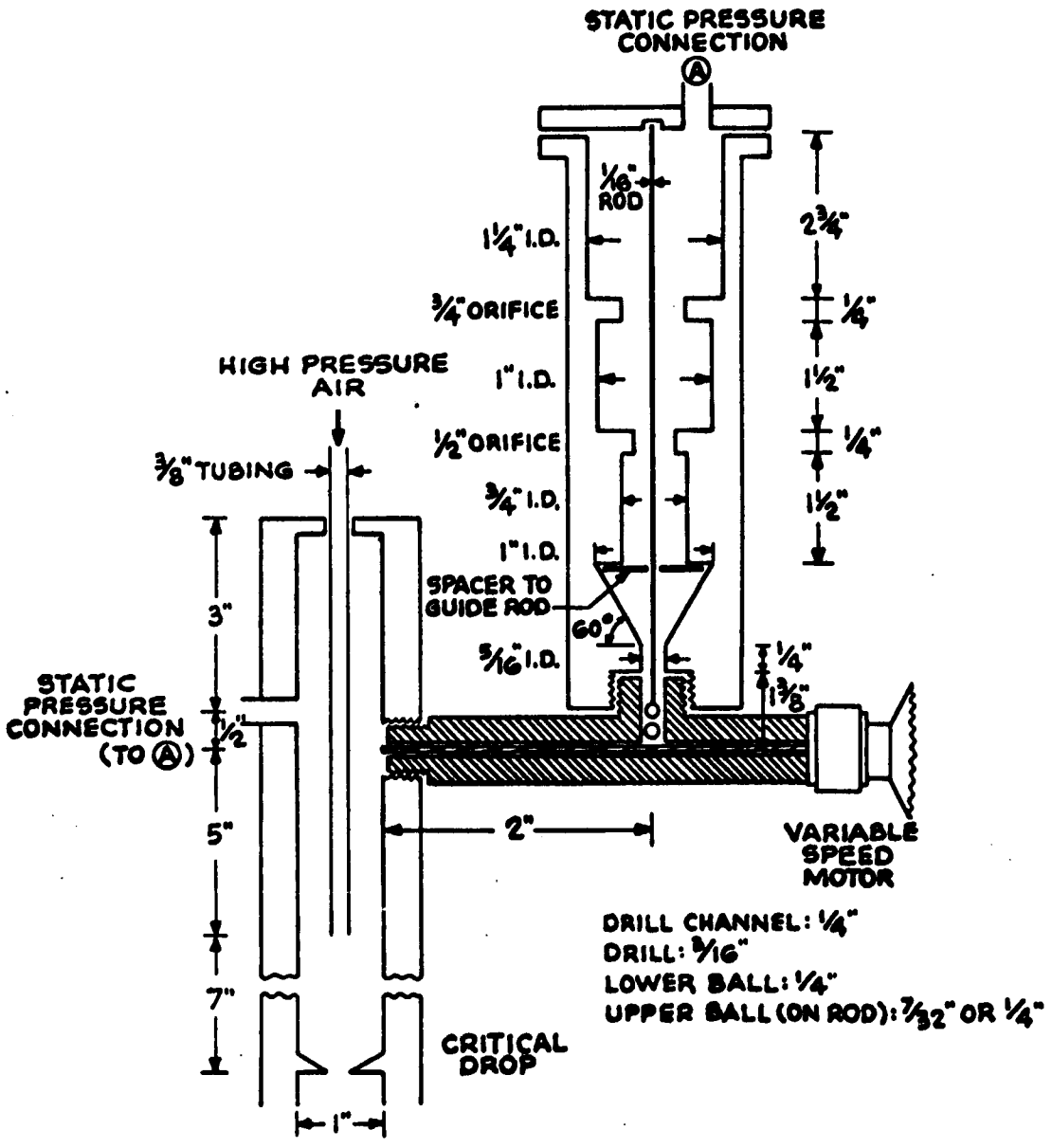

Figure 43. Fly ash feeder.

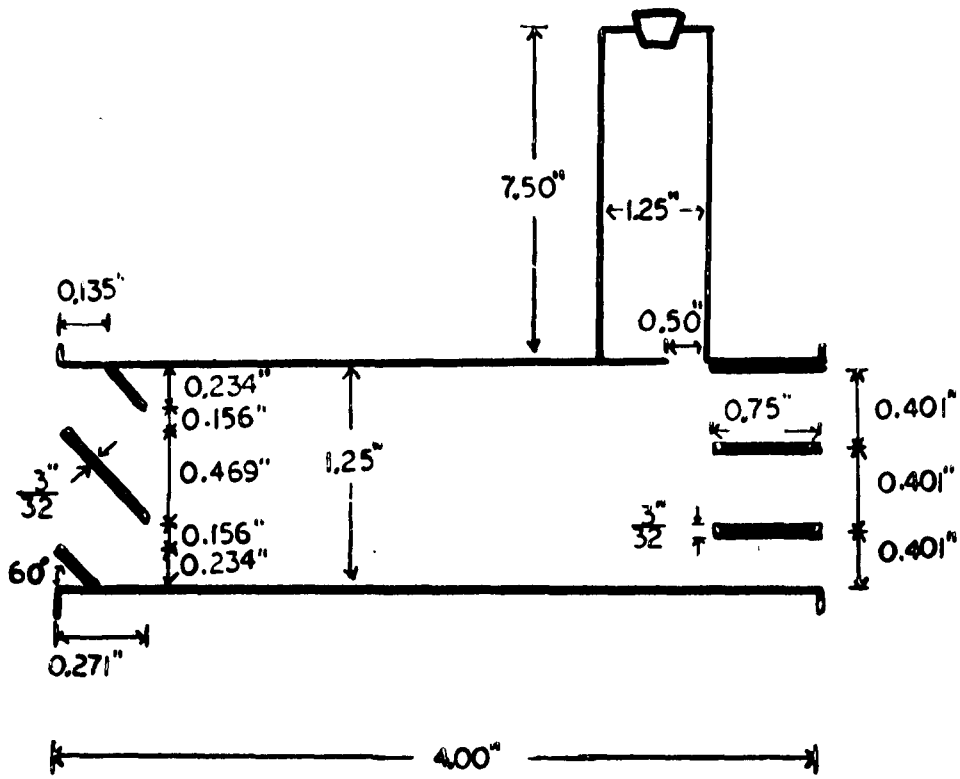

Figure 44. Cross-section of sand bed of panel.

thickness of about 3-1/2 inches. The front louvers, inclined at an angle of 60^{o}, retain the sand at its angle of repose. The rear horizontal louvers also form a free surface. The sand used was 20-30 mesh, as with the horizontal bed. A micromanometer is used for pressure drop measurements across the unit.

The puffback unit has an effective volume of 17 $inches^{3}$. It was operated by filling the tank to the desired puffback pressure, and quickly opening ball valve (C), which afforded a port area of 0.39 $inches^{2}$. This produces a surge flow of air across the panel in the direction opposite to the normal flow of dirty air. The spent solid was collected by removing a rubber stopper at the bottom of the collection bin. It was sieved to separate the ash from the sand, and weighed. The separated sand was recycled and used as fresh solid.

The overall fly ash collection efficiency (weight percent) of the panel was obtained with an isokinetic sampling probe attached to a limiting orifice unit containing a 0.45 micron Millipore filter. The probe, a copper tube of 1/8 inch I.D., 3/16 inch O.D., was centrally located in a one inch I.D.

plexiglas tube.

Experience with the dilute aerosol studies on the clean sand bed indicated that the inlet and exit fly ash streams as well as the test aerosol streams on the panel should pass through tapered sections. These sections are illustrated in Figure 42.

The panel, piping system, and puffback tank were constructed from plexiglas in order to provide visual observation. The louvers and the fly ash feeder's body were constructed out of brass. Presumably electrostatic effects were present. No attempt was made to evaluate the effect of these forces, but it is believed that their influence upon fly ash collection efficiency is not large after a filter cake is formed.

Experimental Procedure for Panel

A typical run on the panel would consist of the following. Each run was performed at constant bed face velocity. The feeder is filled to the top with fly ash. At a particular bed face velocity, V_{Bed}, the pressure drop across the clean bed, ΔP_o, is recorded. A fly ash filter cake is deposited until a pre-determined pressure differential across the bed is

obtained, ΔP_t . The fly ash feeding is then terminated, the air stream is shut off, and the collection bin is emptied of any ash that accumulated during the feeding process. This is called Pre-Puff Ash and consists of ash that did not enter the filter bed but settled out, or filter cake ash, that during the feeding sequence may have fallen off the dirty surface of the panel.

The bed is now cleaned by puffback. The discharged ash and sand is sieved and weighed. This yields the Puff Ash and Puff Sand. If desired, the Millipore filter paper in the isokinetic sampling unit can be weighed to obtain the overall fly ash collection efficiency. The weight of ash required to refill the fly ash feeder is the total weight of ash delivered to the panel during the above operation.

During the feeding process some ash is deposited on the front tapered section which was provided for the inlet test aerosol stream. This section is hereafter referred to as the "ledge". Sand and ash from the puffback process are also carried onto the ledge. The ledge can be cleaned, with the resultant ash and sand being sieved and weighed.

The compressed air stream can now be turned

on again, and the pressure drop after puffback is recorded. This pressure loss, ΔP_d, is the new initial pressure drop for the next cycle. A new filter cake is now deposited until the final pressure differential, ΔP_t, is again attained. The air stream is again shut off, and the bed is again puffed. A new ΔP_d is recorded. The operation from $\Delta P_d(1)$ to $\Delta P_d(2)$ [or from ΔP_o to $\Delta P_d(1)$] constitutes a cycle. Many cycles at the same velocity, puffback pressure, and ΔP_t constitute a run. The bed can be considered to have reached steady state operation when the pressure loss after puffback on two successive cycles, $\Delta P_d(n)$ and $\Delta P_d(n+1)$, are equal.

Then, once steady state has been attained, one more filter cake, up to the same ΔP_t, is deposited. The fly ash feeder is shut off and the compressed air stream may be terminated. A dilute aerosol penetration test is now made across the bed, giving ξ_d. Since the penetration of the 1.1 micron diameter Dow microspheres across the clean bed, ξ_c, has already been recorded (relative to the Tygon bypass), the ratio of these two measurements yields the fractional penetration of the test aerosol across the filter cake, ξ_f.

That is:

$$\xi_f = \frac{\xi_d}{\xi_c}$$

As with the dilute aerosol studies, blank runs (distilled water in an aerosol generator with no latex present) are performed to correct the penetration readings for background dust.

The bed is then cleaned by shock cleaning at the run's puffback pressure using the puffback tank. The term puffback is restricted to the cleaning of the bed after a fly ash filter cake has been deposited, with the resultant pressure loss change from ΔP_t to ΔP_d. Subsequent cleanings after the puffback cleaning are referred to as shock cleanings. The bed is shock cleaned until the clean bed pressure loss ΔP_o is reached (or until many consecutive shock cleanings produce no further change in pressure loss across the bed and no further dislodgement of ash). The spent solid and ash obtained during this cleaning is sieved and weighed.

The ledge is cleaned, and the fly ash feeder is again refilled with a known weight of ash. In this

way an overall material balance for the entire run is obtained. The Millipore filter is weighed in order to obtain the overall fly ash collection efficiency.

The aerosol penetration tests on the panel were performed in two ways:

(1) At an aerosol face velocity, V_A , of about 0.33 cm/sec (0.70 ft/min). This results from using a flow rate of about 2.7 liter/min, which is the capacity of the Royco. Here the entire aerosol stream enters through ball valve (A) (Figure 41). Ball valve (D) is closed. Note that the aerosol test velocity is not equal to the velocity at which the fly ash filter cake was deposited, V_{Bed} .

(2) At an aerosol test velocity equal to the velocity at which the fly ash filter cake was deposited. Here the carrier aerosol stream enters through ball valve (A), but make-up clean air is provided through (D). The Royco samples only a fraction of the effluent. The aerosol velocity under these conditions will be denoted by V_A^B .

All ash and sand quantities for the panel that are expressed in terms of "per unit area" are based on the available free sand surface of the front face. Assuming the sand to have an angle of repose of 35^{o}, this area is 44% of the total bed area in the vertical plane, or 60.3 cm^2 (0.065 ft^2). This will enable a comparison of the panel bed data with the horizontal bed data to be made.

The aerosol and fly ash velocities, however, are computed on the basis of the total projected area of the panel bed in the vertical plane, or 137 cm^2 (0.148 ft^2).

Fly Ash Analysis

The fly ash used in this study was typical power station fly ash, as collected by electrostatic precipitators of high efficiency in a coal-fired power station of the Consolidated Edison Company of New York.

The size distribution of the fly ash was obtained by standard techniques, sieving down to 325 mesh, and using the Andreasen pipette (2) on the -325 portion. Sodium pyrophosphate was used as a dispersant in the water suspension (32). The results

obtained agree with a typical fly ash distribution furnished by Con Edison, as seen in Figure 45. About 50 weight percent was less than 17 microns, with 5 weight percent less than 2 microns. Allen (3) mentions that the ratio of the Stokes diameter to the sieve diameter is of the order one, therefore one could with an apparent error of less than 10% present both kinds of data on the same graph.

It should be noted that all the fly ash in the experiments was first sieved down to 120 mesh before it was used. This was necessary because the larger particles caused difficulty with the fly ash feeder. Thus about 3 weight percent of the power station fly ash was not used.

The effectiveness of the critical drop in dispersing the fly ash feed stream was examined by collecting samples of the feed stream isokinetically. The section containing ball valve (D)(Figures 41 and 42) was replaced by a one inch I.D. plexiglas pipe containing an isokinetic sampling probe with a 0.45 micron Millipore filter. The deposited ash was examined under a microscope and appeared to be dispersed.

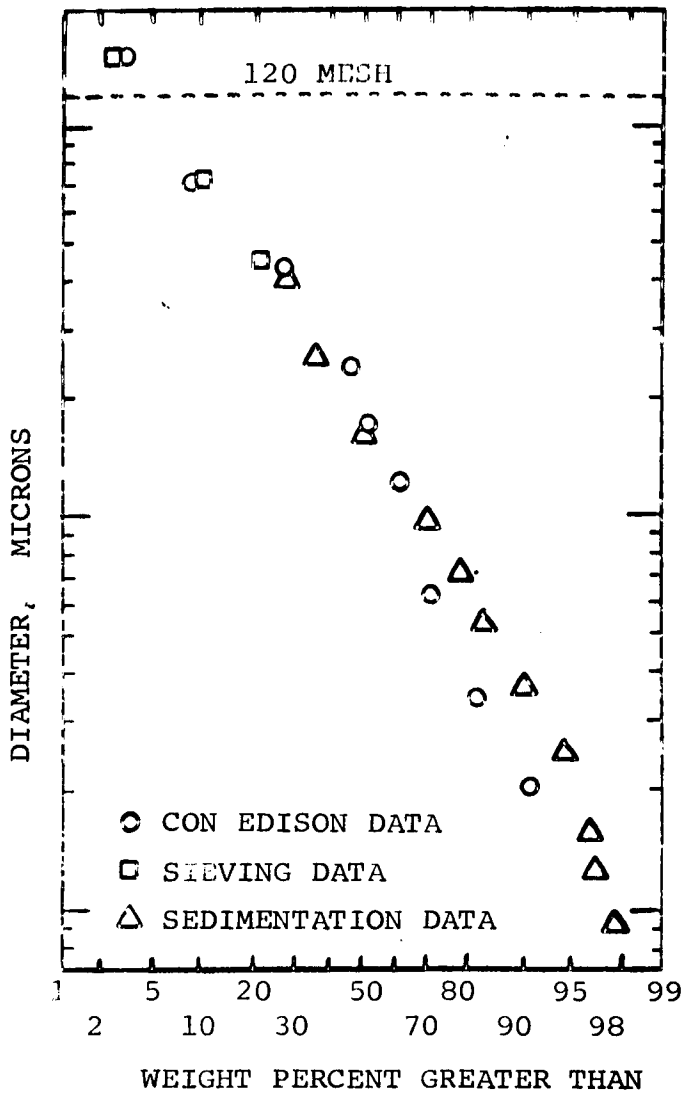

Figure 45. Comparison of obtained fly ash distribution with typical fly ash distribution supplied by Con Edison.

15. PRESSURE DROP AND DILUTE AEROSOL PENETRATION RELATIONSHIPS FOR A FLY ASH FILTER CAKE

Pressure Drop

The pressure loss relationship across a sand bed containing a fly ash filter cake is analagous to that of conventional liquid-solid filtration (42,43).

$$\Delta P_t = \Delta P_o + \Delta P_f \tag{80}$$

where:

ΔP_t = total pressure loss

ΔP_o = pressure loss of clean filter media

ΔP_f = pressure loss attributed to the presence of the fly ash

ΔP_o is given by the usual relationship for flow through porous media; Darcy's law (67):

$$\Delta P_o = K_o V_{Bed} A b \tag{81}$$

where K_o is the permeability constant of the bed.

The relationship for the pressure loss across the fly ash filter cake can be presented in the same form [see equation (79)]. Qualitatively, it is reasonable to assume that if fly ash is deposited solely

by sedimentation on a horizontal sand surface the ash would fall quite randomly, and a certain weight of ash would be required before the entire surface is covered. Some of the ash particles would be carried into the voids and be deposited on interior sand layers, but after an initial increment most of the ash would go toward forming a filter cake. If, after each increment of ash is added, one would pass an air stream through the bed, some of the ash particles may be dislodged from the filter cake (or from the interior sand) and be carried into and possibly through the bed. But, if the weight of ash deposited per unit area, Z , exceeds a certain value, say Z_{po} , a stable filter cake would be formed, and an expression similar to equation (81) may be written for the filter cake.

If, on the other hand, the fly ash filter cake is deposited with the aid of the eventual bed velocity, V_{Bed} , more of the fly ash particles would be preferentially carried towards the voids and a different critical weight of ash would be required. Thus, the critical weight of fly ash per unit area is expected to be a function of the velocity. It is therefore permissible to write

$$\Delta P_f = K_f V_{Bed} (Z - Z_{po}) + \varphi(Z_{po}) \quad (82)$$

where:

K_f = permeability constant for the fly ash filter cake

$\varphi(Z_{po})$ = a function accounting for the pressure loss caused by Z_{po}

The above expression assumes that all of the ash above Z_{po} goes towards forming a filter cake. In general, only a certain fraction of the additional ash above Z_{po}, σ, goes towards the filter cake. What is left, minus the amount that passes through the bed, contributes to a pressure loss caused by ash particles collected in the interior of the sand bed. Thus:

$$\Delta P_f = K_f V_{Bed} \sigma (Z - Z_{po}) + \Delta P_\sigma + \varphi(Z_{po}) \quad (83)$$

or

$$\frac{\Delta P_f}{V_{Bed}} = K_f \sigma (Z - Z_{po}) + \frac{\Delta P_\sigma}{V_{Bed}} + \frac{\varphi(Z_{po})}{V_{Bed}} \quad (84)$$

where ΔP_σ is the pressure loss caused by ash collected in the interior of the bed. It is understood that both σ and K_f may be functions of the velocity. The former is easily seen to be the case, since looking at the extreme, at very high velocities no cake will form and $\sigma \rightarrow 0$; these are the conditions explored by Taub (59). K_f depends on the porosity of the filter cake, ϵ_f , as seen from the Carman-Kozeny equation (67):

$$K_f \propto \frac{(1 - \epsilon_f)^2}{\epsilon_f^3} \tag{85}$$

so that a decrease in ϵ_f (a more compact filter cake) produces an increase in K_f .

Dilute Aerosol Tests

If a dilute aerosol penetration test is performed on a developing filter cake, it is reasonable to expect that:

$$\xi_f = [\exp - \eta_f \sigma (Z - Z_{ao})][\exp - f(\sigma)] \tag{86}$$
$$[\exp - f_1(Z_{ao})]$$

where:

Z_{ao} = critical weight of fly ash deposited per unit area of bed for the aerosol tests

$f_1(Z_{ao})$ = a function accounting for the aerosol removal caused by Z_{ao}

$f(\sigma)$ = a function accounting for the aerosol removal caused by ash collected in the interior of the bed

η_f = attenuation coefficient of the fly ash filter cake

with the understanding that Z_{ao} is not necessarily equal to Z_{po} .

Combining Pressure Loss With Test Aerosol Data

Equations (84) and (85) can be combined to relate the test aerosol collection efficiency of the filter cake to the pressure loss caused by the filter cake. Equation (86) can be rewritten:

$$\ln \xi_f = - \eta_f \sigma (Z - Z_{ao}) - f(\sigma) - f_1(Z_{ao}) \quad (87)$$

and, upon combining with equation (84)

$$\ln \xi_f = - \frac{\eta_f}{K_f} \frac{\Delta P_f}{V_{Bed}} + \alpha \qquad (88a)$$

where

$$\alpha = - \frac{\eta_f}{K_f} \frac{\Delta P_\sigma}{V_{Bed}} + \frac{\varphi(Z_{po})}{V_{Bed}} - f(\sigma) - f_1(Z_{ao}) \qquad (88b)$$

A plot of $\ln \xi_f$ against $\Delta P_f / V_{Bed}$ for constant V_{Bed} describes in more complete detail the behavior of the filter cake. With the use of a 1.1 micron test aerosol, this gives a direct relationship of the effectiveness of the filter cake to an additional deposition of fly ash, since the 1.1 micron diameter particles are in the range of particle size that is the most difficult to filter (62,63). By presenting $\ln \xi_f$ against $\Delta P_f / V_{Bed}$, use is made of the other important characteristic of any filtration device, the power expenditure necessary to overcome the additional resistance imposed by the presence of the filter cake.

The "Effectiveness"

A term called the Effectiveness (Ω) will be used to characterize the cyclic steady state operation of the panel bed filter, with Ω defined by

$$\Omega = \frac{\Delta P_t - \Delta P_d}{\Delta P_t - \Delta P_o} \tag{89}$$

It is easily seen that this is just the ratio of the recovered pressure loss to the total pressure loss caused by the fly ash filter cake. Letting

$$\Delta a = \Delta P_t - \Delta P_d$$

$$\Delta m = \Delta P_d - \Delta P_o$$

it is seen that Δa is the pressure loss caused by the filter cake removed by puffback and Δm is the pressure loss caused by the "permanent" fly ash not removed by puffback. Therefore

$$\Omega = \frac{\Delta a}{\Delta a + \Delta m} \tag{90}$$

Ideally, for steady state operation:

$$\Delta a \approx K_f V_{Bed} \sigma (Z - Z_{po}) \quad (91a)$$

$$\Delta m \approx P_\sigma + \varphi(Z_{po}) \quad (91b)$$

A high value of Ω indicates that most of the fly ash goes into forming a filter cake that can be dislodged, while a low value indicates that a considerable portion of the fly ash penetrates so far into the bed that it is not dislodged by puffback. All other things being equal, a high value of Ω is desirable.

16. EXPERIMENTAL RESULTS - HORIZONTAL BED

Aerosol Penetration Through Filter Cake

A fly ash filter cake deposited on a horizontal sand surface can produce extremely high filtration efficiencies. As seen from Figure 46, deposition at low intensity to about $Z = 0.14$ grams/cm^2 results in a filter cake that has a collection efficiency over 99.99% for 1.1 micron Dow microspheres having a face velocity of 4.5 ft/min. What is even more remarkable, the 0.14 grams/cm^2 produces a filter cake that is at the maximum about 0.23 cm thick, which is about three sand grains in thickness. (The bulk density of fly ash is about 0.60 grams/cm^3, and 20-30 mesh sand has an average grain size of 0.071 cm.) The additional pressure loss due to the presence of the filter cake is only, from Figure 47, about 1.4 inches water.

The validity of relationships of the form presented in equation (84) for $\Delta P_f/V_{Bed}$ vs Z and equation (86) for ξ_f vs Z to characterize the development of the fly ash filter cake are illustrated by the linear portions of Figures 46 and 47.

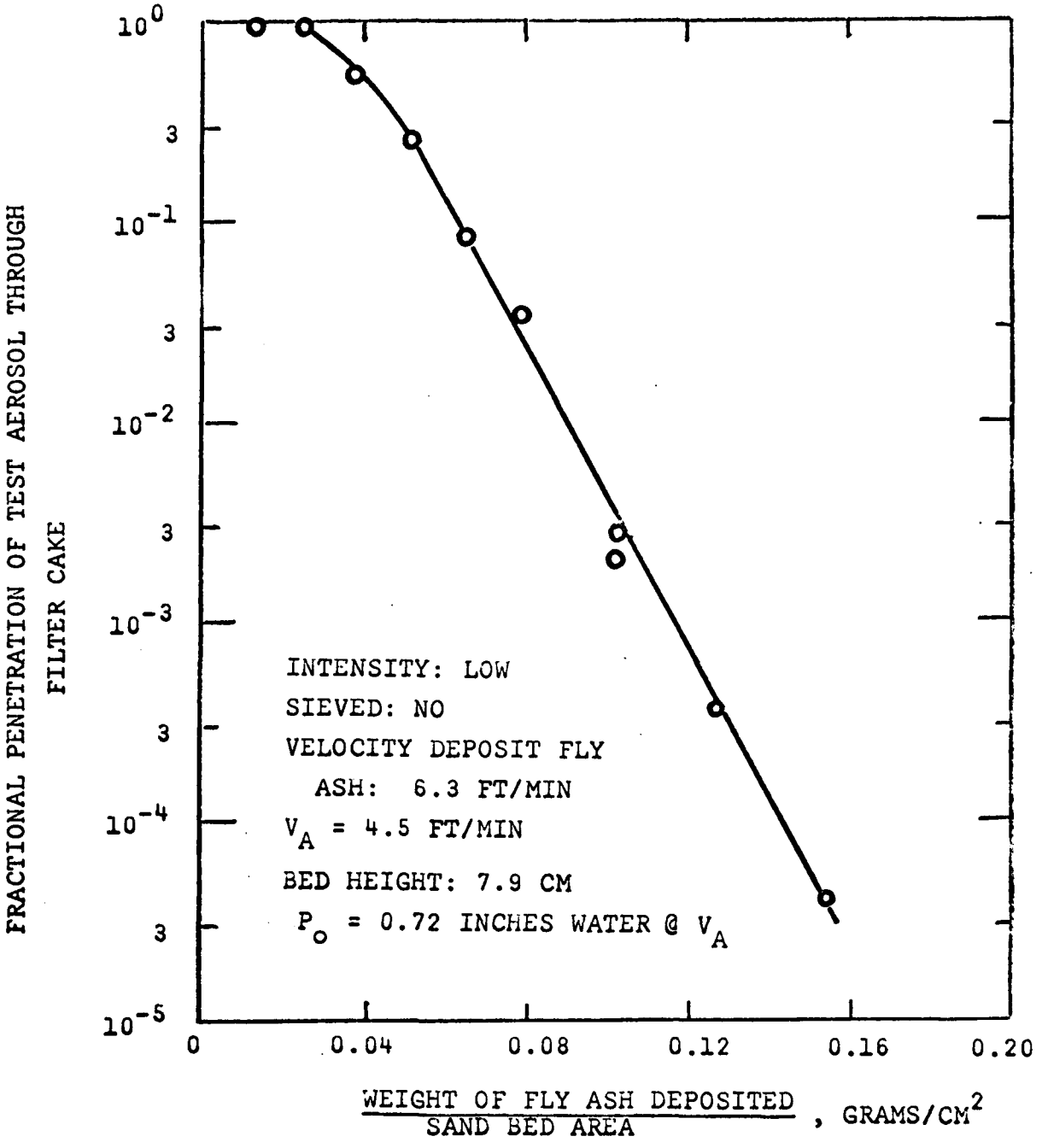

Figure 46. Effect of amount of fly ash deposited on fractional penetration of test aerosol through fly ash filter cake deposited on horizontal sand bed.

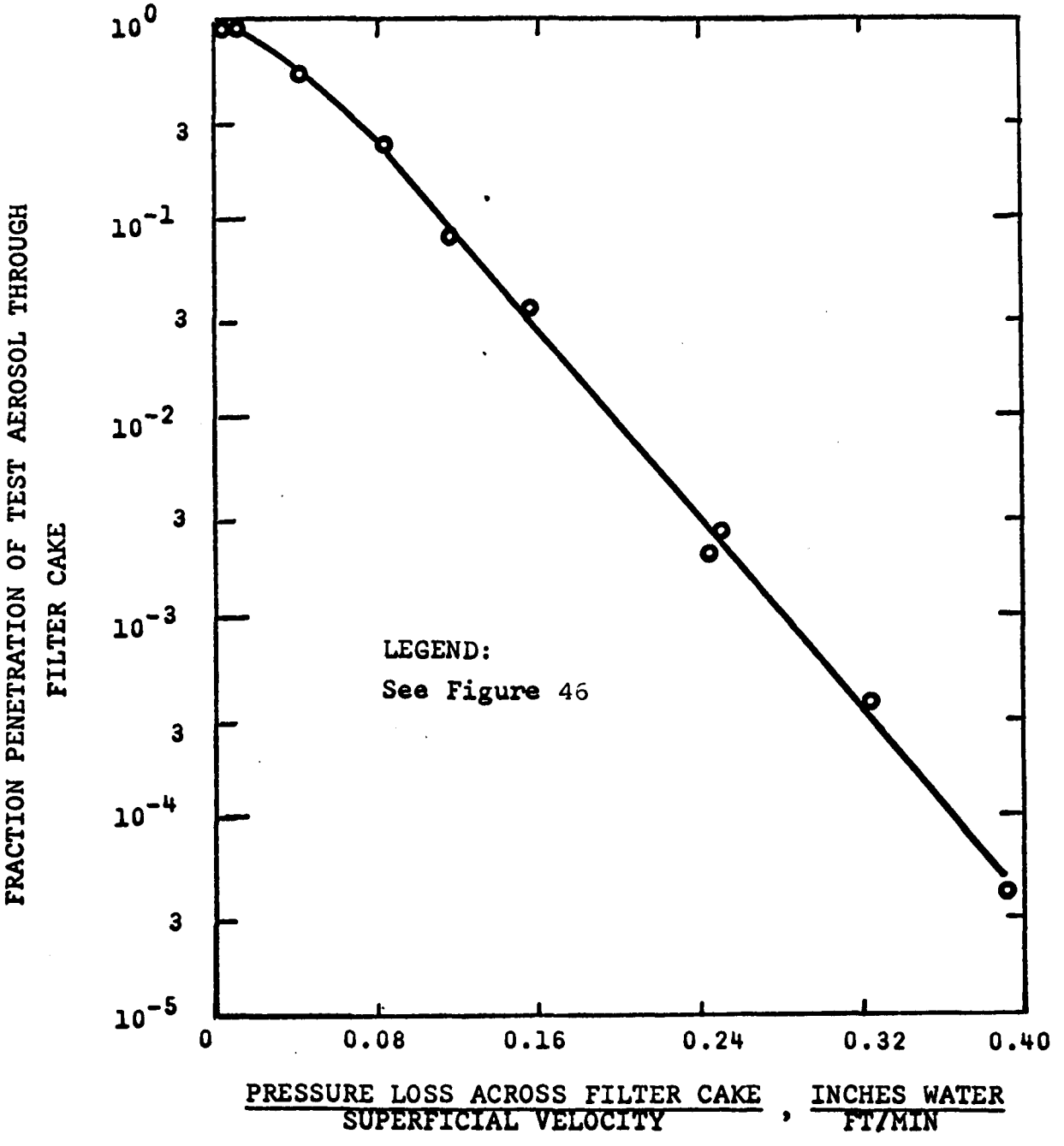

Figure 47. Pressure loss vs aerosol penetration for fly ash filter cake deposited on horizontal sand bed.

Influence of Method of Deposition of Fly Ash on Filter Cake Formation

(1) Effect of Intensity of Deposition

The nature of the filter cake obtained is strongly dependent on the method by which the fly ash was deposited on the sand surface. This can be seen from Figure 48, which shows the effect of intensity of deposition on $K_f\sigma$. This term is the slope of the $\Delta P_f/V_{Bed}$ vs Z curve.

A low intensity of deposition produces a higher $K_f\sigma$, in agreement with Grey (28). Grey argues that a high intensity of deposition reduces the time period for which the upper layer of the bed is active (by jostling, etc., from the falling particles), thus increasing the porosity. Therefore a more compact cake will be formed with a low intensity of deposition.

Decreasing the intensity of deposition increases $\eta_f\sigma$. This result would be expected, for a less porous and less permeable cake is formed.

(2) Effect of Velocity of Deposition

The velocity of deposition also affects the structure of the filter cake. The simplest case is

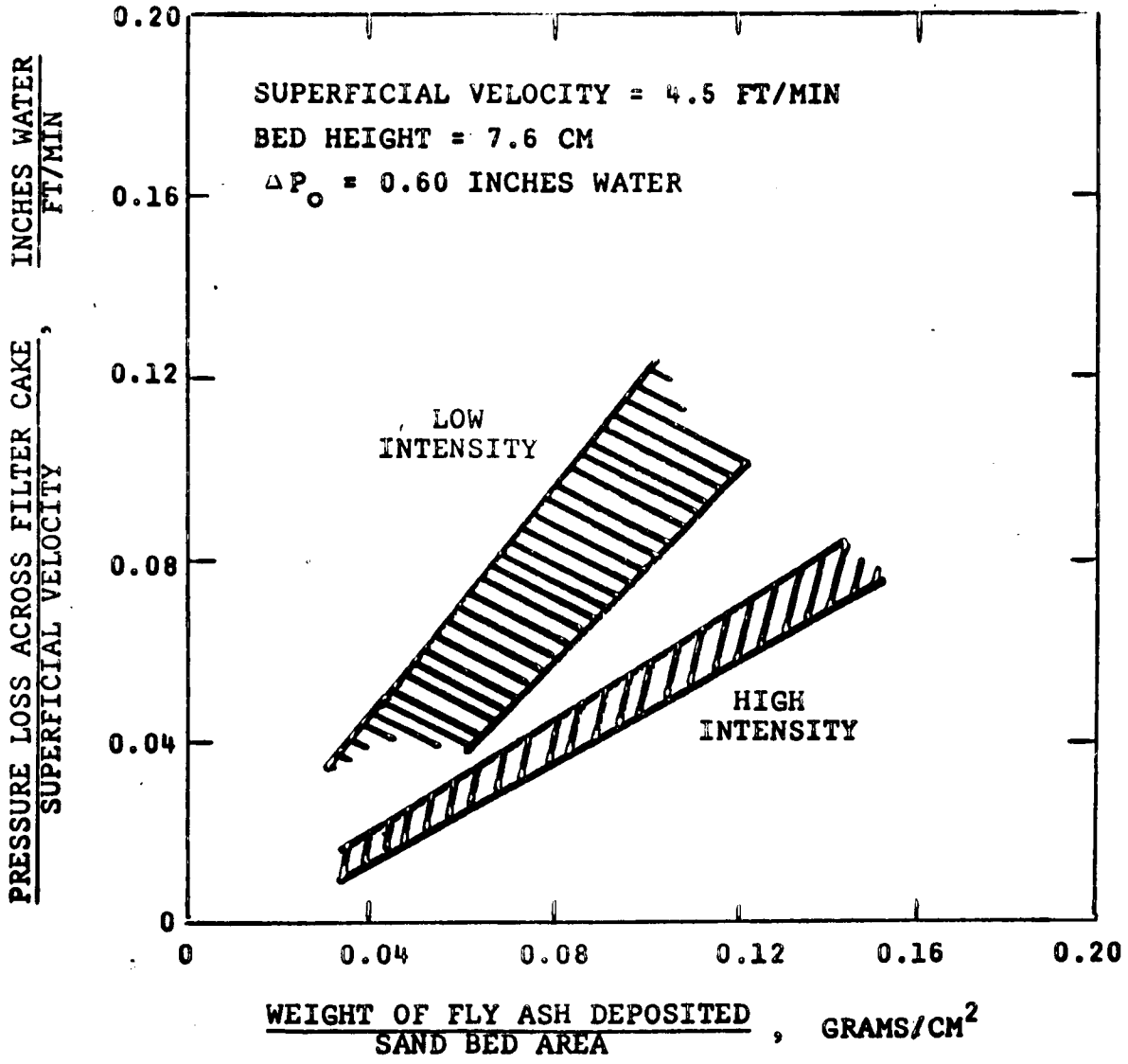

Figure 48. Effect of intensity of deposition of fly ash upon filter cake development.

"Zero Velocity of Deposition", sedimentation. $K_f\sigma$ varied, first increasing, then decreasing with the air velocity of the stream passed through the bed after the fly ash had settled. The same trend, an increase, then a decrease in $K_f\sigma$ was observed on a fly ash filter cake built up by depositing the fly ash at V_{Bed} (Figure 49).

This increase and then decrease with increasing velocity agrees with the trend observed by Borgwardt et al (5) for a filter cake formed in a fibrous filter baghouse . (See Chapter 13 and Figure 32.) However, their values for $K_f\sigma$ were about 2 to 4 times the values obtained in the above runs (and they assumed $\sigma = 1$), and were for a velocity range of about 1.5 to 5 ft/min.

The above mentioned variation in $K_f\sigma$ can be explained in terms of the packing of the fly ash filter cake. If the fly ash is deposited by sedimentation, the ash distributes itself uniformly. The effect of an increase in velocity is to introduce two conflicting phenomena, one tending to increase $K_f\sigma$, the other tending to decrease $K_f\sigma$. The effect of an increasing V_{Bed} decreasing the porosity of a cake and therefore increasing K_f is documented by Grey (28). However, as the bed velocity is increased [but still below the

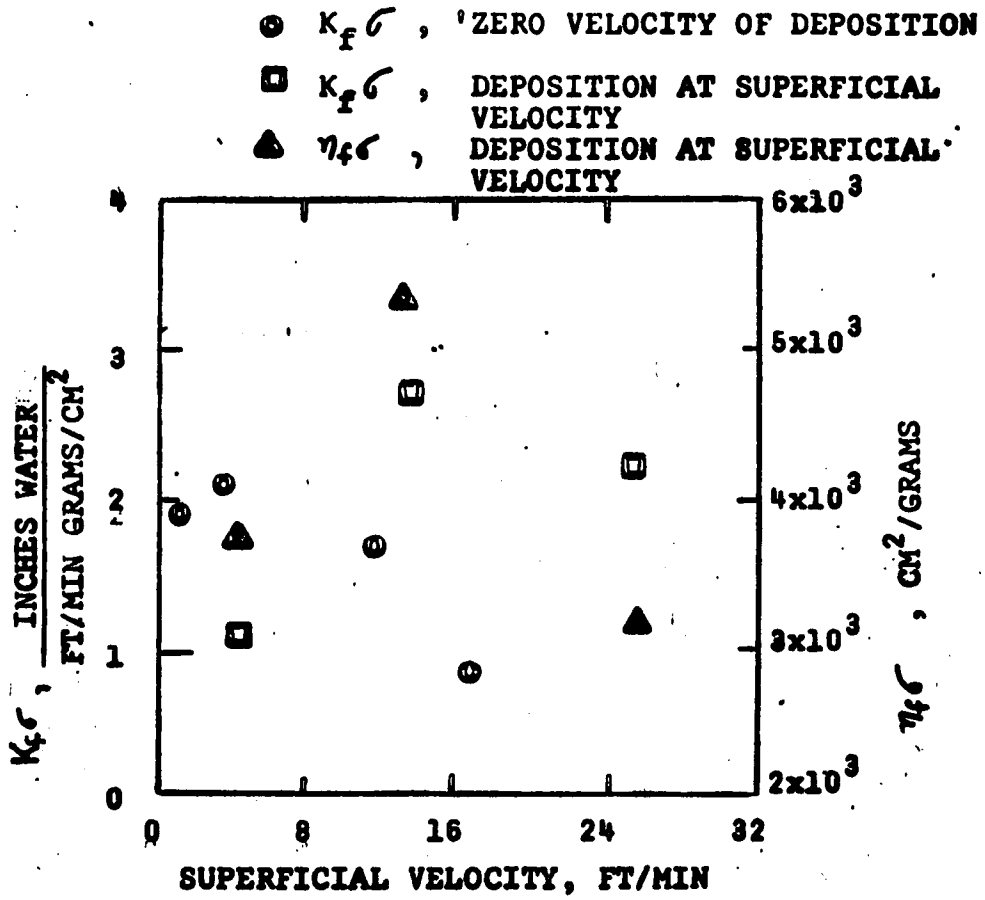

Figure 49. Effect of superficial velocity on filter cake parameters $K_f\sigma$ and $\eta_f\sigma$.

conditions explored by Taub (59)] fly ash is torn away from the sand surfaces and is carried into the interior of the bed. Thus while the porosity of the filter cake is still decreasing because of the higher velocity, σ is decreasing at a faster rate than K_f is increasing, thus an eventual decrease in $K_f\sigma$ (see Figure 49).

The same description applies to the filter cake that is deposited at V_{Bed}, the bed velocity. However, here one has the additional effect of the particles conveyed by the fluid streamlines, and particles are collected by direct interception and inertial impaction (in addition to sieving). This would increase the impact velocity (28), which decreases the porosity, thus increasing K_f. In addition, deposition by sedimentation leads to a higher degree of segregation of the falling ash particles (according to settling velocities), thus increasing the porosity. This occurs because particles of a narrow size range are deposited at any one time. This explains why higher $K_f\sigma$ values were obtained when the fly ash was deposited at V_{Bed} at the higher values of V_{Bed}.

The product of the test aerosol attenuation

coefficient of the filter cake and the fraction of the falling ash that goes towards producing the filter cake, $\eta_f\sigma$, also changes with velocity, as seen in Figure 49. There is apparently a maximum η_f, as would be expected from the dilute aerosol studies. However, the actual effect of V_{Bed} on η_f is masked because the filter cakes were formed at different velocities.

The overall fly ash collection efficiencies were measured for two runs on the horizontal bed. With a V_{Bed} of 24.5 ft/min, and with a cumulative Z of 0.146 grams/cm^2, the overall fly ash efficiency was 98.1%. At a V_{Bed} of 10.9 ft/min, and with a cumulative Z of 0.136 grams/cm^2, the overall efficiency was 99.981%,(1) indicating that 10.9 ft/min filter cake is more compact and a more efficient filtering agent. The above was obtained with a low intensity of deposition, with the fly ash having been passed through the 100 mesh wire screen, and allowed to fall at V_{Bed}.

(1) The weight of fly ash penetrating through the sand bed was the quantity that was measured. Since the overall collection efficiency is the term of interest, 1 - (fraction of fly ash penetrating), expressed on a percent basis is reported.

Fracturing of the Filter Cake and the Use of Aerosol Tests to Disclose the Fractures

On occasion the filter cake cracked, possibly because of its own weight, or because of the impact of the next increment of ash. As the filter cake is deposited, bridges of ash form over the voids in the sand bed's upper surface. The effect of more ash, coupled with the force imparted by the bed velocity, tends to overcome the cohesive forces between the fly ash particles, thus causing fracture. These fractures were quite visible through the plexiglas container, and were in appearance similar to the cracks in dried mud. They occurred quite randomly, with no particular pattern.

The conventional way of presenting the buildup of a filter cake is through ΔP_f vs Z (or $\Delta P_f/V_{Bed}$ vs Z). It is usually assumed that an increase in ΔP_f would, at constant velocity, represent an increase in collection efficiency. This however, is not entirely correct. On occasion, ΔP_f would continue to increase in a linear fashion with Z, while ξ_f would not continue to decrease linearly, but would in fact level off (see Figures 50 and 51). In fact, during some runs ΔP_f would increase, but ξ_f would remain the same or even increase

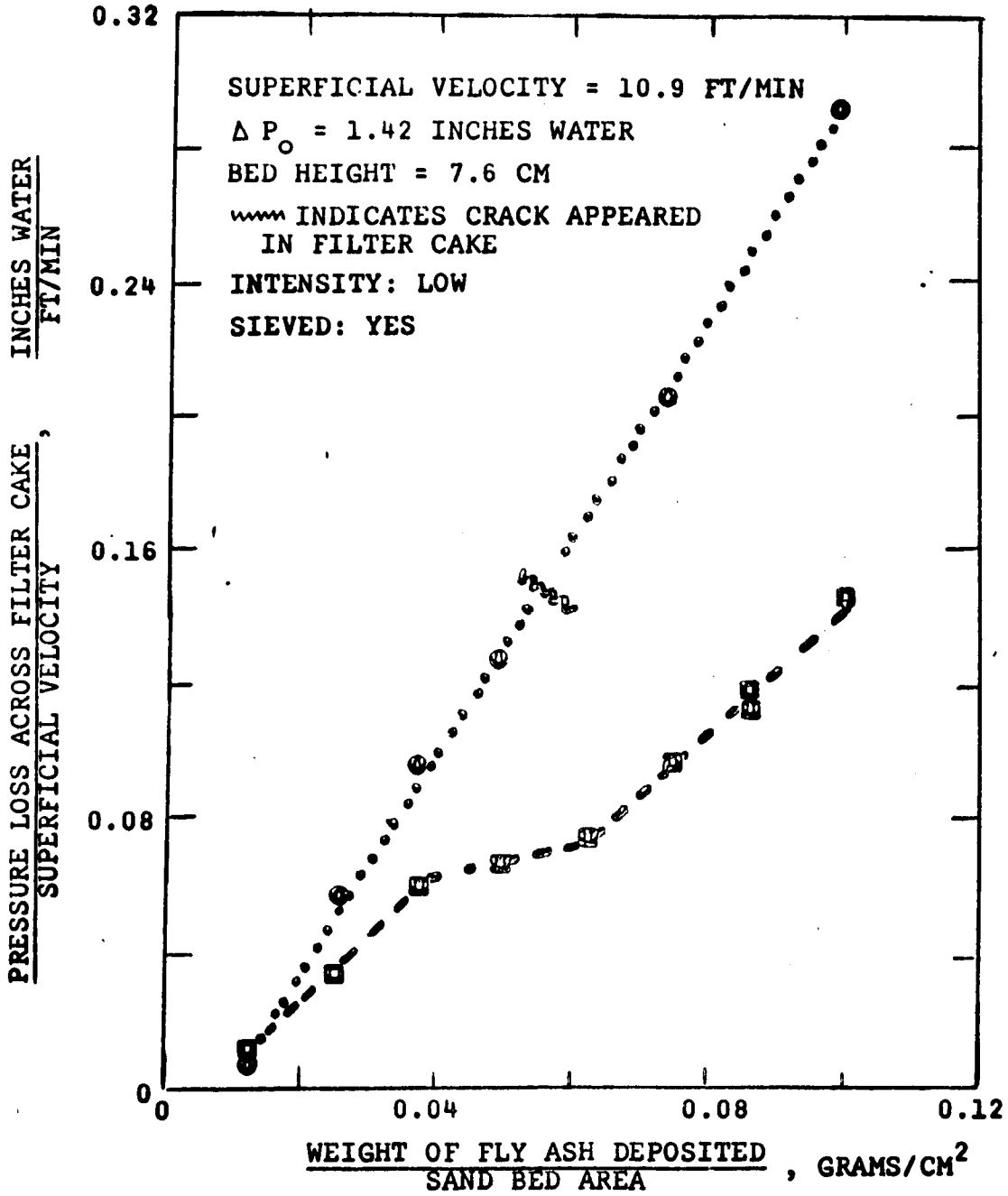

Figure 50. Fly ash deposited at superficial velocity; pressure loss across filter cake vs weight of fly ash added.

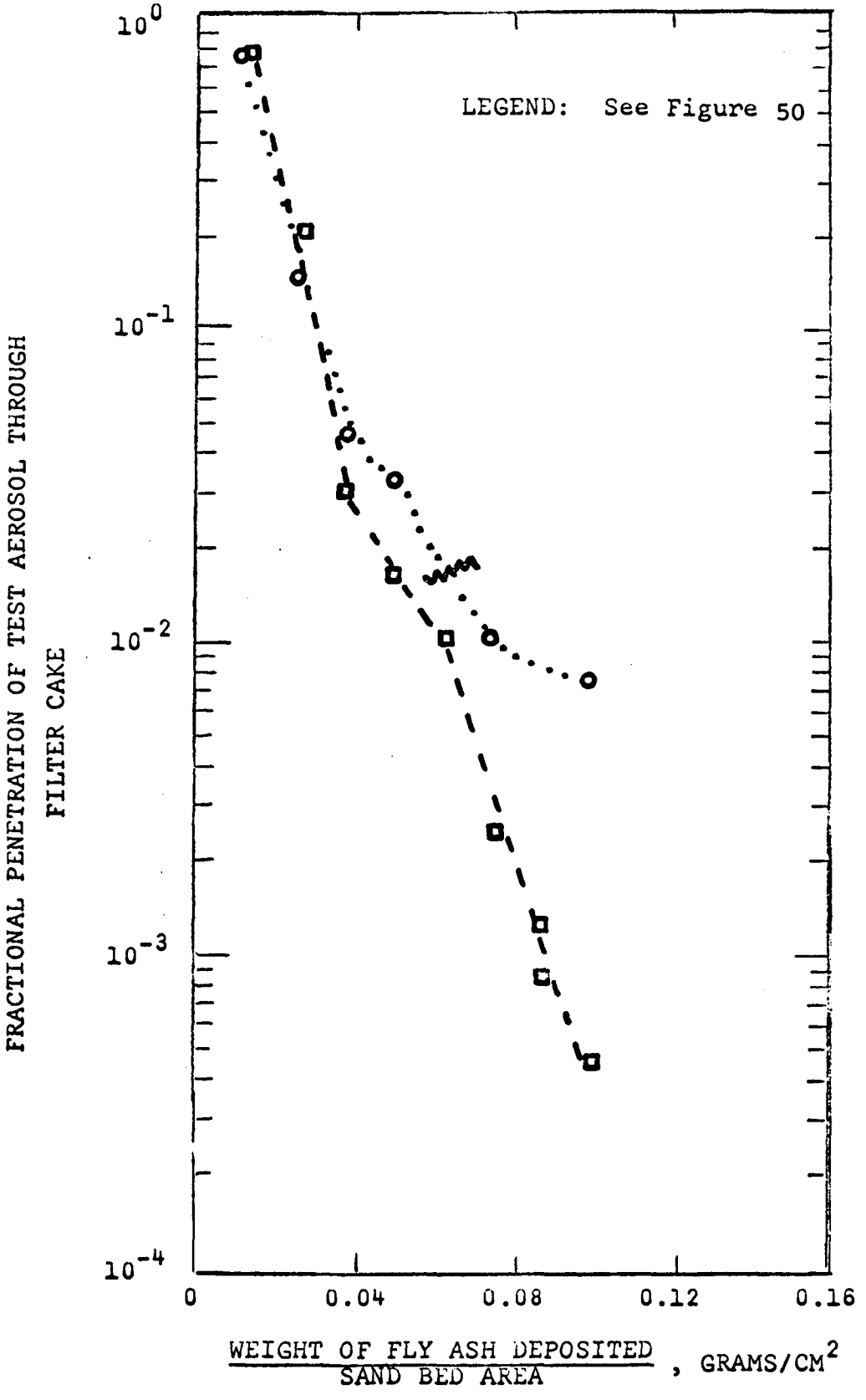

Figure 51. Fly ash deposited at superficial velocity; fractional aerosol penetration through filter cake vs weight fly ash added.

as more ash is added. These irregularities are possibly the results of cracks or pinholes developing in the filter cake. These pinholes might produce a similar effect as those experienced by HEPA or paper filters containing pinholes (7,61). Pressure drop measurements do not disclose these defects, but aerosol penetration measurements can reveal them.

Velocity Shift Measurements

A "Velocity Shift" experiment performed on a developed filter cake disclosed several interesting phenomena, and substantiated other results. A "Velocity Shift" refers to a procedure whereby after constructing a filter cake by deposition of increments of ash at one bed velocity (the base velocity), pressure loss and aerosol penetration measurements are made at another bed velocity. "Velocity Shifts" produced the following effects:

---A decrease from a base velocity of 10.9 to 4.5 ft/min and from a base velocity of 24.5 to 4.5 ft/min can occasionally introduce a fracture in the filter cake. This may have been brought about by the effect an altering of the

aerodynamic path might have on the fly ash filter cake. Curiously, upward velocity shifts did not bring about any fractures.

---When no fracture occurred on a downward "Velocity Shift" from 10.9 to 4.5 ft/min, the value of ΔP_f at V_{Bed} = 4.5 ft/min obtained on the 10.9 ft/min cake was much higher than the value of ΔP_f for the identical Z as on a cake developed at 4.5 ft/min. The value of ξ_f obtained on the "Velocity Shift" bed at V_{Bed} = 4.5 ft/min was much lower than on the 4.5 ft/min cake, again for identical values of Z. This is indicative of a more compact and less porous cake (higher $K_f\sigma$ and higher $\eta_f\sigma$) deposited at 10.9 ft/min.

---An upward "Velocity Shift" from 10.9 ft/min to 24.5 ft/min also has a higher shift value of ΔP_f and a lower shift value of ξ_f than were obtained for a bed developed at 24.5 ft/min for the same Z. This indicates that the 10.9 ft/min bed is more compact, and less porous. Recall identical observations were made from efficiency measurements.

It should be noted that the "Velocity Shift" measurements were performed on a fairly thick filter cake, having an average Z of about 0.12 grams/cm^2.

17. EXPERIMENTAL RESULTS - PANEL BED

Introduction

Exploratory tests were performed on the typical section of the panel bed filter described in Chapter 14. Face velocities (based on the total cross sectional area of the bed- sand plus louvers) of about 5, 11, 22 and 32 ft/min (2.5 to 16 cm/sec) were explored. The fly ash loading varied from about 3 to 12 grams/m^3, depending on the face velocity (V_{Bed}), with no more than a two-fold variation at any particular velocity. Variations in loading had no noticeable effect on the cyclic behavior of the bed. At each velocity, the thickness of the filter cake deposited was varied by performing several runs with different final pressures, ΔP_t. Most runs were performed at a puffback pressure of 15 psig.

General Operating Characteristics

Figure 52 illustrates typical cyclic operation of the panel bed filter. Steady state operation was rapidly attained and easily maintained. This was characteristic of most face velocities, final pressures and puffback pressures. The pertinent characteristics

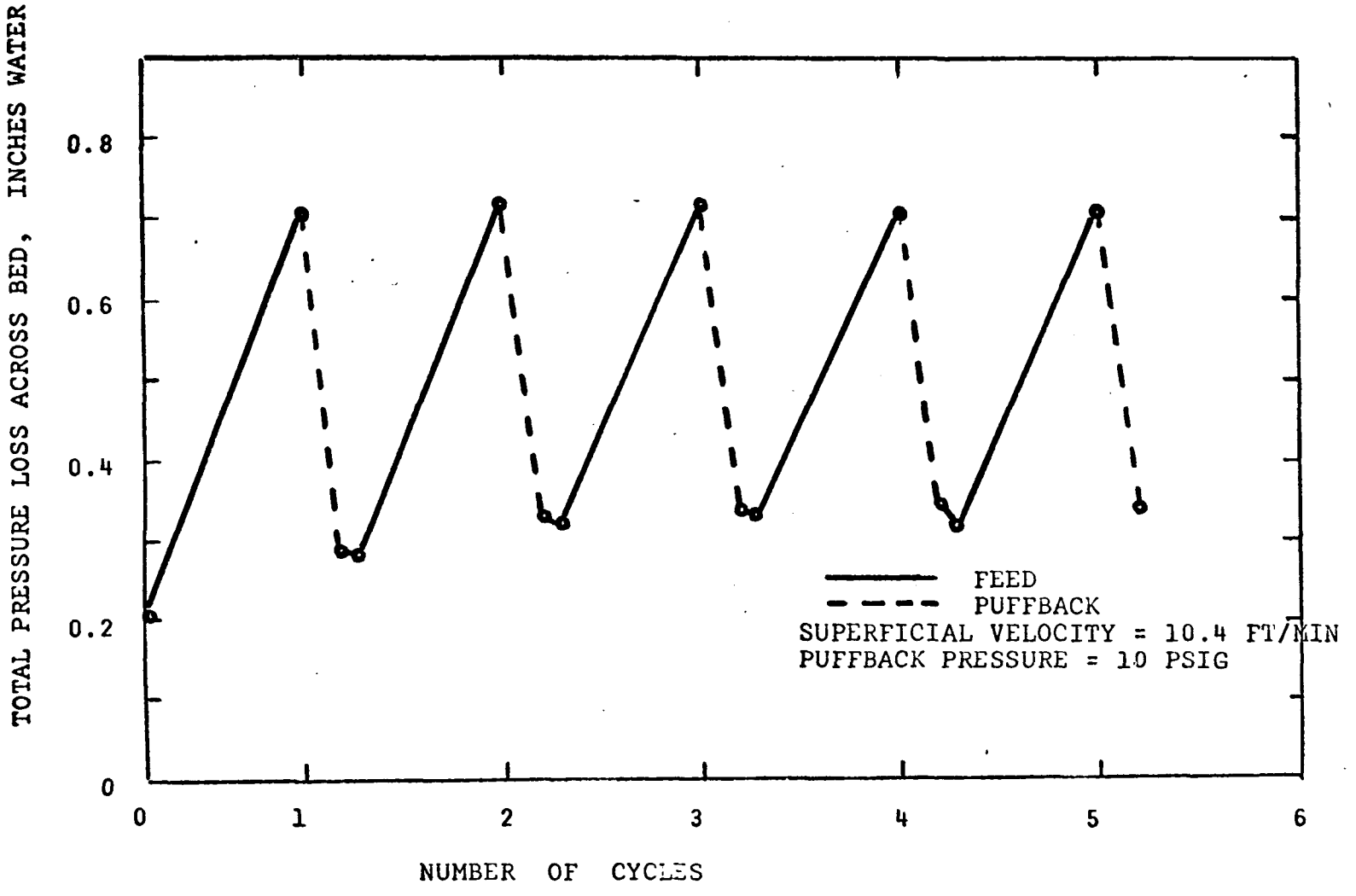

Figure 52. Typical cyclic behavior of granular bed filter (Run P-02).

of this and other runs are enumerated in Table 7.

The overall fly ash efficiencies obtained were all in excess of 99.3%, with many much higher. If more cycles had been performed, naturally the overall efficiencies would have tended to increase. In most cases, the initial fly ash efficiency was in excess of 99%. Comparison of the initial cycle efficiency with the overall cycle (complete run) efficiency indicates that as more cycles are performed, the latter efficiency increases. This is expected from filtration theory, for the first cycle forms the filter cake. The ash left after puffback (permanent filter cake ash) prevents the initial high ash penetration that is characteristic of a clean bed.

A glance at the amount of ash and sand removed by puffback illustrates the power of the puffback technique in regenerating a new filtration surface. From Table 7, Run P-01, the average Puff Ash/Bed Area was 0.149 grams/cm^2, which translates to an equivalent ash thickness removed of 0.25 cm, which is about 3-1/2 sand grains in thickness. The ratio of Puff Ash/Puff Sand was 0.48, which indicates a sand layer of approximately 0.21 cm, which is about 3 sand

Table 7. Representative Values for Panel Bed Filter

Run No.	P-31	P-32	P-33	P-34	P-01	P-02
No. of Cycles	6	7	6	7	7	5
V_{Bed} (ft/min)	4.0	4.3	5.1	5.1	10.4	10.4
Fly Ash Loading (grams/m^3)	8.4	14	7.6	14	6.5	4.4
Puffback Pressure (psig)	15	15	15	15	15	10
ΔP_o (inches water)	0.064	0.075	0.097	0.110	0.19	0.21
ΔP_t (inches water)	0.252	0.504	0.865	1.42[a]	0.71	0.71
ΔP_d (inches water)	0.092	0.126	0.180	0.24	0.29	0.34
$\frac{\Delta P_t - \Delta P_d}{\Delta P_t - \Delta P_o}$, Effectiveness	0.85	0.88	0.89	0.90	0.81	0.74
$\frac{\Delta P_t - \Delta P_o}{V_{Bed}}, \left(\frac{\text{inches water}}{\text{ft/min}}\right)$	0.047	0.057	0.151	0.257	0.050	0.048
Average $\frac{\text{Puff Ash}}{\text{Bed Area}}, \left(\frac{\text{grams}}{cm^2}\right)$	0.074	0.137	0.202	0.178[a]	0.149	0.140
Average $\frac{\text{Puff Ash}}{\text{Puff Sand}}$	0.30	0.37	0.45	0.38[a]	0.48	0.88
Initial Cycle Fly Ash Efficiency-Puff (%)*	99.54	99.79	99.80	99.936	na	na
Overall Fly Ash Efficiency-Puff (%)*	99.83	99.956	99.962	99.986	99.87	99.924
Overall Fly Ash Efficiency-Feed (%)*	99.923	99.982	99.985	99.995	99.933	99.961
V_A (ft/min)**	0.70	0.70	0.70	0.70 & 5.1	na	na
ξ_f**	0.15	0.045	0.086	0.22 & 0.016	na	na

Table 7. (Continued)

Run No.	P-03	P-41	P-22	P-23	P-14
No. of Cycles	4	6	12[b]	8	6
V_{Bed} (ft/min)	10.4	11.1	22.4	22.4	31.6
Fly Ash Loading (grams/m^3)	6.8	6.8	2.5	1.6	1.7
Puffback Pressure (psig)	20	15	15	15	27.5
ΔP_o (inches water)	0.21	0.22	0.45	0.47	0.80
ΔP_t (inches water)	0.71	0.52	0.97	1.36	1.80
ΔP_d (inches water)	0.37	0.34	0.61	0.77	1.46
$\frac{\Delta P_t - \Delta P_d}{\Delta P_t - \Delta P_o}$, Effectiveness	0.68	0.65	0.69	0.66	0.34
$\frac{\Delta P_t - \Delta P_o}{V_{Bed}}$, $\frac{\text{inches water}}{\text{ft/min}}$	0.048	0.025	0.023	0.040	0.032
Average $\frac{\text{Puff Ash}}{\text{Bed Area}}$, $\frac{\text{grams}}{cm^2}$	0.135	0.063	0.058	0.164	0.161
Average $\frac{\text{Puff Ash}}{\text{Puff Sand}}$	0.25	0.25	0.28	0.36	0.24
Initial Cycle Fly Ash Efficiency-Puff (%)*	na	99.57	97.7	99.72	99.47
Overall Fly Ash Efficiency-Puff (%)*	99.82	99.930	99.28	99.64	99.62
Overall Fly Ash Efficiency-Feed (%)*	99.926	99.969	99.78	99.82	99.86
V_A (ft/min)**	na	0.70 & 11.1	0.70	0.70	0.70
ξ_f**	na	0.28 & 0.55	0.73	0.30	0.55

Table 7. (Continued)

* Two ways of reporting the efficiency are used. One is based on the amount of ash puffed off the sand bed surface, the other on the total amount of fly ash fed to the panel.

** When two values are quoted, the first velocity corresponds with the first penetration, the second velocity with the second penetration.

(a) The bed fractured and lost some of its filter cake into the collection bin when the air stream was turned off. The ash quantities reported are based on the residual filter cake; that is, the cake that was eventually puffed off.

(b) A dilute aerosol penetration test was performed after the 8th cycle. The test had an effect on some of the tabulated values, therefore the quantities listed in this table are based only on the first eight cycles.

grains in thickness, was discharged. (Bulk density of ash = 0.60 grams/cm^3, bulk density of sand = 1.44 grams/cm^3.) The Effectiveness, Ω, was 0.81 for the above run. All the above indicate that most of the filter cake is deposited on the front face, with very little penetration of the fly ash into the sand bed. Note that most of the dirty bed pressure loss is recovered (about 80%). The unrecoverable portion is mostly made up of both permanent and non-permanent ash in the interior of the bed. The pertinent parameters for the above run were V_{Bed} = 10.4 ft/min (5.3 cm/sec), ΔP_o = 0.19 inches water, ΔP_t = 0.71 inches water, and puffback pressure = 15 psig.

The shock cleaning sequence listed in Table 8 indicates that only one puff per cycle is sufficient. Most of the pressure recovery ($\Delta P_t - \Delta P_d$) is made in the initial blast. Any shocks performed after the initial puff do not increase the pressure recovery a useful amount. Notice the second shock produced an increase in the bed pressure loss. This is a frequent occurrence during shock cleaning, and is indicative of ash that had not been previously dislodged being removed and carried from the interior of the bed

Table 8.

Comparison of Effect of Additional Cleanings on Bed: Run P-03;

V_{Bed} = 10.4 ft/min; P_o = 0.21 inches water; Puffback Pressure = 20 psig.

Pressure Loss Across Bed Before Operation (inches water)	Type of Operation	Pressure Loss Across Bed After Operation (inches water)	Weight Ash / Bed Area Recovered by Operation ($grams/cm^2$)	Weight Ash / Weight Sand Recovered by Operation
0.71	Final puff on bed before shock cleaing bed	0.36	0.120	0.22
0.36	Initial shock on bed	0.28	0.0410	0.096
0.28	One more shock	0.33	0.0166	0.050
0.33	One more shock	0.24	0.0149	0.035
0.24	Two more shocks	0.24	0.0172	0.033

towards the front face where this ash fills the voids in this region of high dust concentration. Thus the porosity of the residual (permanent) ash layer decreases, and the pressure loss increases.

With reference to Figure 52, it is seen that the pressure loss decreased during the initial minutes of feeding at the beginning of a new cycle on a bed after puffback. This is characteristic of practically every run. The puff had moved ash from the interior of the bed towards the dirty front face. This face was not totally cleaned by the puff, for ash that was not dislodged from the new sand surface remains there. The rest of this residual filter cake consists of ash that was just beneath the initial sand layer. This arrangement is not very stable, and once the air stream is turned on, the ash rearranges itself causing the characteristic dip in pressure loss. If, instead of turning on the feeder simultaneously with the air stream, the air stream alone is passed through the bed, the same distinctive dip is noticed.

While the fly ash was deposited there were instances where the pressure drop decreased suddenly, indicating rearrangement of the filter cake or a

possible tearing away of a portion of the filter cake towards the interior of the bed. In light of the horizontal bed studies these events could also indicate fracturing of the ash surface. These fractures or crevices eventually become filled as more ash is deposited onto the filter cake. These dips in pressure loss become larger as the thickness of the cake increases.

If a cycle is terminated (even before ΔP_t is reached), and clean air alone is passed through the bed at the run's face velocity, the pressure drop across the bed usually decreases a few percent. The percentage decrease was greater as the thickness of the filter cake increased. This change in pressure occurred over an initial period of several minutes, after which even a 12 hour continuation showed no further change in the pressure loss. These results compare favorably with the experiences on the horizontal bed,where passing clean air through the bed at V_{Bed} did not disturb the cake. The slight initial drop that occurs with the panel bed is probably some rearrangement or tearing away of some of the ash, and not a fracturing of the filter cake.

Exploration for Optimum Puffback Pressure

Previous work (55) demonstrated that a face velocity of about 10 ft/min (≈ 5 cm/sec) with a fly ash filter cake producing a pressure loss of about 1/2 inch water would be suitable for a panel bed filter treating the stack gases of a power station. The effect of puffback pressure on the cyclic operation of the panel under the above conditions was first explored. Puffback pressures of 10, 15,and 20 psig were investigated. The results of these runs are presented in Table 7.

The average Puff Ash/Bed Area dislodged is about the same for all three puffback pressures, while the Puff Ash-to-Puff Sand ratio decreases with increasing puffback pressure. This indicates that the bulk of the filter cake that is discharged is localized within the front face (at least at this velocity), and only a small puffback pressure is required to dislodge it. On a virgin bed a shock of 10 psig dislodged no sand. The presence of a filter cake provided a resistance to the air puff, creating a localized buildup of pressure. This force dislodges the ash and the neighboring sand.

A maximum in the Effectiveness, Ω , was obtained with a puffback pressure of 15 psig. A lesser

value of Ω at a puffback pressure of 10 psig is due simply to a smaller burst of air dislodging less ash and sand. A smaller value of Ω at a puffback pressure of 20 psig occurs because the more powerful burst dislodges more ash from the interior of the bed. This ash fills the voids in the neighborhood of the front face, thus creating a lower porosity and therefore a higher ΔP_d.

Notice that the overall fly ash efficiencies decrease as the puffback pressure increases, which is what one would expect. All the efficiencies were in excess of 99.9%.

The above suggested that a puffback pressure of 15 psig would be suitable for an initial exploration of the operation of the panel. This pressure gave a maximum Effectiveness along with a favorable ash-to-sand ratio.

Additional runs were performed at a face velocity of 11.1 ft/min (5.6 cm/sec) and at a puffback pressure of 15 psig, but with a thinner filter cake (lower ΔP_t), to complement the 10.4 ft/min runs. The Effectiveness increases and apparently levels off, while the initial cycle efficiency increases as a

thicker cake is deposited. This indicates that as more fly ash is deposited onto the bed, less penetrates into the interior and more is captured by the filter cake; that is, σ increases.

Effect of Velocity on Cyclic Operation

The cyclic operation of the bed was explored using a V_{Bed} of about 5 and 22.4 ft/min ($\approx$ 2.5 and 11.4 cm/sec) and a puffback pressure of 15 psig. Runs were performed where the thickness of the filter cake was successively increased.

As the bed velocity increases the Effectiveness decreases. Typical values were $\Omega = 0.87$ for 5 ft/min, $\Omega = 0.80$ for 11, and $\Omega = 0.67$ for 22.4 . The initial cycle efficiency and the overall efficiency also decreased as the velocity increased. This would be expected, because as the velocity is increased, more fly ash is collected in the interior of the bed (σ decreases). As more ash is collected in the interior of the bed, the strength or force of the puff is dissipated in the interior of the bed and not concentrated on the front face. A logical consequence of more ash depositing in the interior of the bed is a decrease in the bed efficiency.

It was very difficult to build up a stable, thick filter cake with V_{Bed} = 5 ft/min. At high values of the bed pressure loss, ΔP_t = 1.4 inches water, for example, the pressure loss would fluctuate a great deal and even decrease as much as 0.2 inches water. The Pre-Puff Ash would contain large chunks of fly ash, and if the air stream was turned off and then turned on again the original pressure loss was not recovered; ΔP_t would decrease as much as 0.50 inches water out of a total final pressure loss of ΔP_t = 1.42 inches water. This is indicative of a very unstable filter cake, which would fracture readily, and thus have a low value of $K_f\sigma$. This occurrence is borne out by the horizontal bed studies, which demonstrated that low $K_f\sigma$ values occur at very low velocities.

As ΔP_t is increased, the initial cycle efficiency increased from a value of 99.54% with a ΔP_t of 0.252 inches of water to a value of 99.946% with a ΔP_t of 1.42 inches water. The corresponding increase in the overall cycle efficiency (Puff basis) was from 99.82% to 99.986%. The corresponding increase in the Effectiveness was from 0.85 to 0.90. This is expected, because at this low velocity (5 ft/min) most of

the ash is deposited as a filter cake, with very little penetration, and each succeeding portion of the ash is filtered out by the filter cake that has already been established.

Looking at the other extreme, the filter cake deposited at 22.4 ft/min was more stable than the 5 ft/min cake. The Effectiveness was much lower, about 0.67 with no noticeable trend with increasing ΔP_t. Coupled with the lower value of the overall fly ash efficiency, this is indicative of high penetration of the ash into the bed. Whereas in the lower velocity runs the efficiencies increased as a thicker cake was deposited, at V_{Bed} = 22.4 ft/min there is an apparent leveling off of both the initial cycle efficiency and the overall fly ash efficiency (Puff basis) at about 99.7%. This could arise if one is approaching the higher velocities that Taub (59) explored. The apparent consistency of the Effectiveness indicates the incoming fly ash distributes itself in a constant ratio; that is, a certain fraction goes towards forming the filter cake.

The first run at this velocity (22.4 ft/min) with the lowest ΔP_t, produced an initial cycle

efficiency of 97.7%. This would be indicative of the conditions previously discussed, where it takes a long time to produce a filter cake; hence, the high penetration of the ash.

As mentioned, the filter cake developed at this velocity was more stable than the one deposited at 5 ft/min. If the air stream is turned off, and then turned on again after a slight pause, no change in ΔP_t is observed. Fluctuations in the pressure loss across the bed were noticed during the feed portion of the cycle, but they were not as severe as with the 5 ft/min runs. The Pre-Puff Ash at the higher velocity was very fine, indicating that it was composed of feed ash that settled out and did not enter the panel bed.

Chunks of fly ash filter cake were present in the Puff Ash, however. Examination of the surface of the sand bed after the bed was shock cleaned disclosed the presence of some chunks of ash resting on the louvers. These chunks could have been developed in either of two ways. They could have arisen from the fracturing of the filter cake during the feeding operation, or from a fracture that was created by a puff. In either case, the burst of air was insufficient

to dislodge these chunks of ash.

Limitations of Operating Conditions

An attempt to operate the bed at a face velocity of 31.6 ft/min (≈ 16 cm/sec), with a puffback pressure of 15 psig, and a ΔP_t of 1.12 inches water was unsuccessful. After three cycles, ΔP_d was greater than ΔP_t, as seen in Figure 53. Operation at the same bed velocity, but with a puffback pressure of 27.5 psig and a ΔP_t of 1.36 inches water was unsuccessful for the same reason. After two cycles ΔP_d was greater than ΔP_t. In both cases $\Delta P_t - \Delta P_o$ was about 1/2 inch water.

However, successful operation of the panel was attained with a puffback pressure of 27.5 psig and a ΔP_t of 1.80 inches water, as seen in Table 7.

The increase in ΔP_d above ΔP_t under certain conditions is similar in nature to the increase in pressure during shock cleaning. First of all, at a velocity of 31.6 ft/min one has a very deep penetration of the fly ash. This is confirmed by the low value of the Effectiveness. When the bed is puffed, fly ash in the interior of the bed is carried towards the front face, where it fills the voids in the bed's front surface.

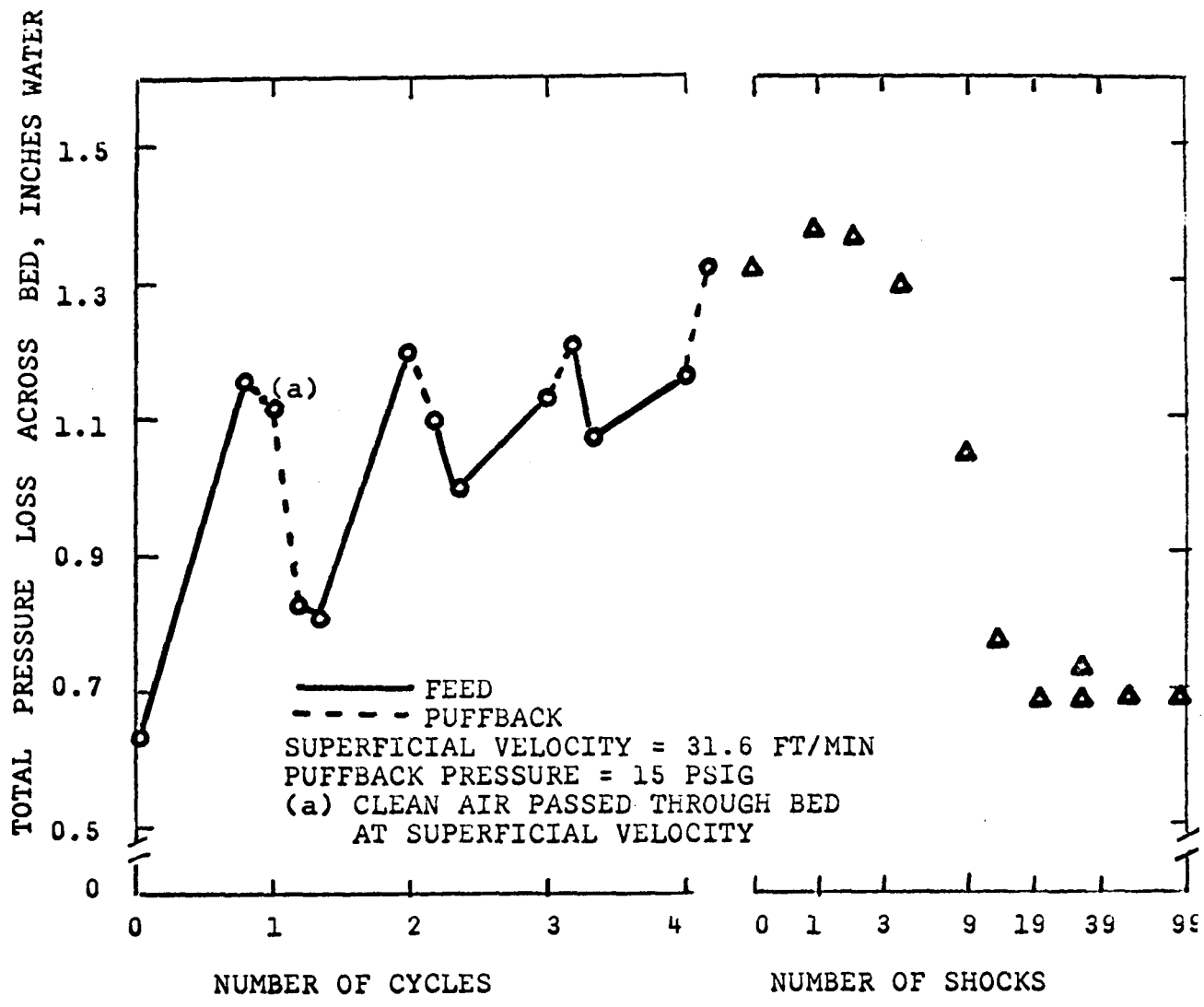

Figure 53. Failure to attain cyclic operation and subsequent shock cleaning on panel (Run P-11).

This arrangement is unstable to a certain extent, as seen by the large dips in the cycle's initial pressure loss. (Figure 53).

The question of why an increase in ΔP_t (from 1.36 to 1.80 inches water) leads to stable cyclic operation can easily be explained. ΔP_d in the stable run is 1.46 inches water, which is above the former ΔP_t. The surface filter cake develops very slowly at this velocity. Apparently, in the successful run the increase in pressure drop due to the filter cake was enough to overcome the effect of the interior ash filling the voids, and thus stable operation was achieved.

Dilute Aerosol Penetration Tests

Initial efforts were directed at performing most of the aerosol tests at a face velocity of about 0.70 ft/min ($\approx$ 0.35 cm/sec). Additional aerosol test velocities would be used to obtain a more complete picture of the filter cake, using information from the dilute aerosol work on clean sand beds (Part One of this dissertation). Knowing the velocity-penetration curve and the thickness of the filter cake one could therefore gain insight to the value of $\eta_f \sigma$ in equation (86) and

the structure of the cake. The above velocity (0.70 ft/min) is in the diffusion regime for aerosol filtration, where excellent agreement was obtained between theory and experiment. The test aerosol was to enter sideshot, through the tapered entrance section (Figure 42).

Figure 54 illustrates the effect of performing the aerosol penetration tests at an aerosol face velocity (V_A) of 0.70 ft/min on a filter cake deposited at a face velocity (V_{Bed}) of 22.4 ft/min. Note the sharp change in the cyclic behavior of the panel after the aerosol test was performed. The pressure loss after puffback, ΔP_d , is higher after the aerosol test, and the Puff Ash quantities decrease. This is indicative of the general behavior of the panel bed if an aerosol test is made at a velocity not equal to V_{Bed} . On-off-on operation of the panel at 22.4 ft/min had no effect on ΔP_t , indicating the integrety of the filter cake at this velocity.

It is now seen that this approach ($V_A \neq V_{Bed}$) is unsuitable for several reasons. The large differences between the two velocities could conceivably cause fracture or rearrangement of the filter cake in a manner similar to the "Velocity Shift" phenomena on the

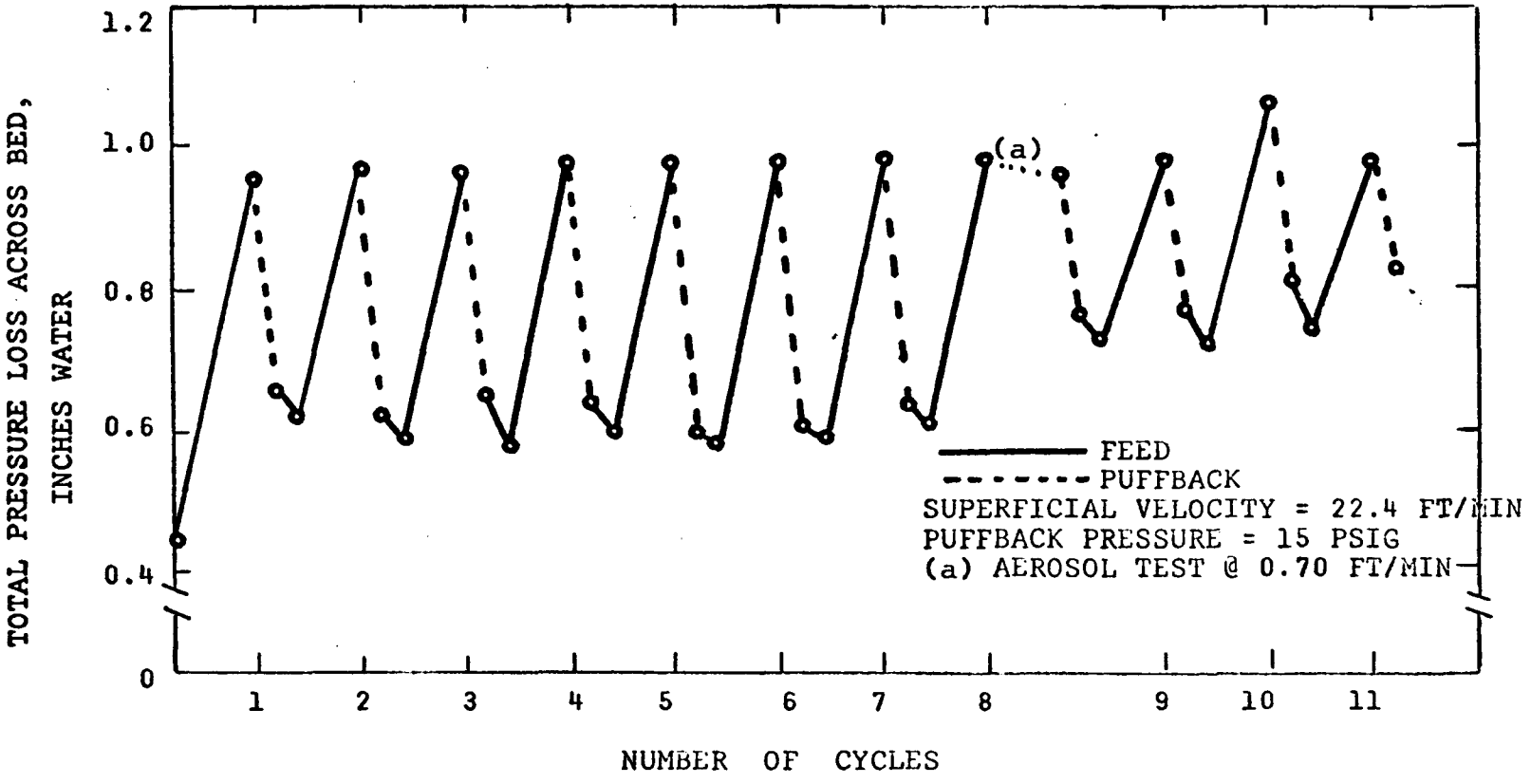

Figure 54. Effect of dilute aerosol test on cyclic operation of panel (Run P-22).

horizontal bed. This would affect the bed's cyclic behavior.

The aerodynamic path of the aerosols is radically different from the path of the fly ash. Therefore the resultant penetrations of the test aerosol do not reflect the penetration of the 1.1 micron fly ash particles. While this by itself is not a problem if one is comparing the thicknesses of filter cakes deposited at the same velocity, no definite correlation can be drawn from filter cakes deposited at different velocities. When this factor is coupled with the possibility that different aerodynamic paths cause fracture, this approach ($V_A \neq V_{Bed}$) is unsuitable.

The results at 22.4 ft/min are indicative of the problem. The table below compares the fractional penetration of the test aerosol at 0.70 ft/min with the total pressure drop due to the filter cake (which reflects the thickness of the filter cake) for four different runs (ΔP_o = 0.45 inches water).

$\Delta P_t - \Delta P_o$ (inches water)	ξ_f
0.53	0.73
0.91	0.30
1.90	0.20
3.78	0.19

Obviously, increasing the filter cake thickness does not change the fractional penetration of the test aerosol a significant amount.

A glance at the results from the aerosol tests performed on the 5 ft/min filter cakes discloses a more radical effect of the aerosol test on the filter cake. This would be expected, for this cake is more loosely packed and is more susceptible to change. Notice the significant change in the pressure loss of the bed after performing the aerosol test, and the changes in the Puff Ash/Bed Area and the Puff Ash-to-Puff Sand quantities (Table 9).

These results indicated that the aerosol tests should be performed at the velocity the filter cake was deposited. Performing the aerosol tests on a 5 ft/min filter cake with a ΔP_t of 1.42 inches water gave the following (ΔP_o = 0.10 inches water):

Aerosol Test Velocity (ft/min)	ξ_f
0.70	0.22
5.1	0.016

On this loosely packed filter cake, performing the aerosol test at 0.70 ft/min fractured the filter cake severely, for the pressure drop after the aerosol test

Table 9.

Effect of Aerosol Tests on Various Bed Parameters:

Run P-33 V_{Bed} = 5.1 ft/min

V_A = 0.70 ft/min

	Pre-Test Cycle	Post-Test Cycle
Bed Pressure Loss After Feeding (inches water)	0.87	0.80
Bed Pressure Loss After Puffback (inches water)	0.18	0.20
Puff Ash/Bed Area (grams/cm^2)	0.193	0.147
Puff Ash/Puff Sand	0.45	0.38

Note: On-off-on operation with the feed air stream had no effect on the above parameters.

was about 0.50 inches water (a loss of about 0.90 inches water). Use of the second method, with the test aerosol at the bed velocity, and with the feed air stream left on as the test aerosol stream was introduced, produced very little change in ΔP_t during the aerosol test. Turning the air stream off and then on again produced some fractures in the cake, but not as severe as with the 0.70 ft/min test.

This confirmed that the test aerosol should be introduced at the bed velocity, and with thick, loosely packed filter cakes the feed air stream must be left on when switching to the aerosol test stream. The simplest way of determining if this precaution is necessary is to shut off the air stream at ΔP_t and then turn it back on again. If no pressure change is noticed, and if the bed still maintains its cyclic behavior, it is probably not necessary to keep the air stream on at all times, and the cake is fairly stable.

The apparent restructuring of the fly ash filter cake after an aerosol test was performed at a velocity different from the deposition velocity, or with a different aerosol aerodynamic path is similar in nature to the fractures brought about in the "Velocity

Shift" experiments on the horizontal sand bed. It is known that the adhesive forces between collectors and dust particles are dependent on the flow velocity (68), and the detachment of particles from collector surfaces also varies with the flow velocity. Likewise, the cohesive forces between the individual dust particles are affected by changes in the flow velocity (68). Furthermore, the shape of the deposited fly ash layer and the size distribution of the fly ash particles on the collector surface is dependent on the flow velocity. Thus, a shift in the bed velocity or an altering of the aerodynamic path of the air stream can both rearrange the filter cake and affect weak points in the filter cake, causing fracture of the cake.

The penetration of 0.016 for the aerosol test stream was the best value obtained in work on the filter panel. This was at ΔP_t = 1.42 inches water, or $\Delta P_f = \Delta P_t - \Delta P_o$ = 1.31 inches water. At this thickness of filter cake (Puff Ash/Bed Area = 0.18 grams/cm^2, and $\Delta P_f/V_{Bed}$ = 0.26 inches water/ft/min) one might expect a penetration of about 10^{-5} from Figure 46 or at least 10^{-3} from Figure 47 in light of the tests conducted on a filter cake resting on a horizontal sand surface. This

discrepancy may be the result of the high voidage of the sand in the test panel, a factor that will be discussed later.

By performing the aerosol penetration tests at V_{Bed} and by using several different aerosol sizes (0.5 microns, 1.1 microns, 2 microns, for example) a complete analysis of the filtration mechanism can be obtained. The test should be performed at various stages of the development of the filter cake. The variation of penetration with particle size as a function of time (and therefore thickness of the filter cake) can be obtained, and from this an instantaneous value of the overall fly ash efficiency can be realized.

Packing of Sand in the Panel

Several factors indicate the average porosity of the sand in the panel is quite high, reflecting poor packing of the sand granules. Figure 55 illustrates the increase in the clean bed pressure drop, ΔP_o, as the puffback pressure is increased. This would be indicative of poor packing, for the higher puffback pressure compacts the sand in the bed.

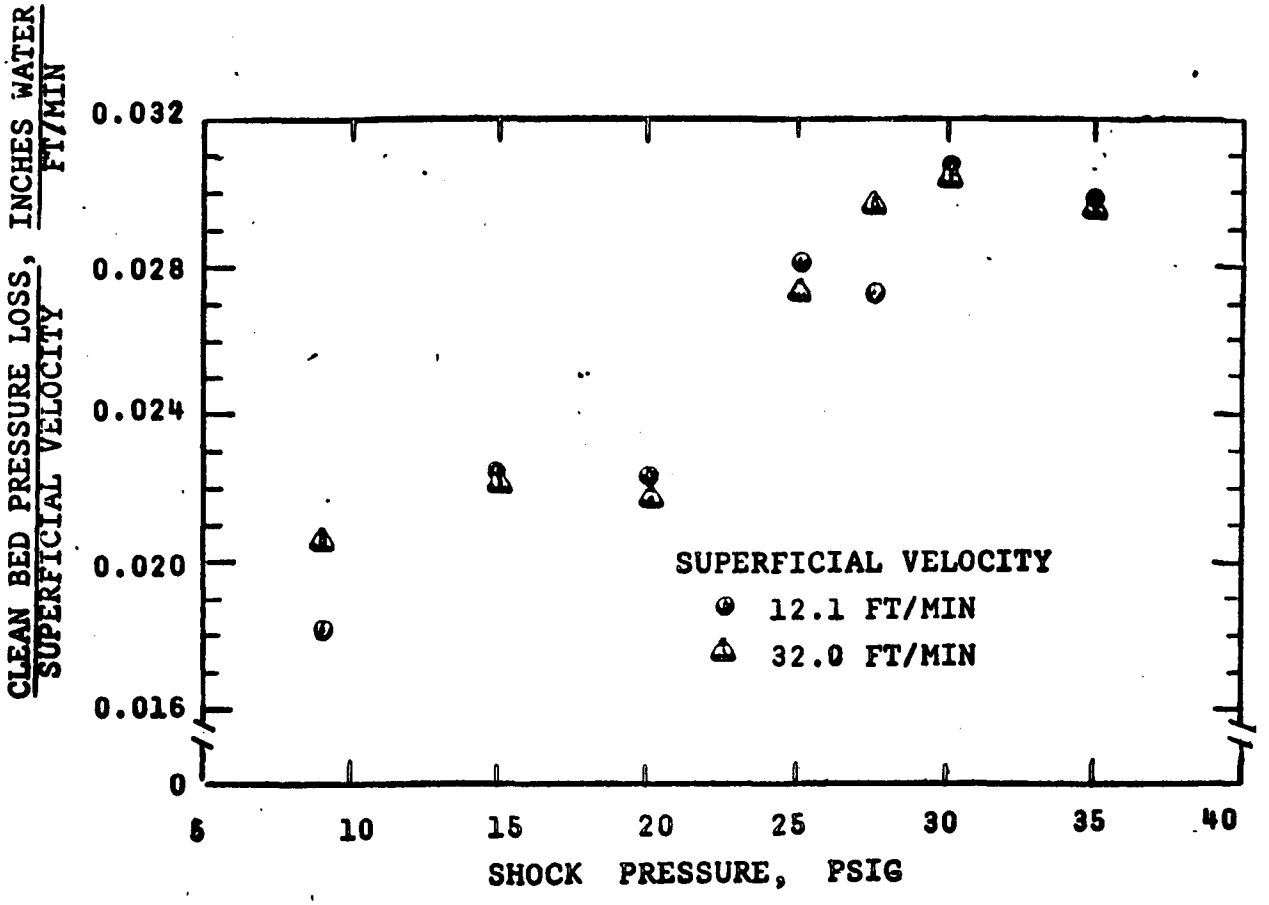

Figure 55. Effect of shock pressure on clean bed pressure loss.

The average porosity of the sand in the panel bed can be calculated from the Carman-Kozeny equation (67):

$$\Delta P_o = K_o' \frac{(1 - \epsilon)^2}{\epsilon^3} V_{Bed}\, b$$

K_o' can be calculated from pressure drop measurements on the horizontal bed, since the porosity of the sand is known. Using this value of K_o', along with pressure loss measurements on the clean panel (at 15 psig puffback pressure) the voidage in the panel is calculated as 0.61.

Aerosol penetration measurements on the virgin panel can also be utilized to calculate an effective porosity of the panel. A fractional penetration of 0.47 was obtained at a face velocity of 0.72 ft/min (0.35 cm/sec). This is clearly in the diffusion regime, and equation (35)

$$E = 5.04\, \rho(\epsilon)^{-1/3}\, Pe^{-2/3} \qquad (35)$$

used along with equation (28)

$$\xi = \exp - \frac{3}{4} \frac{1 - \epsilon}{\epsilon} \frac{E}{r_c} b \qquad (28)$$

generates an effective porosity of 0.55.

It is evident that the effective porosity of the panel is in excess of 0.43, the value for the horizontal bed. This is probably due to the regions of high porosity near the side walls and the top of the sand bed. This provides a convenient bypass for the flow, and may contribute to the high dilute aerosol penetration measurements on the filter cake.

The fly ash, because of the centrifugal force imparted to it as it turns the corner to enter the bed, is forced to the bottom of the inclined sand surfaces. The upper portion of the inclined surface, especially near the louver-sand interface, therefore has a relatively thin filter cake. However, since the aerosol in most cases entered sideshot, it could easily weave its way into regions of low filter cake density near the walls of the panel. This channelling would not have as great an effect on the fly ash efficiencies as it would have on the aerosol efficiencies, because most of the ash is filtered by the first few layers of the sand, if not by the filter cake.

18. CONCLUSIONS

High filtration efficiencies have been demonstrated for operation of a granular bed filter under conditions conducive to the formation of a regenerative filter cake. Steady state cyclic operation at a face velocity of about 11 ft/min produces overall collection efficiencies in excess of 99.9% for a run of seven cycles, for a regenerative filter cake thickness of the order 0.14 grams/cm^2, and with a fly ash pressure loss of about 1/2 inch water just before regeneration by means of puffback.

The fly ash efficiency increases as the number of cycles in a run is increased, because the fly ash left after puffback strains the incoming fly ash, thus preventing the initial "high" penetration that prevails on a virgin sand bed. However, in the range of face velocities, puffback pressures, and filter cake thicknesses explored in this research, the fly ash collection efficiency on the first cycle was never lower than 97.7%. Not surprisingly, at constant face velocity an increase in the thickness of the filter cake increases both the initial cycle efficiency and

the overall efficiency.

The ratio of the pressure loss recovered by puffback to the total pressure loss due to the fly ash, called the Effectiveness, is an indication of the efficiency of the puffback operation. A high value of the Effectiveness is generally desirable, for this means most of the dirty bed pressure loss is recovered. For a face velocity of 11 ft/min, and with a puffback pressure of 15 psig, this ratio was 0.80.

As the face velocity increases, the initial cycle efficiency and the overall cycle efficiency decreases. The Effectiveness also decreases, because a greater portion of the fly ash goes into the interior of the bed and is not strained by the filter cake. Increasing the velocity decreases the fraction of the fly ash that goes into forming a filter cake. At the high velocities explored by Taub (59), above 60 ft/min, no filter cake forms. An Effectiveness of 0.66 and 0.34 for runs of 22 and 32 ft/min respectively was observed for substantially identical thicknesses of fly ash filter cake (as reflected by the quantity of puff ash). The puffback pressures were 15 and 27.5 psig respectively. Both the decline in Effectiveness and the required

increase in puffback pressure indicate the greater penetration of fly ash into the sand at 32 ft/min. Taub's results would indicate that extended operation of a panel bed filter at a velocity above 60 ft/min would yield an Effectiveness close to zero as well as a filtration efficiency close to zero. These results suggest that for the filter cake thicknesses, puffback pressures, and sand size used in this work, about 30 ft/min is a practical upper limit for operation of the panel.

It should be noted, however, that higher velocities tend to produce a cake that is more compact and stable, and less prone to fracture.

The horizontal bed studies demonstrated that a fly ash filter cake deposited on a horizontal sand surface can produce filtration efficiencies in excess of 99.99% against a dilute aerosol stream of 1.1 micron Dow microspheres, for a filter cake thickness of 0.14 grams/cm^2 and a face velocity of 4.5 ft/min. Aerosol penetration tests on a filter cake can disclose characteristics, such as pinholes or cracks developing in the cake, which often cannot be abstracted from pressure drop measurements.

The nature of the fly ash filter cake can be described through the use of the terms $K_f\sigma$, which arises from pressure drop measurements on the cake, and $\eta_f\sigma$, which arises from aerosol penetration measurements. K_f is the permeability constant for the filter cake, η_f is the dilute aerosol attentuation coefficient, and σ is the fraction of the deposited fly ash that goes into forming the filter cake.

A more compact, less porous filter cake, with a larger value of $K_f\sigma$ and $\eta_f\sigma$, is produced if the fly ash is deposited onto the horizontal sand surface with a low intensity of deposition. At first, increasing the face velocity of the fly ash stream increases $K_f\sigma$ and $\eta_f\sigma$, but after a face velocity of about 12 ft/min is reached, both quantities decrease. At low velocities the influence of K_f and η_f prevails, both increasing as the velocity increases; however, as the velocity is increased further, σ begins to decrease as more and more ash penetrates into the interior of the bed until the conditions explored by Taub (59) are reached, where σ effectively goes to zero.

The use of a test aerosol of 1.1 microns diameter is very appropriate for experiments evaluating

the performance of a filter cake resting on a surface. The aerosol is in the size range that is the most difficult to filter (62,63) and most hazardous to health. A plot of the percentage of particles of unit density deposited in the lungs vs particle diameter indicates a deposition of over 50% for about 1 micron particles, with a sharp decrease to less than 10% for 4 micron particles (29).

19. RECOMMENDATIONS FOR FURTHER STUDY

The following recommendations for further investigation are suggested:

(1) In light of the information realized from the horizontal bed studies, a dispersed fly ash stream should be deposited on the sand surface, as in the work on the panel.

(2) The ledge should be removed. This will alleviate the problem of loosing some of the fly ash feed stream as well as some of the Puff Ash and Puff Sand on the ledge.

(3) A different method of introducing the test aerosol stream should be utilized, so that the aerosol stream can follow the same aerodynamic path as the fly ash stream. In addition, all tests should be performed at the fly ash deposition velocity. A new entry point for the test aerosol stream should be provided just below the entrance point of the fly ash stream into the vertical tapered section.

(4) The sand reservoir and the panel section should be reconstructed in order to eliminate any

potential short circuiting of the air streams. This should decrease the average porosity of the granular bed.

(5) A higher puffback pressure might be worth looking into. It has been shown that a higher puffback pressure increases the bed pressure drop by decreasing the porosity. This would help decrease the high voidage mentioned in (3).

(6) A detailed investigation on both the horizontal bed and the panel bed filter on how σ declines toward zero, thus bridging the velocity gap between this work and the study of Taub, is called for.

(7) Studies for both horizontal and vertical beds should examine:

---other sand sizes (or possibly glass beads or lead shot of a very narrow size distribution),

---other bed thicknesses (this would be especially valuable in investigating σ),

---other dusts, including the use of filter aids,

---other test aerosols,

---investigation of the filter cake during a cycle by the aerosol penetration technique.

20. APPENDIX

APPENDIX A. DEVELOPMENT OF THE TRANSFORMATION EQUATION

The equation describing the Brownian motion of a particle in the absence of an external force is

$$m_p \frac{d\bar{V}_B}{dt} = - \frac{\bar{V}_B}{B} + m_p \bar{A}(t) \qquad (A.1)$$

Chandrasekhar (8) demonstrated that this can be transformed into the conventional diffusion equation

$$\frac{\partial n}{\partial t} = \nabla \cdot (\Delta \nabla n) \qquad (A.2)$$

if

$$t >> B\, m_p$$

Now, if external forces, $m_p \bar{K}(\bar{x},t)$, are present, where $\bar{K}$ is the acceleration produced by the external forces, then the particle equation is

$$m_p \frac{d\bar{V}_B}{dt} = - \frac{\bar{V}_B}{B} + m_p \bar{K} + m_p \bar{A} \qquad (A.3)$$

Chandrasekhar demonstrated that this equation also can be transformed, if $t >> B\, m_p$ and $\bar{K}$ does not change

appreciably over distances of the order $(\Delta B m_p)^{1/2}$, giving

$$\frac{\partial n}{\partial t} = \nabla \cdot (\Delta \nabla n - B m_p \bar{K} n) \qquad (A.4)$$

which is Smoluchowski's equation.

The simplest example of an external force is that of gravity, where $\bar{K} = \bar{g}$. Then equation (A.3) becomes

$$m_p \frac{d\bar{V}_B}{dt} = - \frac{\bar{V}_B}{B} + m_p \bar{g} + m_p \bar{A} \qquad (A.5)$$

with its corresponding transformation

$$\frac{\partial n}{\partial t} = \nabla \cdot (\Delta \nabla n - B m_p \bar{g} n) \qquad (A.6)$$

The above equation describes the effect of gravity on Brownian motion.

Now, if there is a fluid moving at constant velocity $\bar{U}_M$, the governing equation becomes

$$m_p \frac{d\bar{V}_B}{dt} = - \frac{1}{B} (\bar{V}_B - \bar{U}_M) + m_p \bar{A} \qquad (A.7)$$

or

$$m_p \frac{d\bar{V}_B}{dt} = - \frac{1}{B} \bar{V}_B + \frac{1}{B} \bar{U}_M + m_p \bar{A} \qquad (A.8)$$

The accompanying transformation is

$$\frac{\partial n}{\partial t} = \nabla \cdot (\Delta \nabla n - \bar{U}_M n) \qquad (A.9)$$

which is the diffusion equation with convective flow (38). It is seen that all other effects on the particle can be considered to be external forces and are equivalent to the term $m_p \bar{K}$ in equation (A.3).

If there is bulk flow and gravity superimposed on the Brownian motion the governing equation is

$$m_p \frac{d\bar{V}_B}{dt} = - \frac{1}{B} (\bar{V}_B - \bar{U}_M) + m_p \bar{g} + m_p \bar{A} \qquad (A.10)$$

or

$$m_p \frac{d\bar{V}_B}{dt} = - \frac{1}{B} \bar{V}_B + \left(\frac{\bar{U}_M}{B} + m_p \bar{g} \right) + m_p \bar{A} \qquad (A.11)$$

so that

$$\frac{\partial n}{\partial t} = \nabla\cdot\left[\Delta\,\nabla n - \left(\bar{U}_M + B\,m_p\,\bar{g}\right) n\right] \qquad \text{(A.12)}$$

If the particle is accelerated because of a change in the fluid velocity (say in the neighborhood of a collector particle), the governing equation becomes

$$m_p \frac{d\bar{V}_B}{dt} + m_p \frac{d\bar{V}_p}{dt} = -\frac{1}{B}\left(\bar{V}_B - \bar{U}_M\right) - \frac{1}{B}\left(\bar{V}_p - \bar{U}_M\right) + m_p\,g + m_p\,A \qquad \text{(A.13)}$$

or

$$m_p \frac{d\bar{V}_B}{dt} = -\frac{1}{B}\bar{V}_B + \left[-m_p \frac{d\bar{V}_p}{dt} + \frac{\bar{U}_M}{B} - \frac{\bar{V}_p - \bar{U}_M}{B} + m_p\,\bar{g}\right] + m_p\,\bar{A} \qquad \text{(A.14)}$$

The above can be transformed into

$$\frac{\partial n}{\partial t} = \nabla\cdot\left[(\Delta\ \nabla n) - \left\{ m_p \frac{d\bar{V}_P}{dt} + \frac{\bar{U}_M}{B} - \frac{\bar{V}_P - \bar{U}_M}{B} + m_p \bar{g} \right\} B\ n\right] \tag{A.15}$$

or

$$\frac{\partial n}{\partial t} = \nabla\cdot(\Delta\ \nabla n) - \nabla\cdot(\bar{U}_M\ n) - \nabla\cdot n\left[- m_p \frac{d\bar{V}_P}{dt} - \frac{\bar{V}_P - \bar{U}_M}{B} + m_p \bar{g} \right] B \tag{A.16}$$

which is equation (15) in dimensional form.

APPENDIX B. SINCLAIR-PHOENIX PHOTOMETER

The commercial Sinclair-Phoenix Aerosol Photometer, model JM-3000-AL was modified as follows (see Figure B.1):

1- Intake manifold was removed, tubing attached directly to aerosol stream.

2- Pump supplied with unit was used only at high flow rates. At low flow rates, to avoid too high a vacuum in the system, a Gast Model 1531 vacuum pump was used.

3- A 100 millimicron Millipore filter was used in the room intake filter system (location FC, Figure B.1).

4- At low flow rates a vacuum pump was connected to the excess discharge rotameter. This was necessary in order to maintain a constant, low flow rate to the photometer.

5- A Dwyer pressure control was connected at point P2 in Figure 12, just upstream of the photometer. The unit would shut down if the vacuum exceeded 10 inches of water at that point. Generally, the system was operated within two to five inches of water of atmospheric pressure.

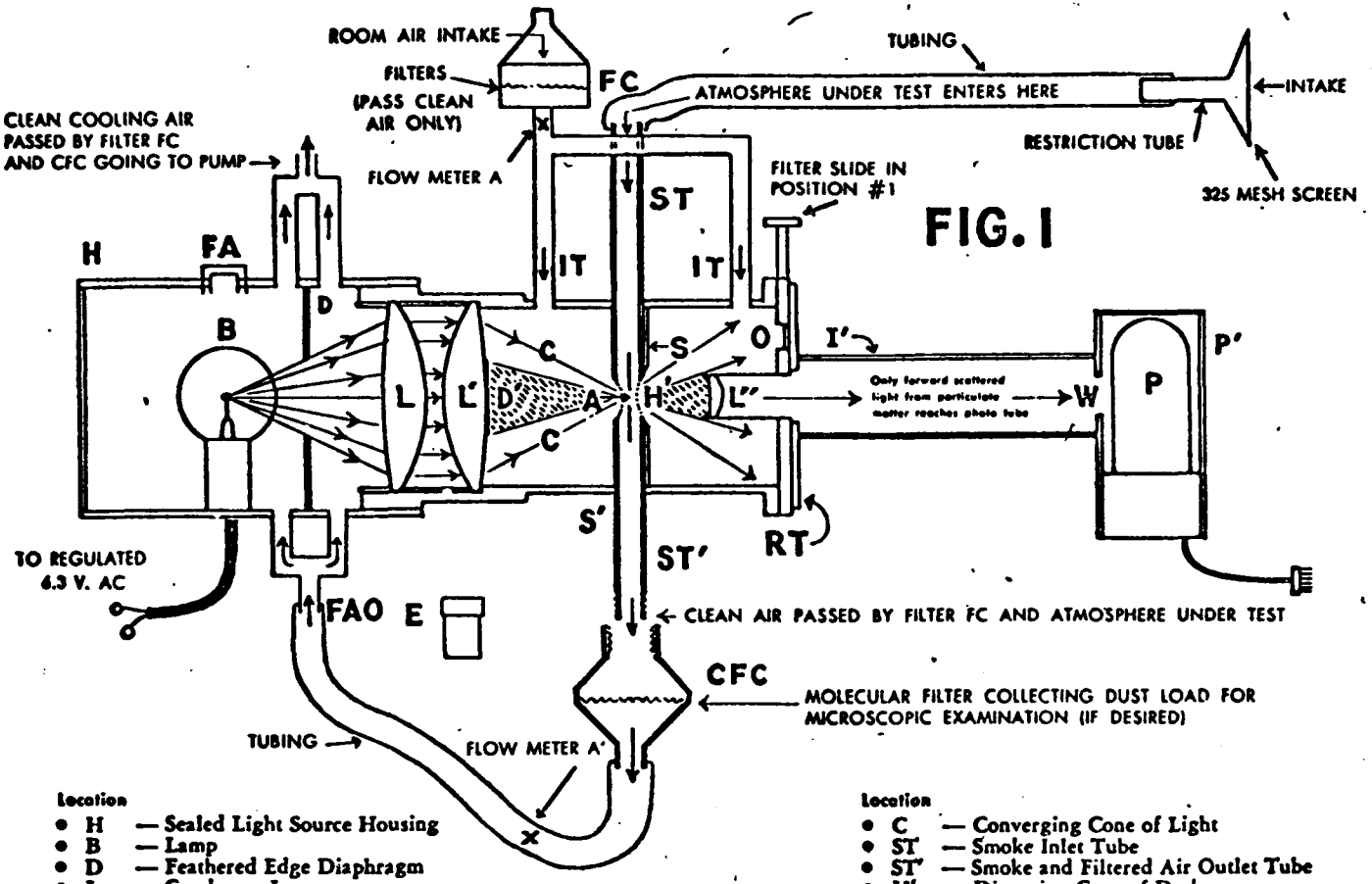

FIG. 1

Location

- H — Sealed Light Source Housing
- B — Lamp
- D — Feathered Edge Diaphragm
- L — Condenser Lens
- L' — Condenser Lens
- D' — Diaphragm Stop Produces converging cone of darkness
- IT — Filtered Air Inlets
- FC — Optical System protector filter and carrier
- E — Removable eyepiece which replaces photomultiplier tube for visual observation of smoke particles, also used for alignment
- CFC — Mass collector filter carrier
- A — Stray Light Limiting Diaphragm
- FA — Filament Alignment Window

Location

- C — Converging Cone of Light
- ST — Smoke Inlet Tube
- ST' — Smoke and Filtered Air Outlet Tube
- H' — Diverging Cone of Darkness
- S — Stray Light Diaphragm
- O — Optical Calibration Filters
- L" — Scattered Light Collecting Lens
- I' — Light Trap Tube
- W — Photomultiplier Tube Diaphragm
- P — Photomultiplier Tube
- P' — Shielded Photomultiplier Tube Housing
- S' — Sealed Optical Housing
- P3 — Cable to Logarithmic Amplifier
- FAO — Lamp Cooling Air Inlet
- RT — Rotatable Light Trap Tube Flange

Figure B.1. Optical system and smoke chamber of Sinclair-Phoenix photometer.

The photometer was readied for operation as follows:

1- First the generator containing distilled water was used to obtain a zero concentration reading on the photometer. This would effectively subtract any background dust or water droplets present in the air stream from the actual aerosol concentration. This was done more to correct for dust than for water vapor. Lundgren and Cooper (40), working with an identical Sinclair-Phoenix photometer and with polystyrene latexes, found that relative humidities of 85% had no effect on light scattering. In any event, the dry air flow was at least 20% of the main flow.

2- The air flow through the "distilled water" generator is now diverted to the aerosol generator. The flow rate used in operation (1) must be maintained. With aerosol flowing through the Tygon bypass, a reading of about 90% full scale on the recorder is obtained. The photometer gain has to be increased in order to obtain this reading. However, in doing this the background concentration response would also increase. Therefore, it is necessary to

switch back to the pure water generator and establish a new zero point at this increased gain. This procedure is repeated many times until, with no further adjustment to the instrument, pure water gives a reading of zero and aerosol a reading of about 90%.

3- Operation (2) is required only at the start of a sequence of runs performed without shutting the photometer off. Only the null (water) calibration has to be repeated whenever a new velocity is investigated.

The operation of the photometer is illustrated by Figure B.1. It is, however, not a true forward light scattering instrument, but collects light scattered between about 4 and 40 degrees.

APPENDIX C. AEROSOL PENETRATION MEASUREMENTS ON STRAIGHT SECTIONS

Refer to Figure C.1. It is seen that the penetration of the aerosol through the bed unit with respect to the blank unit is:

$$\text{Relative Penetration} = \frac{F_{abcdefg}\, F_{bed}}{F_{stwxyzg}\, F_{blank}}$$

where F_i is the fraction of aerosol remaining after passing through unit 'i'. Now $F_a = F_s$, and $F_f = F_z$. Then the above can be written as

$$\text{Relative Penetration} = \frac{F_{bcde}}{F_{twxy}} \frac{F_{bed}}{F_{blank}}$$

Figure C.2 shows some of the data obtained on a long unit (12 inch entrance and exit sections) and a short unit (7 inch entrance and exit sections) against Tygon tubing. Figure C.3 indicates that the losses in the Tygon tubing are negligible, since measurements made on a 55 inch length with respect to a 220 inch length, the latter having many bends and loops, shows no difference. Note there are no differences in the data

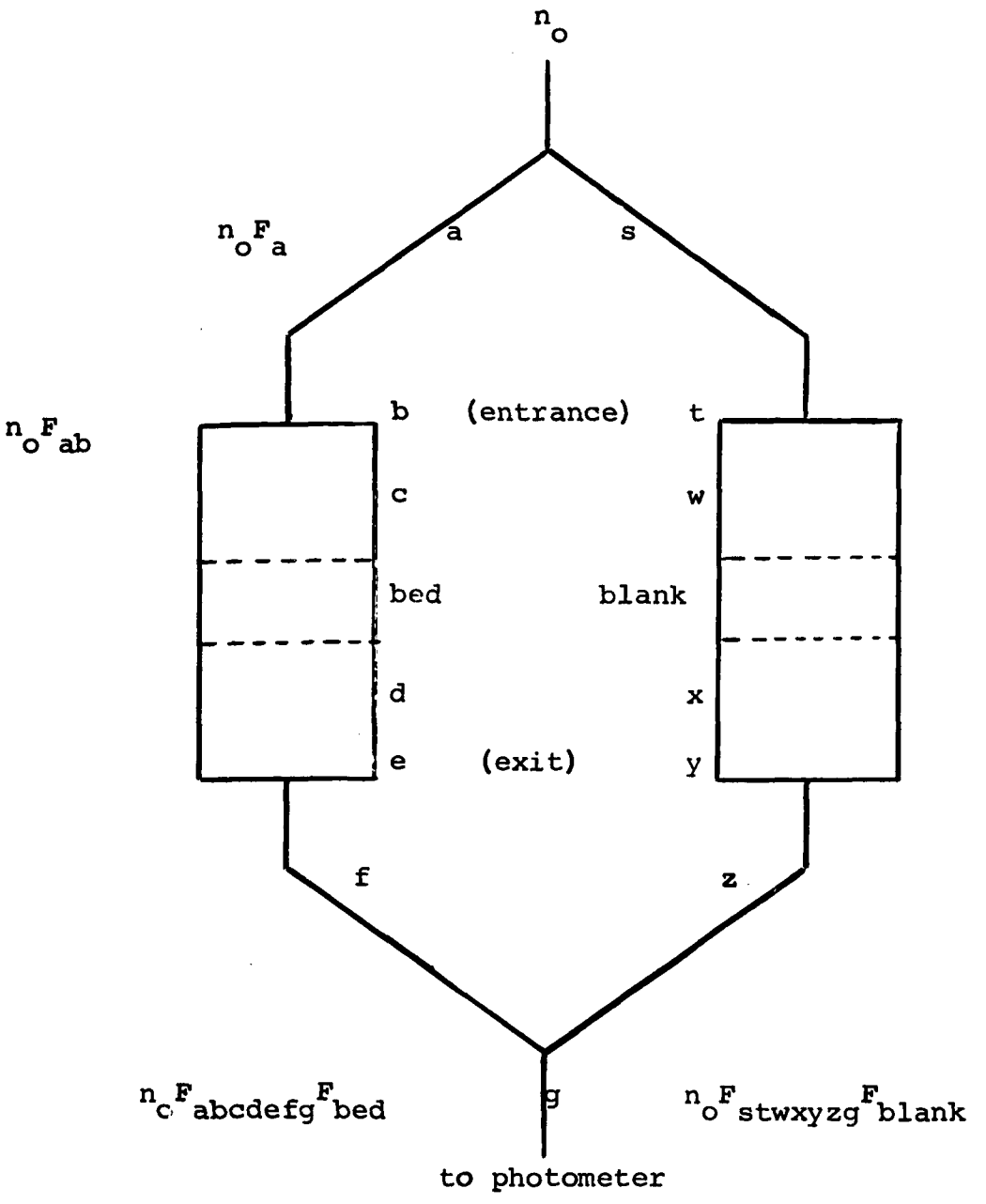

$F_{i.....n}$ = fraction of aerosols remaining after passing through units i to n

Figure C.1. Schematic for aerosol penetration measurements: straight sections.

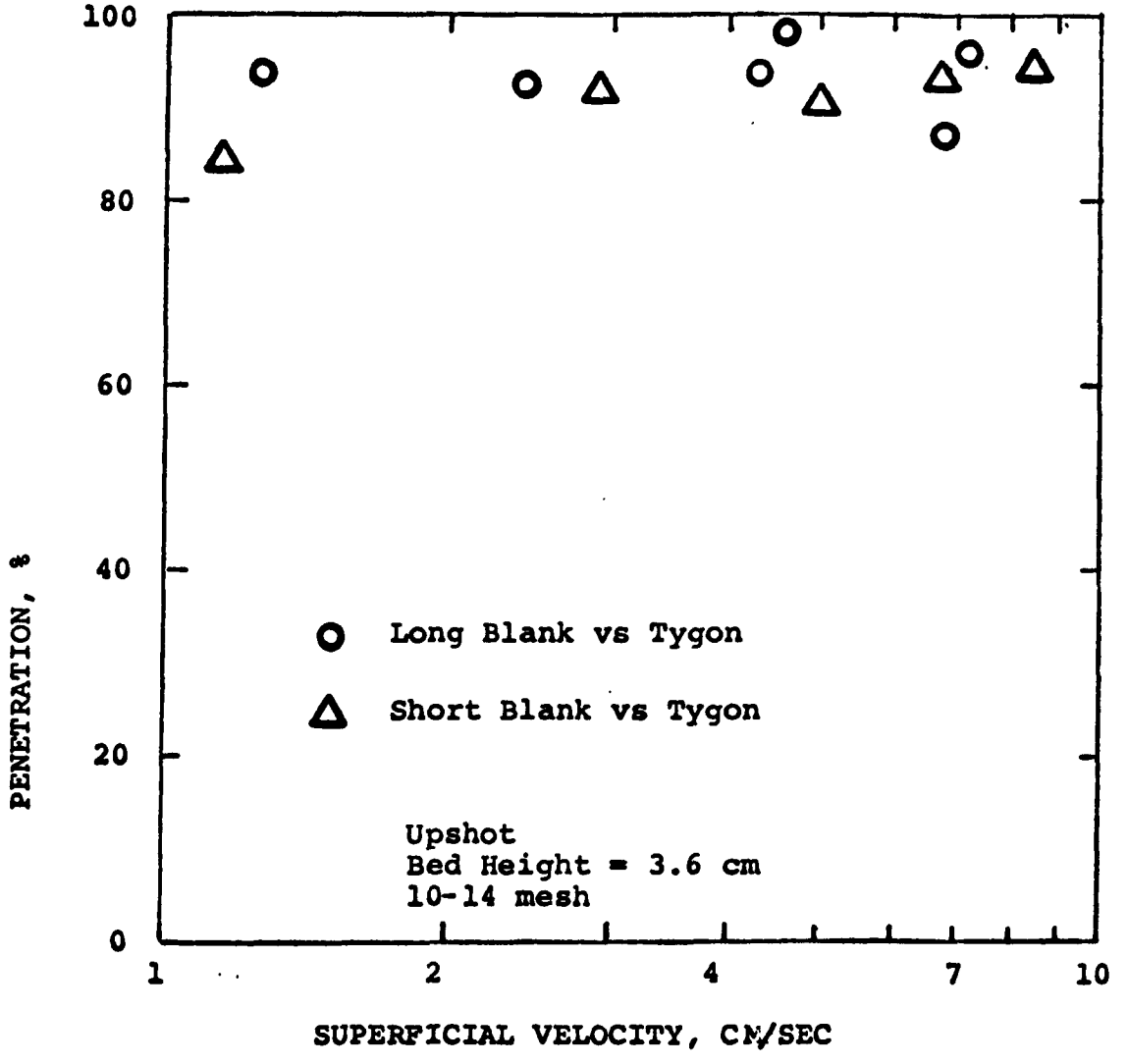

Figure C.2. Relative penetration of blank unit with respect to Tygon tubing.

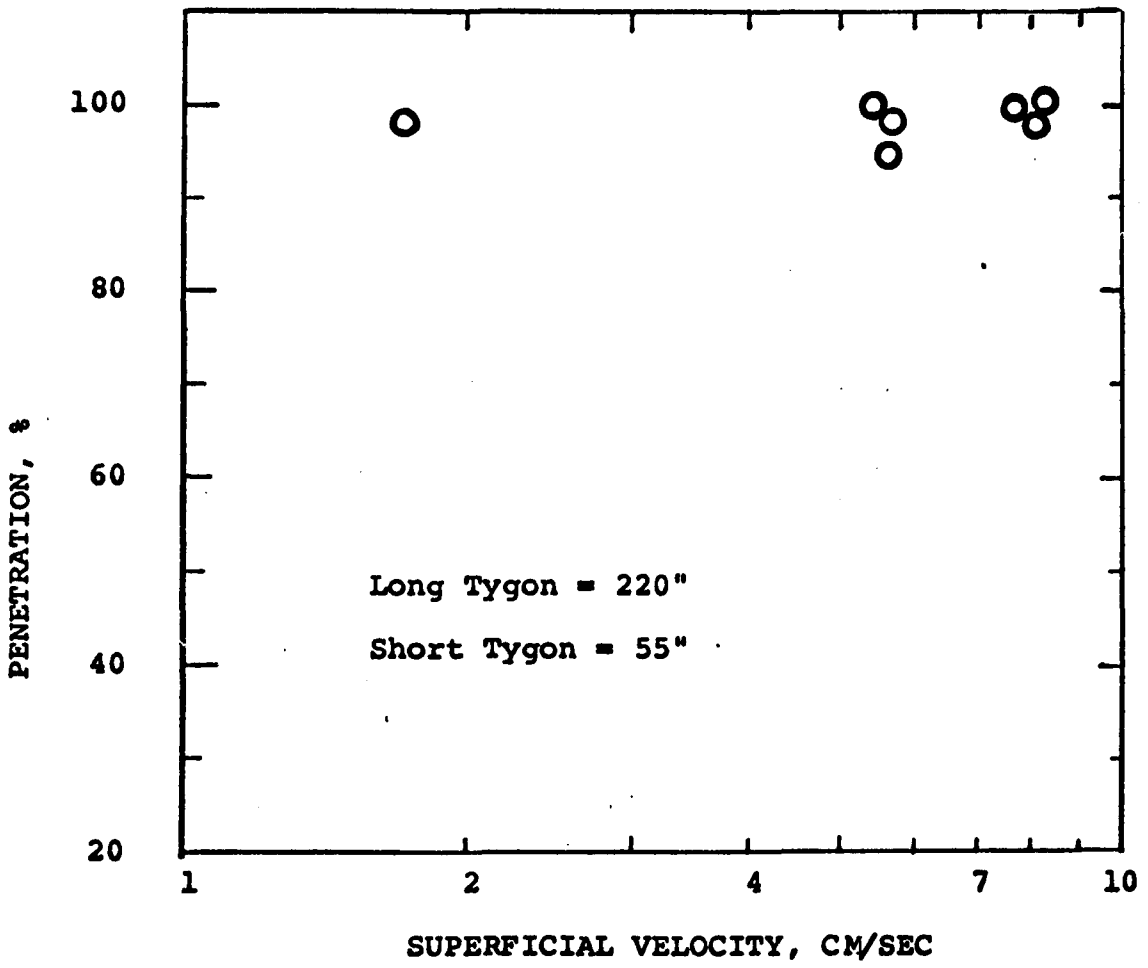

Figure C.3. Relative penetration through long Tygon with respect to short Tygon.

obtained on the long and short blank against Tygon. Therefore it can be said that $F_w = F_x = F_{blank} \approx 1$. The relationship then becomes

$$\text{Relative Penetration} = \frac{F_{bcde}}{F_{ty}} F_{bed}$$

Also, it can be assumed that $F_c = F_d \approx 1$. Then

$$\text{Relative Penetration} = \frac{F_{be}}{F_{ty}} F_{bed}$$

or

$$F_{bed} = \frac{F_{ty}}{F_{be}} \text{Relative Penetration}$$

but F_{bed} is the penetration through the sand bed, and is equal to ξ. F_{ty} and F_{be} are the entrance and exit losses on the blank and bed units.

Figure C.4 shows that for both upshot and downshot flow, a short unit gives higher penetrations. Figure C.2 established that there were little differences between the two empty units. However, with the presence of a bed, the flow patterns tend to spread out. The abrupt change, especially with large aerosol particles,

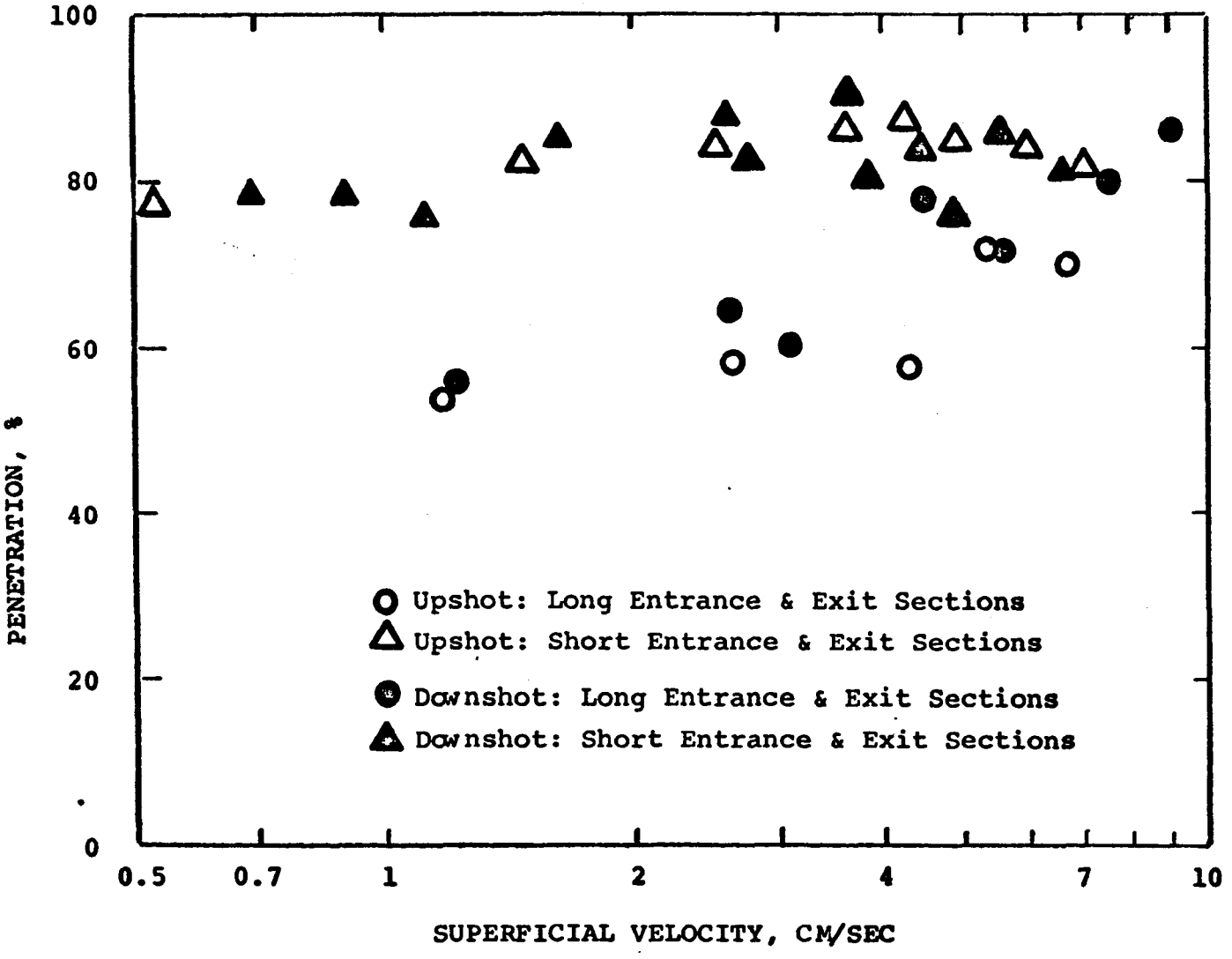

Figure C.4. Comparison of data obtained on long and short units.
Bed height = 3.6 cm
10-14 mesh sand

at the exit causes the particles to be lost. For this reason tapered entrance and exit sections were used.

APPENDIX D. AEROSOL PENETRATION MEASUREMENTS ON TAPERED SECTIONS

The rationale is similar to the straight sections previously discussed. However, initially measurements are made on the unit with no bed present (blank) with respect to a 55 inch length of 3/8" I.D. Tygon. Then, at the same flow rate the measurements are repeated with the sand bed present.

The penetration measurement with the blank is (Figure D.1):

$$\text{Relative Penetration (blank)} = \frac{F_{ab'c'de}\, F_{blank}}{F_{xze}\, F_{tube}}$$

The penetration measurement with the sand bed is:

$$\text{Relative Penetration (bed)} = \frac{F_{abcde}\, F_{bed}}{F_{xze}\, F_{tube}}$$

The penetration through the sand bed is just the ratio of the above two ratios. That is,

$$\frac{\text{Relative Penetration (bed)}}{\text{Relative Penetration (blank)}} = \frac{F_{bc}}{F_{b'c'}} \frac{F_{bed}}{F_{blank}}$$

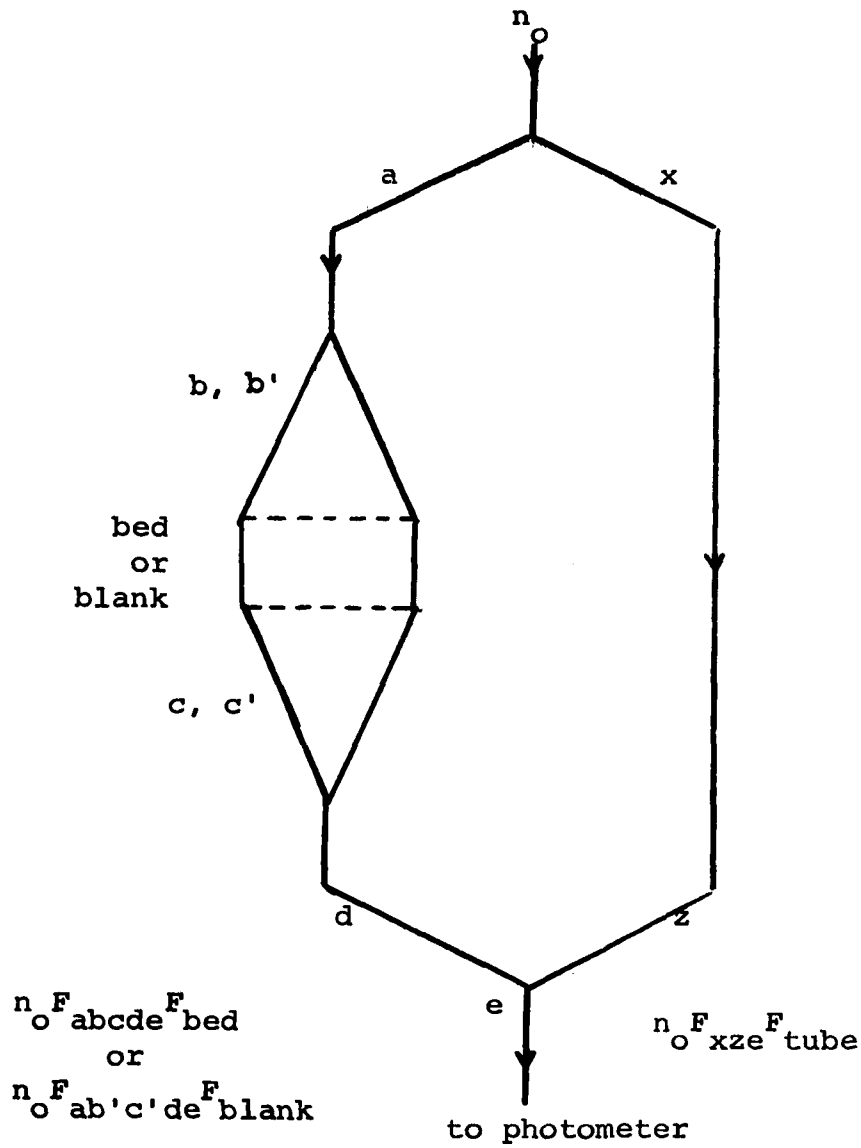

(' indicates blank measurement)

Figure D.1. Schematic for aerosol penetration measurements: tapered sections.

or, assuming $F_{bc}/F_{b'c'} = 1$

$$\frac{\text{Relative Penetration (bed)}}{\text{Relative Penetration (blank)}} = \frac{F_{bed}}{F_{blank}}$$

The above expression can be rearranged to read:

$$F_{bed} = \frac{\text{Relative Penetration (bed)}}{\text{Relative Penetration (blank)}} F_{blank}$$

But F_{blank} is approximately one, since Figure D.2 indicates that the length of the blank chamber has no effect on the penetration. Therefore:

$$F_{bed} = \frac{\text{Relative Penetration (bed)}}{\text{Relative Penetration (blank)}}$$

Since F_{bed} is just ξ, the fractional penetration through the sand bed, the above expression becomes:

$$\xi = \frac{\text{Relative Penetration (bed)}}{\text{Relative Penetration (blank)}}$$

For convenience a calibration curve for the above equation as a function of velocity was prepared. This curve is shown in Figure D.2. Note the difference between upshot and downshot flow at low velocities.

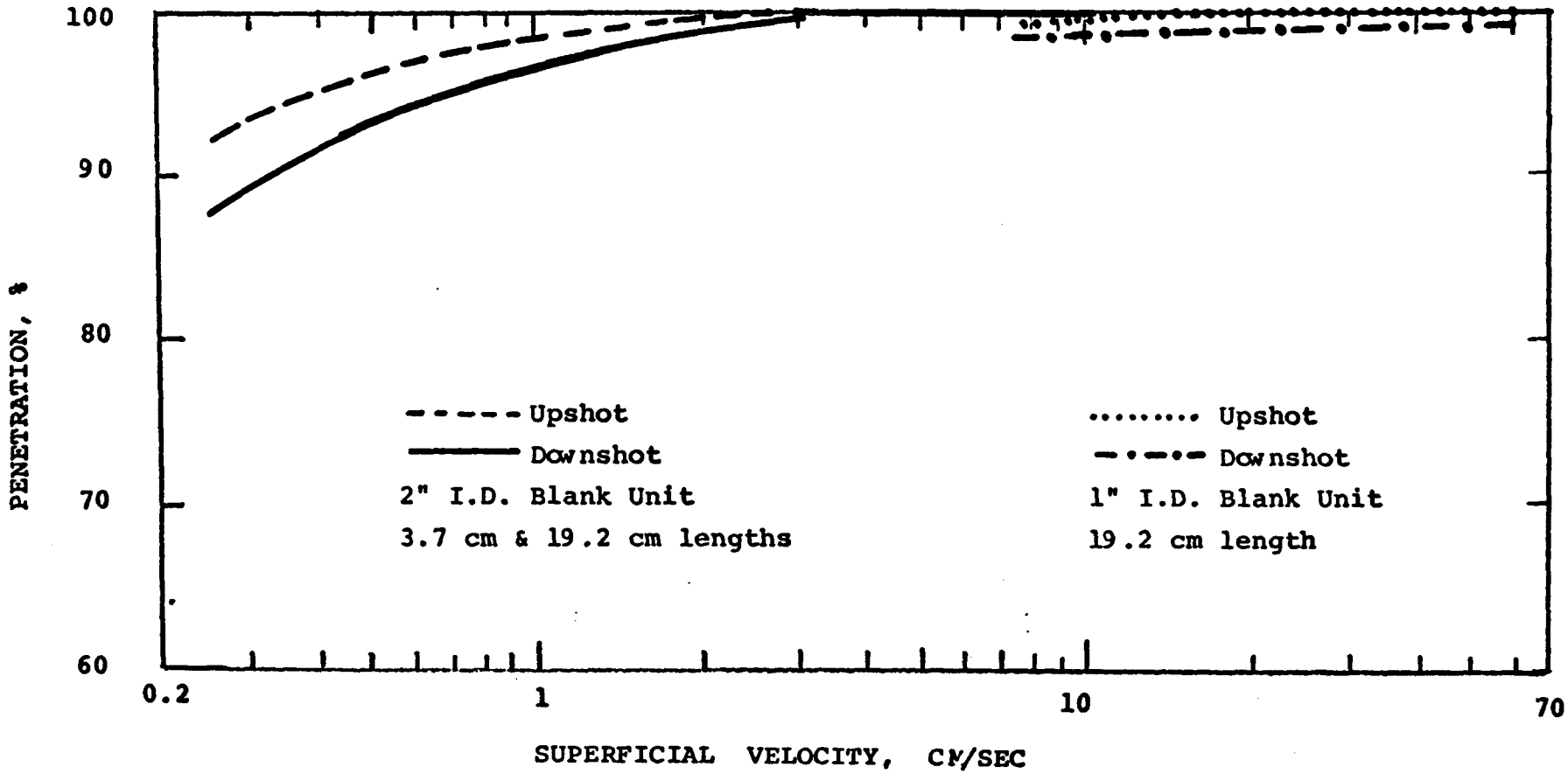

Figure D.2. Calibration curve for blank tapered sections. Penetration through blank section with respect to Tygon.

APPENDIX E. ROYCO COUNTER

A Royco model 220-4 Airborne Particle Monitor with a model 263 display was used to measure the test aerosol concentration from both the horizontal bed and the panel bed. This unit continuously counts the number of particles that are sampled at a flow rate of about 3 liters/min, and supposedly displays the results in four size ranges:

--particles greater than 0.3 microns diameter
--particles greater than 0.5 microns diameter
--particles greater than 1.0 microns diameter
--particles greater than 2.0 microns diameter.

The instrument was set up to continuously count for one minute, retain the number on the display for about 15 seconds, then recycle to zero to begin counting again.

The optical system of the monitor is illustrated in Figure E.1. The particle monitor projects a beam of light through a stream of air and detects the presence of particles by sensing the light scattered by the particles with a phototube positioned at 90° to the main projection axis. Hence, as opposed to the Sinclair-Phoenix which is a forward scattering instrument, this

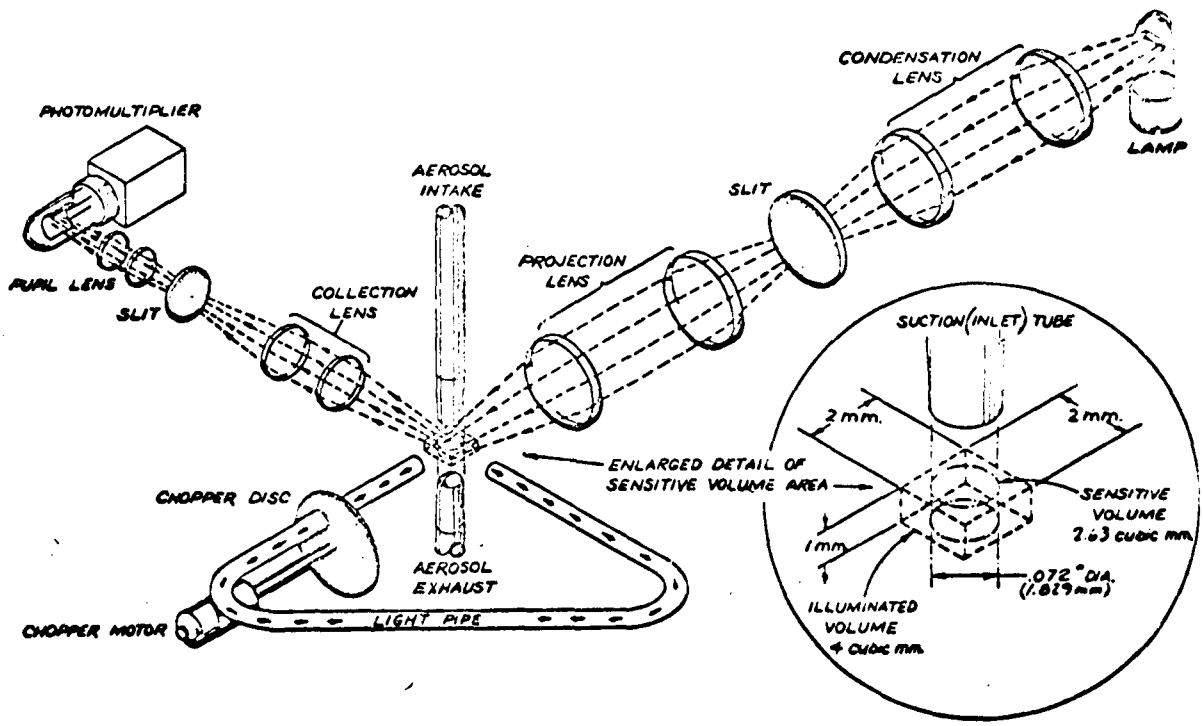

Figure E.1. Optical system of the Royco particle counter.

is a right angle scattering device. When no particle is passing through the viewing field, the phototube sees a dark field. If a particle is present, light is scattered into the phototube during the time that the particle is present in the viewing field. Since the amount of light reaching the photomultiplier tube varies with the size of the particle, the output of the tube is fed into an electric pulse height analyzer which classifies the particles according to size. Since the instrument actually counts the particles, the concentration is kept below 10^5 particles per minute to prevent coincidence losses from having two particles present in the sensing volume at the same time.

The instrument has an internal calibration to correct for decreases in the intensity of the lamp with time.

Although the output from the Royco indicated the test aerosol had a certain degree of heterodisperseness (see Chapter 6), the extent of heterodisperseness is not as large as indicated. Rimberg and Thomas (51) evaluated the model 220 for the AEC, and found that the counter indicates a wide range of sizes for an aerosol that is actually monodispersed. The origin of the

discrepancy is thought to lie in the optical system. If the illumination of the optically sensitive volume is non-uniform and non-homogeneous, monodispersed particles at different points in the sensitive volume can generate different scattered light pulses. The photomultiplier, which may not be uniformly sensitive, can also produce electrical pulses which are different, even if the scattered light pulses are identical. Thus, a monodispersed aerosol could conceivably produce a pulse spectrum, and appear as an heterodispersed aerosol.

21. BIBLIOGRAPHY

1. American Petroleum Institute (Department of Chemical Engineering, University of Cincinnati), Removal of Particulate Matter from Gaseous Wastes: Filtration, p37, New York (1961).

2. Amstein, E.H., and Scott, B.A., "The Measurement of Particle Size Distribution by Sedimentation Methods," Journal Applied Chemistry, 1, Supplementary Issue No. 1, pS10, (1951).

3. Allen, T., Particle Size Measurements, Chapman and Hall, Ltd., London (1968).

4. Baggaley, R., U.S. Patents 746,255 and 746,261 (December 8, 1903).

5. Borgwardt, R., Harrington, R., and Spaite, P., "Filtration Characteristics of Fly Ash from a Pulverized Coal-Fired Power Plant," Journal Air Pollution Control Association, 18, p387 (1968).

6. Brandt, H., "The Possibilities of Further Developments in Dust Removal Techniques," Staub Reinhaltung der Luft (in English), 25, p23 (1965).

7. Burchsted, C.A., "Requirements for HEPA Filters," Contamination Control, p12, November 1967.

8. Chandrasekhar, S., "Stochastic Problems in Physics and Astronomy," Reviews of Modern Physics, 15, p1 (1943).

9. Chen, C.Y., "Filtration of Aerosols by Fibrous Media," Chemical Reviews, 55, p595 (1955)

10. Corn. M., "Adhesion of Particles," in Aerosol Science, C.N. Davies, editor, Academic Press, New York (1966).

11. Corn, M., and Silverman, L., "Removal of Solid Particles from a Solid Surface by a Turbulent Air Stream," American Industrial Hygiene Association Journal, 22, p377 (1961).

12. Davies, C.N., "Viscous Flow Transverse to a Circular Cylinder," Proc. Phy. Soc., B, 63, p288 (1950).

13. Davies, C.N., "The Separation of Airborne Dusts and Particles," Institution of Mechanical Engineering; Proceedings 1-B, No. 1-12, p185 (1952-53).

14. Davies, C.N., "Deposition from Moving Aerosols," in Aerosol Science, C.N. Davies, editor, Academic Press, New York (1966).

15. Dorman, R.C., "The Role of Diffusion, Interception, and Inertia in the Filtration of Airborne Particles," in Aerodynamic Capture of Particles, E.G. Richardson, editor, Pergamon Press, London (1960).

16. Dorman, R.C., "Filtration," in Aerosol Science, C.N. Davies, editor, Academic Press, New York (1966).

17. Engelbrecht, H.L., "The Gravel Bed Filter-A New Approach to Gas Cleaning," Journal Air Pollution Control Association, 15, p43 (1965).

18. Fairs, C.L., and Godfrey, E., "The Problems of Dust in Chemical Industry," in Dust in Industry, Society of Chemical Industry, London (1948).

19. Fiechter, L.B.,British Patent 194,730 (September 20, 1923).

20. First, M., and Silverman, L., "Predicting the Performance of Cleanable Industrical Fabric Filters," Journal Air Pollution Control Association, 13, p581 (1963).

21. Fournier, J., British Patent 450,048 (June 9, 1936).

22. Friedlander, S.K., "Theory of Aerosol Filtration," Industrial and Engineering Chemistry, 50, p1161 (1958).

23. Friedlander, S.K., Particle Diffusion in Low-Speed Flow," Journal Colloid and Interface Science, 23, p157 (1967).

24. Friedlander, S.K., and Pasceri, R.E., "Aerosol Filtration by Fibrous Filters," in Biochemical and Biological Engineering Science, N. Blakebrough, editor, Vol.1, Academic Press, New York (1967).

25. Fuchs, N.A., The Mechanics of Aerosols, Pergamon Press, London (1964).

26. Gavett, W., U.S. Patent 2,287,983 (June 30, 1942).

27. Graff, R., Pfeffer, R., and Squires, A.M., "Capturing Sulfur with Calcined Dolomite," paper presented at Second International Clean Air Congress, Washington, D.C., December 1970.

28. Gray, W.A., The Packing of Solid Particles, Chapman and Hall, Ltd., London (1968).

29. Green, H.L., and Lane, W.R., Particulate Clouds:Dusts, Smokes and Mists, 2nd Edition, Spon, Ltd., London (1958).

30. Happel, John, "Viscous Flow in Multiparticle Systems: Slow Motion of Fluids Relative to Beds of Spherical Particles," A.I.Ch.E. Journal, 4, p197 (1958).

31. Hartmann, U., German Patent 176,943 (January 20, 1906).

32. Herdan, G., Small Particle Statistics, 2nd Revised Edition, Butterworths, London (1960).

33. Herne, H., "The Classical Computations of the Aerodynamic Capture of Particles by Spheres," in Aerodynamic Capture of Particles, E.G. Richardson, editor, Permamon Press, London (1960).

34. Irani, R., and Callis, C., Particle Size: Measurement, Interpretation and Application, John Wiley (1963).

35. La Mer, V.K., Gendron, P.R., and Gruen, R.S., Nuclear Science Abstracts, Vol. 5, No. 755 (1951).

36. Lamb, H.,Hydrodynamics, 6th Edition, Cambridge University Press (1932).

37. Langmuir, I., Filtration of Aerosols and the Development of Filter Materials, part IV, Report # OSRD-865 (1942).

38. Levich, V.G., Physicochemical Hydrodynamics, Prentice-Hall (1962).

39. Lucas, H.G., Note on Multiple Orifice Fine Particle Feeder, U.S. Bureau of Mines, Morgantown, West Virginia, Private Communication (1967).

40. Lundgren, D.A., and Cooper, D.W., "Effect of Humidity on Light Scattering Methods of Measuring Particle Concentration," Journal Air Pollution Control Association, 19, p243 (1969).

41. Lunge, G., A Theoretical and Practical Treatise on The Manufacture of Sulfuric Acid and Alkali with the Collateral Branches, 1st Edition, Vol. 3, p248, Jan van Voorst, London (1880).

42. McCabe, W., and Smith, J.C., Unit Operations of Chemical Engineering, McGraw Hill (1956).

43. Orr, Clyde, Particulate Technology, Macmillan Company, New York (1966).

44. Pich, J., "Theory of Aerosol Filtration," in Aerosol Science, C.N. Davies, editor, Academic Press, New York (1966).

45. Pfeffer, Robert, "Heat and Mass Transport in Multi-particle Systems," Industrial and Engineering Chemistry Fundamentals, 3, p380 (1964).

46. Pfeffer, R., and Happel, J., "An Analytical Study of Heat and Mass Transfer in Multiparticle Systems at Low Reynolds Numbers," A.I.Ch.E. Journal, 10, p605 (1964).

47. Ramskill, E.A., and Anderson, W.L., "The Inertial Mechanism in the Mechanical Filtration of Aerosols," Journal of Colloid Science, 6, p416 (1951).

48. Ranz, W.E., and Wong, J.B., "Impaction of Dust and Smoke Particles," Industrial and Engineering Chemistry, 44, p1371 (1952).

49. Rigg, G. (to New Jersey Zinc Co.), U.S. Patent 1,095,676 (May 5, 1914).

50. Rimberg, D., and Thomas, J.W., "Comparison of Particle Size of Latex Aerosols by Optical and Gravity Settling Methods," Journal of Colloid Interface Science, 32, p101 (1970).

51. Rimberg, D., and Thomas, J.W., "Response of an Optical Counter to Monodispersed Aerosols," Atmospheric Environment, 4, p681 (1970).

52. Smith, H.F., (to Gas Research Company), U.S. Patent 1,608,678 (November 30, 1926).

53. Squires, A.M., "Method and Apparatus for Treating Fluids and Non-Fluid Materials," U.S. Patent 3,296,775 (January 10, 1967).

54. Squires, A.M., "Apparatus and Method for Fluid-Solid Contacting," Application for U.S. Letters Patent.

55. Squires, A.M., and Pfeffer, R., "Panel Bed Filters for Simultaneous Removal of Fly Ash and Sulfur Dioxide: I. Introduction," Journal Air Pollution Control Association, 20, p523 (1970).

56. Stern, A., Air Pollution, Vol. III, 2nd Edition, Academic Press, New York (1968).

57. Stern, S.C., Zeiler, H.W., and Schekman, A.I., "The Aerosol Efficiency and Pressure Drop of a Fibrous Filter at Reduced Pressures," Journal Colloid Science, 15, p546 (1960).

58. Strauss, W., and Thring, M.W., "Studies in High-Temperature Gas Cleaning," Journal Iron and Steel Institute (London), 196, p62 (Sept, 1960).

59. Taub, Steven I., Ph.D. dissertation, Carnegie-Mellon University (1970).

60. Thomas, D.G., and Lapple, C.E., "Deposition of Aerosol Particles in Fibrous Filters," A.I.Ch.E. Journal, 7, p203 (1961).

61. Thomas, J.W., "Aerosol Penetration Through Pinholed Filters," Health Physics, 11, p667 (1965).

62. Thomas, J.W., and Yoder, R.E., "Aerosol Size for Maximum Penetration Through Fiberglas and Sand Filters," AMA Arch. Ind. Health, 13, p545 (1956).

63. Thomas, J.W., and Yoder, R.E., "Aerosol Penetration Through a Lead Shot Column: A Method of Particle Size Estimation," AMA Arch. Ind. Health, 13, p550 (1956).

64. Wasser Luft und Betrieb, editorial note by Dr. R., 5, p27 (1961).

65. Wong, J.B., Ranz, W.E., and Johnstone, H.F., "Collection Efficiency of Aerosol Particles and Resistance of Flow through Fibrous Mats," Journal Applied Physics, 27, p161 (1956).

66. Zenz, F.A., (to Ducon Co.), U.S. Patent 3,410,055 (November 12, 1968).

67. Zenz, F.A., and Othmer, D., Fluidization and Fluid-Particle Systems, Reinhold Publishing Company, New York (1960).

68. Zimon, A.D., Adhesion of Dust and Powder, Plenum Press, New York (1969).

22. VITA

Leon Carl Paretsky was born in Brooklyn, New York on November 23, 1943. He received his elementary and secondary education in the New York City school system. He entered the Polytechnic Institute of Brooklyn in September 1960, and graduated in June 1964 with a Bachelor of Science in Chemical Engineering (cum laude).

He worked during the summer of 1964 at Brookhaven National Laboratory before commencing his graduate studies in September 1964 at the City College of the City University of New York. He received his Master of Engineering (Chemical) from the City College. While pursuing his doctoral degree he was employed at various times as a Part-time Lecturer in the Chemical Engineering Department of the City College.

He currently resides in Brooklyn with his wife, Celia, and son, Peter.